Spring August 2014

MICROBE-MINERAL RELATIONSHIPS AND BIOGENIC MINERAL TRANSFORMATIONS IN ACTIVELY VENTING DEEP-SEA HYDROTHERMAL SULFIDE CHIMNEYS

TZIHSUAN J. LIN
University of Massachusetts - Amherst

MICROBE-MINERAL RELATIONSHIPS AND BIOGENIC MINERAL TRANSFORMATIONS IN ACTIVELY VENTING DEEP-SEA HYDROTHERMAL SULFIDE CHIMNEYS

A Dissertation Presented

by

TZI-HSUAN JENNIFER LIN

Submitted to the Graduate School of the
University of Massachusetts Amherst in partial fulfillment
of the requirements for the degree of

DOCTOR OF PHILOSOPHY

May 2014

Microbiology Department

MICROBE-MINERAL RELATIONSHIPS AND BIOGENIC MINERAL TRANSFORMATIONS IN ACTIVELY VENTING DEEP-SEA HYDROTHERMAL SULFIDE CHIMNEYS

A Dissertation Presented

by

TZI-HSUAN JENNIFER LIN

Approved as to style and content by:

_____

James F. Holden, Chair

_____

M. Darby Dyar, Member

_____

Susan B. Leschine, Member

_____

Klaus R. Nusslein, Member

_____

John Lopes, Department Head

Microbiology

DEDICATION

To:

Every child asking why

ACKNOWLEDGMENTS

I would like to thank James F. Holden for being a constant source of inspiration, guidance and support throughout the years. I aspire to be the scientist and mentor he is. I thank Helene Ver Eecke and Samantha Zelin, for being outstanding mentors during my first couple of years and their lasting friendship and advice. I thank current and past lab members: Kyunghwa Baek, Lucy Stewart, Katarina Olsson, Sarah Hensley, Begum Topcuoglu, Emily Moreira, Gabriel El Sebae, Srishti Kahyap, Molly Williams and James Llewellyn for great scientific discussions, great times in the lab and wish them every success. I am indebted to Burcu Unal, Roberto Orellana and Jesus Alvelo for their many hours of stimulating conversation and friendship. There are a lot of great people in the department, too numerous to name, that I am thankful for. I am grateful for the sharing of equipment and materials within the department. I would like to thank our collaborators M. Darby Dyar and Elly Breves, for their vital and continued advice and support throughout my Ph.D. I would also like to thank our collaborators John W. Jamieson, Mark D. Hannington, Håkon Dahle, Janice L. Bishop, Melissa D. Lane, David A. Butterfield, Deborah S. Kelley and John A. Baross for their expertise and invaluable support to this interdisciplinary dissertation, without which it would never have been possible. I thank my committee members Susan R Leschine and Klaus R Nüsslein for their additional guidance and support.

I am grateful for all my friends for always being there. I would especially like to thank my parents, Cheng-Shih Lin and Show-Mei Sung, for raising me to be a curious scientist, for their continued love and support, and my siblings: Eunice, Anica and Ian for always saying the wrong thing and pushing me to be the best I could be. I would lastly like to thank An-Hsiang Adam Chu, for always believing in me and being my ultimate cheerleader.

ABSTRACT

MICROBE-MINERAL RELATIONSHIPS AND BIOGENIC MINERAL TRANSFORMATIONS IN ACTIVELY VENTING DEEP-SEA HYDROTHERMAL SULFIDE CHIMNEYS

MAY 2014

TZI-HSUAN JENNIFER LIN

B.S., NATIONAL YANG MING UNIVERSITY

PH. D., UNIVERSITY OF MASSACHUSETTS AMHERST

Directed by: Dr. James F. Holden

This dissertation uses a combination of microbiology, mineralogy, and geochemistry to understand dissimilatory iron reduction in hyperthermophilic archaea and the role and potential impact of these and other vent microorganisms within active deep-sea hydrothermal vent chimneys. The central objective of the dissertation is to determine if mineral composition and chimney type are among the primary determinants of microbial community composition and hyperthermophilic, dissimilatory iron reducer growth, in addition to other environmental factors such as nutrient availability, temperature, pH, and chlorinity. This is done using samples and organisms collected from the Endeavour Segment of the Juan de Fuca Ridge in the northeastern Pacific Ocean. The goals of this dissertation are: 1) to correlate microbial community compositions within three Endeavour hydrothermal chimneys with their mineral compositions using mineral spectroscopic techniques that have not been applied previously to hydrothermal chimneys, 2) to characterize the growth and Fe^{2+} production rates and constraints of two novel hyperthermophilic iron reducers isolated from Endeavour hydrothermal chimneys, and 3) to determine the mineral end-products of these iron reducers using mineral spectroscopic techniques that have not been applied previously with hyperthermophiles.

This was first done by collecting three active hydrothermal chimneys and their associated high-temperature fluids from the Endeavour Segment, Juan de Fuca Ridge to evaluate the linkages among mineralogy, fluid chemistry, and microbial community composition within the chimneys. To identify mineralogy, Mössbauer, mid-infrared thermal emission, and VNIR spectroscopies were used for the first time on vent chimneys, in addition to thin-section

petrography, x-ray diffraction (XRD) and elemental analyses. A chimney from the Bastille edifice was rich in Fe-sulfide and composed primarily of chalcopyrite, marcasite, sphalerite, and pyrrhotite (i.e., type I chimney) while chimneys from the Dante and Hot Harold edifices were rich in anhydrite (type II-III chimneys). The bulk emissivity and reflectance spectroscopies corroborated petrography, XRD, and elemental analyses, demonstrating the potential of these techniques for future shipboard analysis. The microbial community within the Bastille chimney was most closely related to mesophilic and thermophilic anaerobes of the deltaproteobacteria, especially sulfate reducers, and anaerobic hyperthermophilic archaea, while those within the Dante and Hot Harold chimneys were most closely related to mesophilic and thermophilic aerobes of the beta-, gamma- and epsilonproteobacteria. Numerical modeling of energy availability from redox reactions in vent fluids suggests that aerobic oxidation of sulfide and methane should be the predominant autotrophic microbial metabolisms at 25°C and 55°C and that anaerobic oxidation of methane should prevail at 80°C. While the microbial community compositions of all three chimneys show aerobic sulfide-oxidizing epsilonproteobacteria, the predominance of mesophilic sulfate reducers in the Bastille chimney suggests that type I chimneys may promote anaerobic metabolisms.

The next two goals, namely characterizing the growth and Fe^{2+} production rates and constraints of two novel hyperthermophilic iron reducers isolated from Endeavour hydrothermal chimneys, and determining their mineral end-products using mineral spectroscopic techniques that have not been applied previously with hyperthermophiles, were carried out in parallel.

Hyperthermophilic iron reducers are common in hydrothermal chimneys found along the Endeavour Segment in the northeastern Pacific Ocean based on culture-dependent estimates. However, information on the availability of Fe(III) (oxyhydr)oxides within these chimneys, the types of Fe(III) (oxyhydr)oxides utilized by the organisms, rates and environmental constraints of hyperthermophilic iron reduction, and mineral end products are needed to determine their biogeochemical significance and are addressed in this study. Thin-section petrography on the interior of a hydrothermal chimney from the Dante edifice at Endeavour showed a thin coat of Fe(III) (oxyhydr)oxide associated with amorphous silica on the exposed outer surfaces of pyrrhotite, sphalerite and chalcopyrite in pore spaces, along with anhydrite precipitation in the pores that is indicative of seawater ingress. The iron sulfide minerals were likely oxidized to Fe(III) (oxyhydr)oxide with increasing pH and E_h due to cooling and seawater exposure,

providing reactants for bioreduction. Culture-dependent estimates of hyperthermophilic iron reducer abundances in this sample were 1,740 and 10 cells per gram (dry weight) of material from the outer surface and the marcasite-sphalerite-rich interior, respectively. Two hyperthermophilic iron reducers, *Hyperthermus* sp. Ro04 and *Pyrodictium* sp. Su06, were isolated from other active hydrothermal chimneys on the Endeavour Segment. Strain Ro04^T grew on peptides, reduced poorly crystalline iron oxide to black ferromagnetic magnetite and produced acetate and minor amounts of ethanol. It did not grow on any other terminal electron acceptor or purely by fermentation. Strain Su06^T also catabolized peptides but only when H_2 was present and reduced poorly crystalline iron oxide to magnetite and nitrate to N_2. They both grew between 82°C and 97°C (T_{opt} 90-92°C) and pH 5.0 and 9.0, but strain Ro04^T had a pH optimum of 8.0 while strain Su06^T had a pH optimum of 5.0. 16S rRNA gene sequence similarity analysis indicated they are 98.4% identical to each other and are most closely related (>98%) to *Hyperthermus butylicus* DSM 5456^T, *Pyrodictium abyssi* DSM 6158^T, *Pyrodictium occultum* DSM 2709^T and *Pyrodictium brockii* DSM 2708^T. The complete genome for Strain Su06 was obtained and genome comparisons done *in silico* between Strain Su06^T against *Hyperthermus butylicus* and *Pyrolobus fumarii*, revealed that Strain Su06 is a novel species. Strain Ro04^T had growth characteristics most similar to *H. butylicus* while strain Su06 was more similar to *P. abyssi*. However, the ability of the strains to reduce iron and their inability to reduce sulfur compounds clearly distinguished them from all of their closest relatives. Phylogenetic, genomic, and phenotypic data indicate that strain Ro04^T is novel species of *Hyperthermus* and strain Su06^T is a novel species of *Pyrodictium*. The name *Hyperthermus hephaesti* is proposed for strain Ro04^T and *Pyrodictium delaneyi* is proposed for Su06^T. Mössbauer spectroscopy of the iron oxides before and after growth demonstrated that both organisms form nanophase (<12 nm) magnetite [Fe_3O_4] from laboratory-synthesized ferrihydrite [$Fe_{10}O_{14}(OH)_2$] with no detectable mineral intermediates. They produced up to 40 mM Fe^{2+} in a growth-dependent manner while all abiotic and biotic controls produced < 3 mM Fe^{2+}. Hyperthermophilic iron reducers may have a growth advantage over other hyperthermophiles in hydrothermal systems that are mildly acidic where mineral weathering at elevated temperatures occurs.

TABLE OF CONTENTS

Page

LIST OF TABLES

LIST OF FIGURES

CHAPTER 1

INTRODUCTION

1.1 Central Objective and Goals

This dissertation uses a combination of microbiology, mineralogy, and geochemistry to understand dissimilatory iron reduction in hyperthermophilic archaea and the role and potential impact of these and other vent microorganisms within active deep-sea hydrothermal vent chimneys. The central objective of the dissertation is to determine if mineral composition and chimney type are among the primary determinants of microbial community composition and hyperthermophilic, dissimilatory iron reducer growth, in addition to other environmental factors such as nutrient availability, temperature, pH, and chlorinity. Hydrothermal chimneys from the Endeavour Segment hydrothermal vent field in the northeastern Pacific Ocean are a reliable source of hyperthermophilic iron reducers (*Ver Eecke et al., 2009*) and are the source of field samples for this study. Two novel hyperthermophilic iron reducers from Endeavour Segment hydrothermal chimneys are the main biological subjects of this study and are analyzed for their growth and mineral transformation capabilities.

The goals of this dissertation are: 1) to correlate microbial community compositions within three Endeavour hydrothermal chimneys with their mineral compositions using spectroscopic techniques that have not been applied previously to hydrothermal chimneys, 2) to characterize the growth and Fe^{2+} production rates and constraints of two novel hyperthermophilic iron reducers isolated from Endeavour hydrothermal chimneys, and 3) to determine the mineral end-products of these iron reducers using mineral spectroscopic techniques that have not been applied previously with hyperthermophiles. This dissertation is the result of collaborations between microbiologists, mineralogists, petrologists, geochemists, and molecular ecologists. Realistically, none of the analyses herein could be completed by one researcher. Rather, it was my role to be the point-person to bring these disparate pieces of data together along with my own microbiological analyses to produce a holistic picture of life and hyperthermophilic iron reduction within hydrothermal chimneys (Fig. 1.1).

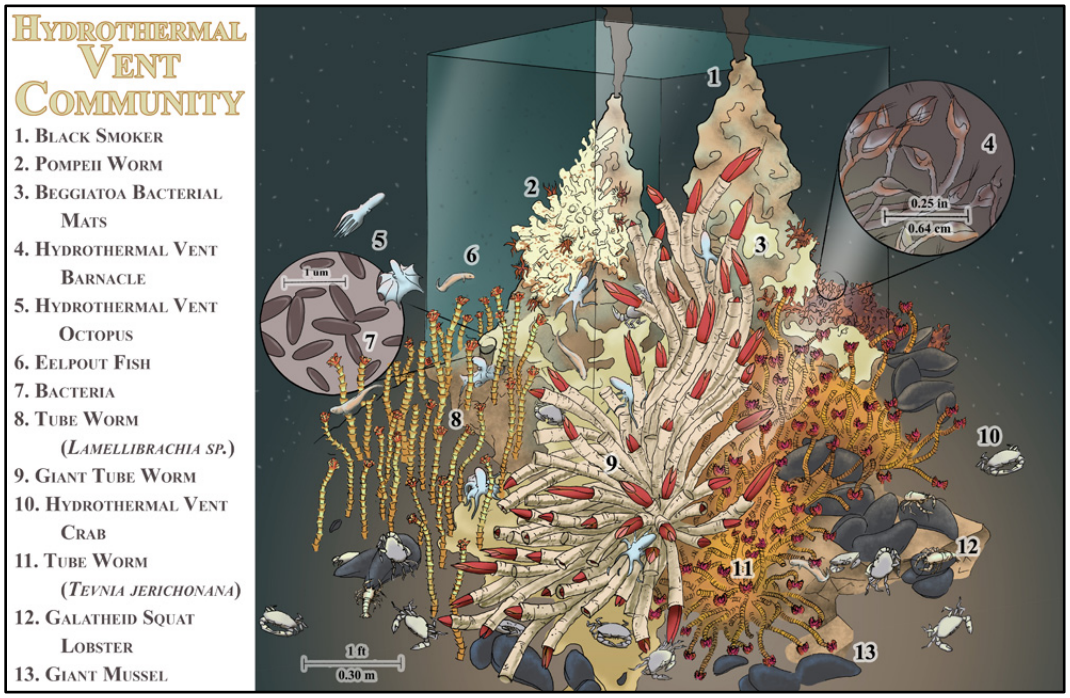

Figure 1.1 General composition of a hydrothermal vent system with each important component labeled with numbers. This figure depicts the thriving and ecologically diverse nature of hydrothermal vent systems with their characteristic features (National Geographic Society).

The dissertation consists of five chapters. This introductory chapter will review the literature on deep-sea hydrothermal vents, factors influencing microbial community structures and distribution patterns within hydrothermal vents, the physiology and characteristics of dissimilatory iron reduction, mineral biosignature production and identification, and the astrobiological implications of these organisms. Chapter 2 is a microbial and mineralogical description of the interior habitable zones of three active hydrothermal chimneys from the Endeavour Segment, Juan de Fuca Ridge. Chapter 3 examines magnetite formation from ferrihydrite by two hyperthermophilic iron reducers (*Hyperthermus hephaesti* Ro04 and *Pyrodictium delaneyi* Su06) from Endeavour Segment hydrothermal chimneys. Chapter 4 taxonomically characterizes these two novel isolates**.** Chapter 5 provides the implications and significance of this dissertation.

1.2 Deep-Sea Hydrothermal Vents

Many environments on Earth are seemingly inhospitable due to extreme temperatures, high pressures, and high and low pHs. Surprisingly, so-called 'extremophiles' are found living in many of these environments that have adapted unique mechanisms to allow them to thrive under and even require these extreme conditions. One such extreme environment is deep-sea hydrothermal vents.

Deep-sea hydrothermal vents were first discovered along the Galápagos Rift in the eastern Pacific Ocean in 1977 (*Corliss et al., 1979*). Numerous factors led to the discovery of hydrothermal venting with the main hypothesis being that hydrothermal activity at mid-ocean ridges is the logical outcome of subseafloor seawater interacting with shallow hot rock due to plate-tectonics (Fig. 1.2). The theory of plate tectonics is that the Earth's lithosphere is divided into dozens of plates that float and move about the Earth's surface with convection cells of weak, partially-molten asthenosphere within the upper mantle driving the separation and convergence of the plates (Fig. 1.3). At mid-ocean spreading centers, two tectonic plates diverge due to upwelling within the mantle. The tensile weakness along the edge of the plates and the gravitational downward drift of the plates allow for upwellings of magma that create new crust between the diverging plates and flows onto the seafloor as lava. The basalt at mid-ocean

spreading centers subsides as it cools, permiting seawater to percolate down into the crust to regions heated by magma lenses that form

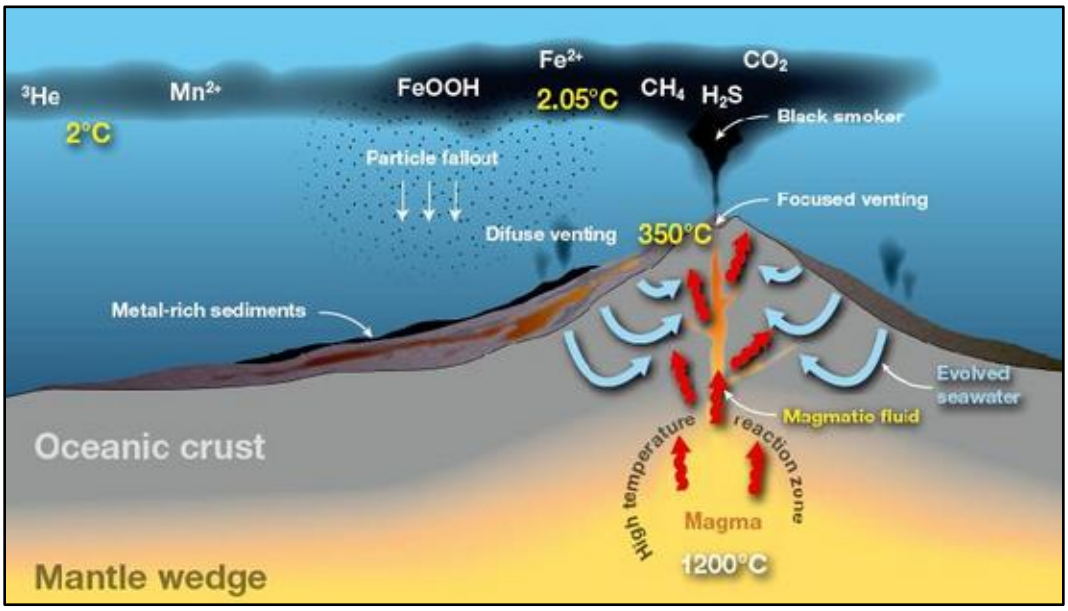

Figure 1.2 Detailed description of how and why hydrothermal vents are formed. Different magma source pockets are found beneath the Earth's crust and heat up the surrounding rock. Seawater that has percolated into the Earth's crust through cracks and pores mixes with the hot rock to produce hydrothermal fluid. When this hydrothermal fluid comes into contact with cold, oxic seawater, heavy metals and minerals precipitate out, causing the black smoke effect.

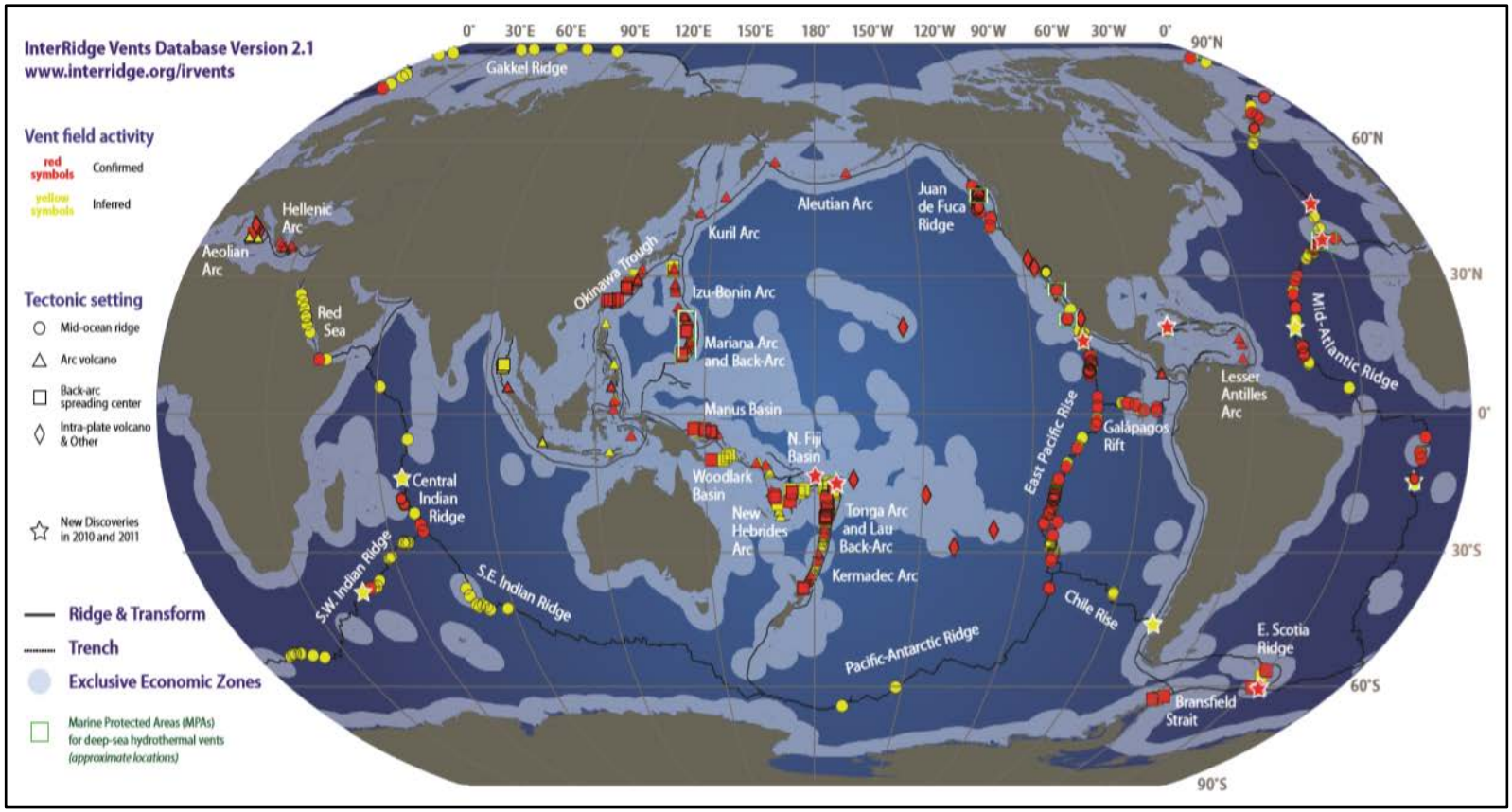

Figure 1.3 Confirmed and inferred hydrothermal activity worldwide. Hydrothermal fields are ubiquitous throughout the Earth's oceans, found especially where mid-ocean ridges and transformations occur.

below the spreading centers. The heating of this seawater drives hydrothermal fluid circulation deep into the subseafloor (*Delaney et al., 1998*).

Several researchers anticipated the discovery of high-temperature fluids along mid-ocean spreading centers due to plate tectonics, seafloor mineral deposits on land, and unusual biological communities found within these regions (*Talwani et al., 1971; Corliss et al., 1979; Skinner, 1983;*). The study of hydrothermal vents revealed the role they play in the transfer of mass and energy from the crust and the mantle to the oceans (*Von Damm et al., 1985*). Basalt-hosted mid-ocean spreading centers also spread laterally at varying rates due to varying fluxes of magma to the spreading center (*Baker et al., 1995; 2004*). The East Pacific Rise is a fast-spreading system, the Juan de Fuca Ridge in the northeastern Pacific Ocean is an intermediate-rate spreading system, and the Mid-Atlantic Ridge is a slow spreading system.

At discrete points along mid-ocean spreading centers, focused flows of hydrothermal fluids rise from the seafloor as distinct jets that can reach temperatures over 400°C. Upon mixing with cold seawater, the heavy metals within hydrothermal fluids that were extracted from subseafloor rock by high-temperature water-rock reactions precipitate out and form the characteristic 'black smokers' and large mineral deposits found at hydrothermal vents (Fig. 1.4) (*Summit & Baross, 2001; Kelley et al., 2002*). These jets of hydrothermal fluid often form metallic spires called hydrothermal chimneys. The formation of these chimneys typically involves two major growth stages: a sulfate mineral-dominated stage and a sulfide-mineral dominated replacement stage. These two stages determine mineral zoning within black smokers and are affected by permeability, which affects the mixing of the two end-member solutions and resulting precipitation (*Haymon, 1983; Tivey & Delaney, 1986; Tivey et al., 1999; Tivey, 2004).* These stages begin with precipitation of anhydrite ($CaSO_4$) from heated seawater where hot hydrothermal fluid comes into contact with the seawater. Anhydrite continues to build upward and outward, acting as a physical boundary between the hydrothermal fluid flow and the surrounding seawater. Metastable pyrrhotite (FeS) precipitates from the cooling hydrothermal fluid onto the surface of anhydrite, then is dissolved and re-precipitated as pyrite and marcasite (both FeS_2). This seals the pores in newly-formed hydrothermal chimneys and allows for chalcopyrite (Fe-Cu sulfide) to begin accumulating within the inner flow channels of the chimneys. This marks the initiation and development of metal sulfide precipitation and the build-

Figure 1.4 Large hydrothermal deposit typically found at the Endeavour Segment of the Juan de Fuca Ridge. These so-called “black smokers” are formed when hot, reduced, hydrothermal fluid comes into contact with cold, oxic seawater and minerals precipitate out, forming the structures and the smoke that billows out of these chimneys.

up of other metal sulfide compounds such as wurtzite and sphalerite (Fe-Zn sulfides) (*Goldfarb et al., 1983; Haymon, 1983; Tivey & Delaney, 1986; Tivey, 2007*).

This generalized view on the growth of hydrothermal chimneys does not take into account differences in vent fluid composition, temperature, pH, vent fluid density, oxygen fugacity, rates of fluid flow, and diffusive versus advective transport. These become important factors that contribute to abundances and types of minerals within hydrothermal chimneys and may influence the microbial community compositions found on and within the chimneys.

1.2.1 Hydrothermal Vents on the Endeavour Segment, Juan de Fuca Ridge

Along the Juan de Fuca Ridge in the northeastern Pacific Ocean, the Juan de Fuca Plate spreads to the east while the Pacific Plate spreads to the west. The Juan de Fuca Plate is then subducted beneath the North American Plate, forming the Olympic and Cascade mountains. This mid-ocean spreading center has a spreading rate of 6 cm per year and is the primary source of hydrothermal venting in the northeastern Pacific Ocean. The Juan de Fuca Ridge is 500 km long, but it is comprised of several shorter segments (*Karsten et al., 1986*). One such segment towards the northern end of the Ridge is the Endeavour Segment.

The Endeavour Segment is 90 km long with an axial valley as its most prominent feature (*Tivey and Delaney, 1986*). Along the floor of the valley, there are five major hydrothermal vent fields spaced 2-3 km apart named Sasquatch, Salty Dawg, High Rise, Main Endeavour and Mothra (going north to south). The Endeavour Segment is characterized by high levels of seismicity, intense phase separation of hydrothermal fluids (*i.e.*, the partitioning of hydrothermal fluid into a brine and metal-rich phase and a volatile-rich phase due to intense subseafloor heating of seawater), steep gradients in volatiles and temperature across and within vents, dense and diverse biological communities, and varying degrees of hydrothermal venting (*Kelley et al., 2012*).

The hydrothermal vents along the Endeavour Segment differ significantly from most other hydrothermal vents on Earth. One of the main differences is the presence of extremely large, steep-sided mineral deposits at Endeavour that rise up to 45 m above the seafloor and are up to 50 m across at the base (*Delaney et al., 1992, Robigou et al., 1993*). They result from high concentrations of ammonia in Endeavour hydrothermal fluids that increase the pH of the fluids

and enhance the deposition of sulfide minerals and silica (*Tivey et al., 1999*). Although each vent deposit edifice is distinct, there are distinguishing and characteristic features of deposits within the Main Endeavour and High Rise vent fields. These include the presence of numerous smaller chimneys that form on top of the main edifices and the presence of multiple overhanging mineral flanges along the sides of the edifices. The Mothra vent field is the southernmost hydrothermal field and has the largest venting area on the Endeavour Segment. It consists of five or more active and inactive vent deposits that are spread 40-200 m apart (*Kelley et al., 2001*). These deposits are different from other Endeavour venting areas because they contain significantly fewer black smokers, generally lack flanges, and mostly consist of steep-sided pinnacles that are highly porous and vent at lower temperatures.

There are four main chimney types at Endeavour and elsewhere on the Juan de Fuca Ridge that are distinguished by their fluid flow characteristics and mineral assemblages (Fig. 1.5) (*Koski et al., 1994*). Type I chimneys are columnar structures that form due to the rapid, focused flow of buoyant, high-temperature hydrothermal fluid from small-diameter orifices. Initial growth of these chimneys is rapid. These have the classic form of growth with chalcopyrite lining the inner fluid flow path; silicate-rich zones within the outer surface; and minerals such as wurtzite, sphalerite and marcasite within the middle region. Type II chimneys are bulbous and have relatively higher porosity and sluggish fluid flow rates through them. They form sulfate- to sulfide-dominant structures, with minor amounts of sphalerite, pyrite, wurtzite, chalcopyrite and pyrrhotite within the pores. These chimneys do not contain the clear mineral zonations found in type I chimneys. Both type I and type II chimneys are formed from high-temperature venting. Type III chimneys have lower fluid temperatures circulating through them and are Zn-rich. Anhydrite is abundant in these chimneys but conclusions on whether it is a requirement for growth cannot be made due to the minimal number of representative samples. Type IV chimneys have a lower temperature depositional history compared to other vent deposit types. Fluid temperatures in most Type IVs do not exceed 250°C.

In 1998, portions of four large hydrothermal sulfide-sulfate-silicate edifices were brought to the surface from the Mothra vent field for scientific examination and for display at the American Museum of Natural History in New York City (*Delaney et al., 2001*). One of these edifices, named ‘Roane’, was a porous, diffusively venting structure that was 8 m in height, with interior fluid temperatures ranging between 210°C and 278°C. The top 3 m of the Roane spire

were brought to the surface, and a detailed mineralogical study of its growth history and mineral composition was performed (*Kristall et al., 2006*). It was suggested that Roane was formed gradually and had extensive seawater influx and hydrothermal fluid mixing within its interior due to its lack of a well-defined open central conduit. Its central core contained Fe-sulfide minerals such as pyrite, marcasite and pyrrhotite, Fe-Zn-sulfides such as wurtzite and sphalerite, and the Fe-Cu-sulfide chalcopyrite. Non-sulfide phases such as silicates and sulfates formed near the outer portions of the spire, and the interior pore spaces of this region contained extensive clays and other Fe(III) (hydr)oxides. In 2004, a small hydrothermal chimney that had grown on the remaining stump of the Roane edifice (since the removal of the top portion) was sampled and used as the inoculum for the *Hyperthermus* sp. Ro04 strain discussed in this dissertation.

1.3 Microbial Communities and Distribution Patterns

Biogeography is the study of the distribution of organisms and populations over space and time. It aims to determine where organisms live, their abundances, and why they are where they are. Microbial biogeography is often described by the Baas-Becking hypothesis, which states 'everything is everywhere - the environment selects' (*Baas-Becking, 1934*). This statement is both supported and disputed within microbiology. In the case of hydrothermal vents, the evidence supports the idea that the environment does indeed select. The oceanic subseafloor, primarily composed of sediments and igneous crust, is potentially a diverse and rich microbial habitat. It was estimated that sedimentary marine microbes (including microbes within the igneous crust) comprise up to 25% (290 Pg C) of the total biomass on Earth (*Whitman et al.*, 1998; *Lipp et al., 2008*). This estimate was recently modified due to improved calculations of sediment thickness globally, which suggest that subseafloor sedimentary microbes comprise 0.35% (4.1 Pg C) of Earth's total biomass, which is 10-45% of the previous estimates (*Kallmeyer et al., 2012*). These studies did not take into account microbial abundances within igneous ocean crust, which may include an additional 200 Pg C (*Heberling et al., 2010*), but biomass estimates in marine igneous crust are very poorly constrained. One place with access to microbes that live in igneous crust is at submarine hydrothermal vent sites. These sites are the most biologically productive sites in the deep-sea, accounting for up to 10^{13} g of biomass from chemosynthetic organisms alone (*McCollom and Shock, 1997*). The most pronounced limitation to life at

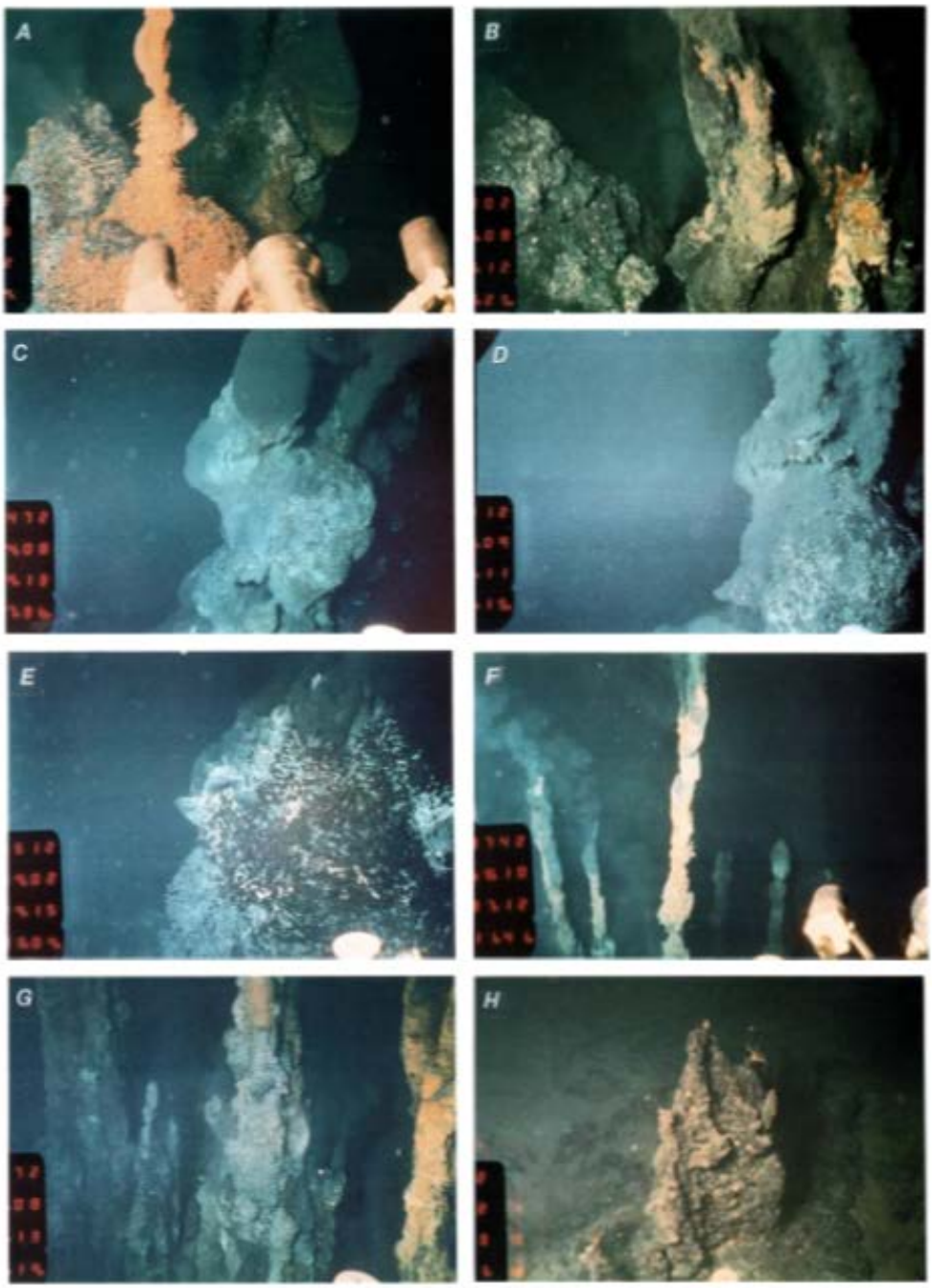

Figure 1.5 Different types of hydrothermal chimneys that form due to fluid out-flow velocity, fluid mineral composition, size and shape of exit route etc. (*Koski et al., 1994*)

hydrothermal vents is temperature. Pure hydrothermal fluids often reach temperatures that exceed 300°C, but the highest known growth temperature for a microorganism is 122°C (*Takai et al., 2008*). Organisms in hydrothermal vents are often defined by their temperature limits for growth, namely mesophiles (optimal growth temperatures [T_{opt}] of 20-50°C), thermophiles (T_{opt} of 50-80°C), and hyperthermophiles (T_{opt} greater than 80°C). Another limitation on life at these sites is nutrient availability. Carbon, nitrogen, phosphorous and trace elements are all essential for life (*Holland & Baross, 2003; Hoehler, 2007*). One hyperthermophilic methanogen is capable of nitrogen fixation (*Mehta & Baross, 2006*), but is the only known example of this process at elevated temperatures. Phosphorus limitation in hydrothermal vents has not been examined. Many microorganisms in vents are chemoautotrophs and serve as a source of organic carbon in this system (*Jannasch & Mottl, 1985*). These chemoautotrophic metabolisms are driven by redox disequilibria found in the mixture of chemically reduced hydrothermal fluid and oxidized seawater.

The energy available for chemoautotrophic growth has been modeled in mixtures of hydrothermal fluid and seawater. One of the first bioenergetics models for autotrophic microbial growth in hydrothermal vents suggested that vents favor the growth of aerobes that oxidize H_2S, CH_4, Fe^{2+} and Mn^{2+} at temperatures below 38°C, and anaerobes that oxidize H_2 and reduce S°, and SO_4^{2-} to H_2S, and CO_2 to CH_4 above 38°C (*McCollom & Shock, 1997; Amend et al., 2011*). H_2 availability has been suggested to partition anaerobic metabolisms in anoxic sediments and aquifers on land (*Lovley & Goodwin, 1988*), with H_2 availability as a key determinant for the presence of methanogens in hydrothermal vents (*Flores et al., 2011; Ver Eecke et al., 2012*). Phylogenetic analyses of microbes from various niches within vent environments support the idea that aerobic sulfur oxidizing bacteria belonging to the epsilonproteobacteria often are the most abundant organisms present (*Brazelton et al., 2006; Huber et al., 2007; Takai et al., 2010*).

Studies that correlate hydrothermal chimney mineral composition with their local microbial community compositions are limited for hydrothermal vent sites such as the Endeavour Segment (*Schrenk et al., 2003; Ver Eecke et al., 2009; Zhou et al., 2009*) and elsewhere (*Takai et al., 2001; Kormas et al., 2006; Pagé et al., 2008; Olins et al., 2013*). At the Endeavour Segment, it was observed that microbial abundance of both bacteria and archaea vary from zone to zone (*Schrenk et al., 2003*). Zones deeper within the chimney were suggested to have minimal amounts of seawater mixing and were characterized by high temperatures and

anoxia. The microbial communities shifted from being mesophilic bacteria and archaea near the exterior of the chimney to predominantly hyperthermophilic archaea in its interior. Hyperthermophiles found in the hotter zones of chimneys generally belonging to the Thermococcales, Desulfurococcales, Methanococcales and Archaeoglobales (*Takai et al., 2001; Schrenk et al., 2003; Kormas et al., 2006; Pagé et al., 2008; Zhou et al., 2009*). Microbial communities have been observed in hydrothermal vent deposits that are mostly composed of metal sulfide and silicate (*Schrenk et al., 2003; Kormas et al., 2006; Zhou et al., 2009*) to predominantly sulfate dominant chimneys (*Pagé et al.,* 2008; *Olins et al., 2013*). In all zones, microbial communities were also observed to be associated with mineral surfaces which suggest a mechanistic and dependent attachment (*Schrenk et al., 2003*).

Very little attention has been given to iron-reducing microorganisms in hydrothermal vents. McCollom and Shock (1997) stated that there is very little energy available for iron reduction in vents due to the high insolubility of iron in these systems, unless another form of Fe(III) is available. A study of the mineral composition of a vent chimney showed that Fe^{3+} (hydr)oxide minerals can be abundant (*Kristall et al., 2004*). This oxidized iron could be a major source of Fe^{3+} for iron reducers in vent environments. Iron reducing microorganisms have been found in several hydrothermal vents (*Slobodkin et al., 2001; Kashefi et al., 2002; Kashefi & Lovley, 2003; Ver Eecke et al., 2009*).

1.4 Dissimilatory Iron Reduction

Iron is the most common element by mass and fourth most abundant mineral in the Earth. Whether iron is present in a reactive form is one of the major limiting factors for growth of iron-metabolizing microorganisms. Iron exists in a range of oxidation states with the most common being Fe^{2+} and Fe^{3+}. Thermodynamically, Fe(III) (hydr)oxide reduction has a higher energy yield than either sulfate reduction or methanogenesis (Table 1.1). In natural environments such as soils, shallow aquifers, sediments and subsurface materials, crystalline Fe(III) (hydr)oxides, which are not as easily reduced, are more abundant then amorphous Fe(III) (hydr)oxides (*Schwertmann & Taylor, 1977*). Amorphous Fe(III) (hydr)oxides, which are thermodynamically more favorable for growth and metabolically more relevant, tend to exist at near neutral pH

Table 1.1: Redox potential tower of major microbial metabolisms

Reaction	Redox potentials of selected half-reactions at 25°C and pH 7 E_h (V)
$O_2 + 4H^+ + 4e^- \leftrightarrow 2H_2O$	0.81
$NO_3^- + 6H^+ + 6e^- \leftrightarrow ½ N_2 + 3H_2O$	0.75
$NO_3^- + 2H^+ + e^- \leftrightarrow NO_2^- + H_2O$	0.42
$NO_3^- + 10H^+ + 8e^- \leftrightarrow NH_4^+ + 3H_2O$	0.36
$Fe^{3+} + e^- \leftrightarrow Fe^{2+}$	0.36
$SO_4^{2-} + 8H^+ + 6e^- \leftrightarrow S + H_2O$	-0.20
$SO_4^{2-} + 10H^+ + 8e^- \leftrightarrow H_2S + 4H_2O$	-0.21
$CO_2 + 8H^+ + 8e^- \leftrightarrow CH_4 + 2H_2O$	-0.24
$H^+ + e^- \leftrightarrow 1/2H_2$	-0.41
$Fe^{2+} + 2e^- \leftrightarrow Fe$	-0.85

(*Lovley, 1991; Straub, 2001*). In anaerobic, non-sulfidogenic environments, they are the predominant form of iron used for growth by microorganisms (*Lovley, 1991; Coleman et al, 1993; Coates et al, 1999; Saffarini et al, 2002)*. Amorphous Fe(III) (hydr)oxides have high surface areas and intrinsic reactivity. Specifically, ferrihydrite, an amorphous Fe(III) (hydr)oxide, was suggested to be an important environmental terminal electron acceptor for microbial respiration (*Hansel et al., 2003; 2005*). Reduction of small amounts of crystalline Fe(III) (hydr)oxides in the environment also has a significant influence on local inorganic geochemistry due to the release of soluble Fe^{2+}, phosphate, and trace minerals. These effects, the redox transition between Fe(II) to Fe(III), and the coupled abiotic-biotic iron reduction patterns have a significant role in environmental biogeochemistry both on modern and early Earth.

1.4.1 Discovery and History of Iron Reduction

It was proposed that the early Earth 3.8 Ga ago was hot and Fe(II) rich, and that Fe(III) and H_2 could have been generated photochemically thus providing energy sources for ancient life (*Gold, 1992*). Therefore, iron respiration may have been one of the earliest forms of microbial respiration (*Walker et al, 1984; Lovley, 2004*). While abiotic mechanisms of iron reduction likely predominate in the environment today, microbially mediated iron redox reactions are a significant subsurface process that occurs in anoxic environments (*Lovley et al, 1988*). Fe(III) respiration occurs in discrete clades of microorganisms in both bacteria and archaea (*Caccavo et al., 1996; Lonergan et al., 1996*; *Dobbin et al., 1996, 1999; Slobodkin et al., 1997; Vargas et al., 1998; Francis et al., 2000*), prompting the question of conservation of dissimilatory Fe(III) reduction mechanisms throughout microbial evolution. It was later shown that separate and distinct strategies are used by the mesophilic bacteria *Geobacter* and *Shewanella* in contrast with the hyperthermophilic archaeon *Pyrobaculum islandicum* (*Feinberg et al., 2008*). Therefore, it is unlikely that one specific mechanism was conserved across all iron-reducing microorganisms.

Microbial iron reduction was first observed in fermentative organisms and was thought to be used as a minor electron sink (*Runov et al., 1926; Roberts et al., 1947*). The first organisms that were proven to use dissimilatory iron reduction as energy and maintenance mechanisms were *Pseudomonas* (*Balashova et al., 1978*); *Geobacter metallireducens* GS-15, an obligate anaerobe isolated from anaerobic sediments in the Potomac River (*Lovley et al., 1987*); and

Shewanella oneidensis, a facultative anaerobe isolated from sediments in Oneida Lake, NY (*Myers and Nealson, 1988a*). These organisms use organic compounds as electron donors and reduce Fe(III) (hydr)oxide as a terminal electron acceptor *(Lovley, 1991; Nealson & Myers, 1990*). Dissimilatory iron reduction was later found to be a major respiratory pathway in many *Geobacter* and *Shewanella* species (*Gorby et al, 1991; Myers & Myers, 1994; Childers et al, 2002*).

In 1999, thermophilic and hyperthermophilic iron reducers were grown from a deep subsurface petroleum reservoir in Western Siberia. It was confirmed that the samples contained both bacteria and archaea through sequencing of 16S rRNA genes (*Slobodkin et al., 1999*). The first report of a hyperthermophilic, Fe(III) reducing isolate came in 2001 (*Slobodkin et al., 2001*). It reported that bacterial and archaeal hyperthermophilic iron reducers were enriched at hydrothermal vents at the 13°N East Pacific Rise vent field and that an archaeal species of *Thermococcus* was isolated that catalyzed the reaction. Fe(III) reducers from this environment utilized peptone, molecular hydrogen, and acetate as electron donors and produced a black magnetic end-product (*Slobodkin et al., 2001*). It was suggested that accumulation of magnetic iron oxides within the walls of black smokers may partly be due to microbial iron reduction processes occurring at high temperatures (*Slobodkin, unpublished*). The finding of hyperthermophilic iron reducers in hydrothermal vents suggests that these organisms are ecologically versatile, ubiquitous in nature, and potentially participate in significant organic carbon turnover. As a result of their probable relevance on local and global geochemistry and carbon fluxes, appreciation of the intricacies of how these organisms use an insoluble terminal electron acceptor is essential.

1.4.2 Mechanisms of Iron Reduction

1.4.2.1 Iron reduction in mesophiles

Many mesophilic bacteria reduce insoluble Fe(III) (hydr)oxides for energy and cell maintenance. The physiology of dissimilatory iron reduction has been studied primarily in two genera of mesophilic bacteria: *Geobacter* and *Shewanella*. In general, dissimilatory reduction of insoluble iron involves three known mechanisms: 1) direct cell contact with the iron, 2) secretion of iron chelators that solubilize the iron and return it to the cell for reduction without direct contact, and

3) the reduction and release of extracellular electron shuttles for iron reduction without direct contact (Fig. 1.6) (*Weber et al., 2006*). Proteins involved in iron reduction have been purified and characterized from *Geobacter* and *Shewanella* (e.g., *Seeliger et al, 1998*; *Gaspard et al, 1998*; *Magnuson et al, 2000*; *Leang et al, 2003*). Because *Geobacter* and *Shewanella* are both Gram-negative bacteria, they require a mechanism to deliver electrons across their periplasm to the outer cell wall membrane. In both organisms, this is done using polyheme *c*-type cytochromes (*Weber et al, 2006*). The outer cell wall membrane proteins and mechanisms for electron transfer from the cell to iron differ between these two organisms. *Shewanella* spp. use both a flavin as an extracellular electron shuttle (*von Canstein et al, 2008; Marsili et al, 2008*) and conductive pili to transfer electrons directly to insoluble iron (*Gorby et al., 2006*). *Geobacter* spp. need to be in direct contact with Fe(III) (hydr)oxide unless an exogenous electron shuttle is provided and transfer electrons by direct contact with the iron via conductive pili (*Reguera et al, 2005*).

1.4.2.2 Iron reduction in hyperthermophiles

Iron reduction has been studied in hyperthermophilic archaea and hyperthermophilic bacteria. The first two cultures of obligate iron-reducing hyperthermophiles were *Geoglobus ahangari* and *Geothermobacterium ferrireducens* from marine and terrestrial sites, respectively (*Kashefi et al., 2002a*; *2002b)*. The physiological mechanisms of iron reduction in hyperthermophilic archaea are unknown. *Pyrobaculum* species (i.e., *P. aerophilum, P. islandicum, P. arsenaticum, P. calidifontis*) all reduce Fe(III) (hydr)oxide (*Kashefi & Lovley, 2000; Feinberg et al., 2008*), but only one of them contains a polyheme *c*-type cytochrome suggesting that a mechanism other than those found in *Geobacter* and *Shewanella* are used (*Feinberg et al., 2008*).

1.5 Minerals

In naturally-occurring environments, a diverse array of minerals is present in varying abundances, types, and solubility levels. There are more than 3,000 known mineral species, each with its own distinctive chemical and physical properties, composition, and atomic structure. Some minerals are environmentally and industrially relevant as raw materials of nearly all types

of manufacturing. Many minerals participate in global carbon cycling and microbial respiration in the subsurface.

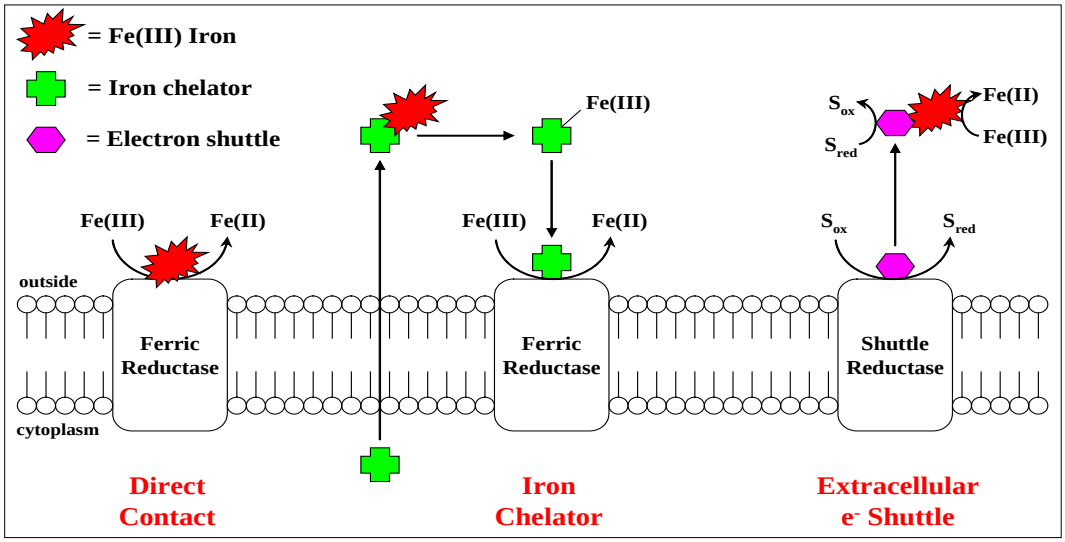

Figure 1.6 Dissimilatory iron reduction can occur through several mechanisms depicted above Direct contact occurs when the microbe requires a direct interface with the iron oxide mineral in order to transfer electrons from its terminal reductase to its terminal electron acceptor. A second mechanism is to produce a chelator that binds to the insoluble iron oxide mineral and brings it back to the terminal reductase to be reduced. The third mechanism is to produce an extracellular electron shuttle that gets secreted by the cell and reduces the iron oxide mineral while getting oxidized itself so that it can be recycled and reused.

Iron is of particular importance. It exists in a wide range of oxidation states, though Fe^{2+} and Fe^{3+} are the most commonly-occurring. Iron oxide minerals are fundamentally important in understanding the evolution of oxygen on the Earth's surface. The importance of biogeochemical cycling of Fe is well-recognized (*Van Cappellen et al., 1998*; *Johnson et al., 2000*) and microorganisms that utilize iron as an energy source are ubiquitous in nature and occur in environments such as anaerobic soil sediments (*Lovley et al., 1993*), deep-sea hydrothermal vents (*Ver Eecke et al., 2009*), freshwater and saltwater sediments (*Lovley et al., 2004*) and heavy metal contaminated sites (*Orellana et al., 2013*). Biogenically-formed minerals are paramount to our knowledge of biomarkers and few studies have analyzed these transformed minerals after dissimilatory iron reduction. The characteristics of bio-reduced mineral products and reactants have not been well-studied due to the high complexity of culturing dissimilatory iron reducers, the numerous forms of both Fe(III) oxide and Fe(II) oxide (some amorphous and x-ray amorphous), inaccessibility of instrumentation that can accurately identify distinctive iron types, and data that are hard to analyze. The impact and niche of this dissertation is the conjoined effort to study both the microbiology and the minerals involved in hyperthermophilic iron reduction in parallel. This section emphasizes the importance and bridges this interface.

1.5.1 Microbe-Mineral Interactions

Microbes in the biosphere have been shown to be active and influential in a multitude of geomicrobial processes in multiple environments: element bio-transformations (*Stolz et al., 2002*), biogeochemical cycling (*Nazaries et al., 2013*), metal and mineral transformations (*Purvis & Pawlik-Skowronska, 2008; Gilmour & Riedel, 2009; Uroz et al., 2009*) metal speciation, toxicity, mobility, mineral formation, dissolution and deterioration (*Gadd, 2004; 2008*), decomposition, bio-weathering (*Edwards et al., 2005*), and soil and sediment formation (*Huang et al., 2004*). It has also been shown that metals are involved in most aspects of microbial growth, metabolism and differentiation (*Gadd, 1992a*). The ubiquity of microbes found within these environments, and the significant effects of the microbes and minerals on each other, signify their mutual importance.

Most microbial studies have been done in uniform suspensions using liquid media, solid plates, and chemostats. More recent work has shown that a majority of microbial activity

involves interaction with solid surfaces. Their properties are different from those in liquid culture and are much more complex when in contact with solid surfaces (*Hamilton and Characklis, 1989*). Different mineral substrates produce variable growth rates, development of resistance to toxic metals and/or antibiotics, and changes in morphology and/or motility. In addition, some organisms use minerals as terminal electron acceptors for energy gain, and this is the focus of this dissertation. It has also been suggested that bacteria behave as geochemically reactive solids and that cell wall reactivity differs with varying conditions (*Ferris et al., 1986; 1987*). The field of geomicrobiology has grown dramatically and multiple studies looked at microbe-mineral interactions, as elucidated on below.

1.5.2 Abiotic vs. Biotic Iron Transformation Processes and Products

Ferrihydrite is the most bio-available form of Fe(III) oxide and the primary terminal electron acceptor used by iron reducers. Ferrihydrite is a reactive, poorly crystalline Fe(III) oxide that has high solubility, redox potential, and surface area relative to other Fe(III) oxide minerals such as goethite and lepidocrocite (*Manceau and Combes, 1988*; *Cornell and Schwertmann, 2003*). Mineral transformations and products from ferrihydrite differ from abiotic to biotic processes and upon generation of Fe(II) after microbial respiration, aging and stabilization of the terminal electron acceptor: reactive ferrihydrite, accelerates, and secondary mineral transformations develop that affect biogeochemical cycles of Fe as well as other minerals (*Fredrickson et al., 1998, Hansel et al., 2003*). During dissimilatory iron reduction, secondary mineralization of ferrihydrite was shown to occur via a coupled biotic-abiotic pathway that resulted in magnetite and goethite production *(Hansel et al., 2003*; *2005*). These coupled biotic-abiotic processes, rates, constraints and products, depend on the Fe (II) concentrations in the environmental milieu and on the mineral itself. Understanding these coupled processes separately and together, from both the microbial and mineral standpoint, is crucial to the development of a microbe-mineral interface model.

1.5.3 Iron Oxide Identification Techniques

In order to understand these coupled processes, highly sensitive and accurate methods of identifying different types of iron oxides must be developed. Numerous techniques are used in the identification of iron oxides, some more common than others. Historically, electron microprobe and XRD have been used the most due to high accessibility, easy sample manipulation and interpretation, and an in-depth body of data. Several alternative methods and instruments have been developed that provide higher accuracy and sensitivity to iron oxide identification, specifically, but it must be stated that these methods and instruments must be used in unison to provide a complementary and full bodied study. One of these alternative methods, Mössbauer spectroscopy, can identify iron compounds based on valence state and their magnetic properties (*Bancroft 1973*; *Dyar et al., 2006*). This has been used to identify multiple iron oxides in a wide variety of samples (*Murad & Johnston, 1988; Jumpertz et al., 1993*). It can also determine the composition and abundance of iron-bearing minerals, such as those found at hydrothermal vent sites that are often difficult to identify. Several other instruments include synchrotron spectroscopy, visible/near-infrared spectroscopy (VNIR), Fourier transform infrared spectroscopy (FTIR), thermal emission spectroscopy (TES), and microscopy techniques such as scanning electron microscopy (SEM) and transmission electron microscopy (TEM). These all provide valuable pieces of information that need to be used to build a complete identification. Successful identification of biotic vs. abiotic iron oxides will aid in the development of microbe-mineral models and biosignatures.

1.5.4 Significance

Microbial interaction with minerals in both synthetic and natural environments has long been known. Microbial biomineralization, in which microbial activity influences the transformation of mineral substrates, has become an important area of research in multiple fields: microbiology, geology, astrobiology, mineralogy, geochemistry, etc. Microbes influence the formation and degradation of minerals; mineral reduction (*Lovley et al., 2000*), biosorption (*Beveridge and Murray, 1976*), production and excretion of metabolite(s) and many more. The resultant biominerals are of particular interest to this research. The nature of these biominerals depends on a number of factors such as the nature of cell surfaces, cellular micro-environments, and the presence of reactive anions (sulfides, phosphates, etc.). These bio-minerals may undergo

further crystal structure changes that may aid in the deposition of solid phase minerals over geological time scales (*Beveridge et al., 1983*). One suite of processes that contributes significantly to biomineralization is the oxidation/reduction of iron oxides in anoxic environments. The formation of sedimentary iron deposits, magnetite, siderite, etc., have all been attributed to microbial influence: precipitation and deposition of Fe(III) oxides and hydroxides by both enzymatic, e.g. *Gallionella* sp., and non-enzymatic processes, e.g. *Leptothrix* sp. (*Ehrlich & Newman, 2009*) is one example. These processes and their resultant biominerals have relevance to both environmental and application-based processes. Some of these include biocorrosion of metals, bioleaching of metals from ores, bioweathering of rocks/minerals, bioremediation, and biosignature production. Respiration of minerals, in particular iron oxides, by microbes has been the subject of several studies with the focus being on biochemical pathways and not on the identification of mineral products. These mineral products are critical to the understanding of life on early Earth and extraterrestrial planets due to their potential use as biogenic markers. Biosignatures are not well-studied but greatly relevant to geomicrobiology and astrobiology. Detection and identification of specific minerals that accurately signify certain metabolisms is essential for the development of biosignatures in this field.

1.6 Astrobiological Implications

Astrobiology is an interdisciplinary field that is defined by NASA as the study of the origin, evolution, distribution, and future of life in the universe. This field also addresses the search for life, habitable environments, and detection of evidence for potential life and most relevant to this dissertation; biosignatures on Earth, extraterrestrial planets, and in the Solar System. The main goals of the NASA astrobiology program are to determine whether there is life beyond Earth and, if so, how it can be detected. Most ongoing studies target the search for water, chemical biosignatures, and biomarker gases in the atmosphere. Another topic of avid research has been the origination and initiation of extremophilic life under harsh, extraterrestrial conditions. These studies have been carried out using terrestrial extremophiles as analogs (*Olsson-Frances and Cockell, 2010*).

Life, which will be defined here as being able to undergo self-sustaining processes coupled with growth and adaptation, began on Earth approximately 3.5 Ga. All life on Earth is

made up of carbon, water, and heritable genetic information in the form of nucleic acids. The earliest evidence for life is in microbial mats that have been compressed into the sedimentary rock record (*Noffke et al., 2013*), representing what is possibly the last universal common ancestor (LUCA), or the most recent organism from whence all the organisms now living on Earth descended. This theory is based upon the idea that "all the organic beings which have ever lived on this earth have descended from some one primordial form, into which life was first breathed," as written by Charles Darwin in *On the Origin of Species* in 1859. This forms the deepest branch in Carl Woese's phylogenetic tree of life (Fig. 1.7) and is composed of hyperthermophilic microorganisms.

1.6.1 Last Universal Common Ancestor (LUCA)

It has been proposed that RNA was the first biological macromolecule to perform, pre-LUCA, the catalytic and information storage processes that are now done by proteins and DNA (*Benner and Ellington, 1991*). Cells then evolved the DNA, RNA, and proteins that are commonly found in all living organisms today and formed the LUCA. The history of life since the LUCA is primarily based on the phylogenetic tree of life drawn from sequence comparisons of the small ribonucleotide subunit of ribosomal RNA and shows three distinct branches: the Eukaryotes, the Archaea, and the Bacteria. However, the tree of life poses another question: what metabolism(s) was the LUCA able to use for energy generation? Based on whole genome sequences, the LUCA must have generated a proton motive force and used a membrane ATP synthase to produce ATP as energy since this protein is commonly found in all three domains of life (*Gogarten et al., 1989*; *Koch and Schmidt, 1991*). The LUCA might have possessed an electron transport chain to produce the proton motive force, and it has been suggested that nitrate, sulfate and sulfur respiratory chains were the metabolic energy chains. Further evidence from culture-based studies suggests that sulfur respiration and Fe(III) reduction are competitors for the first form of microbial respiration.

1.6.2 Biogenic Products as Biosignatures

Life and biosignatures are inextricably linked. Both are composed of substances that are identifiable and quantifiable. A biosignature is any substance produced by living organisms that provides scientific evidence of life and characterizes past or present life on Earth or on extraterrestrial planets. Several biosignatures have been used by various research groups to answer

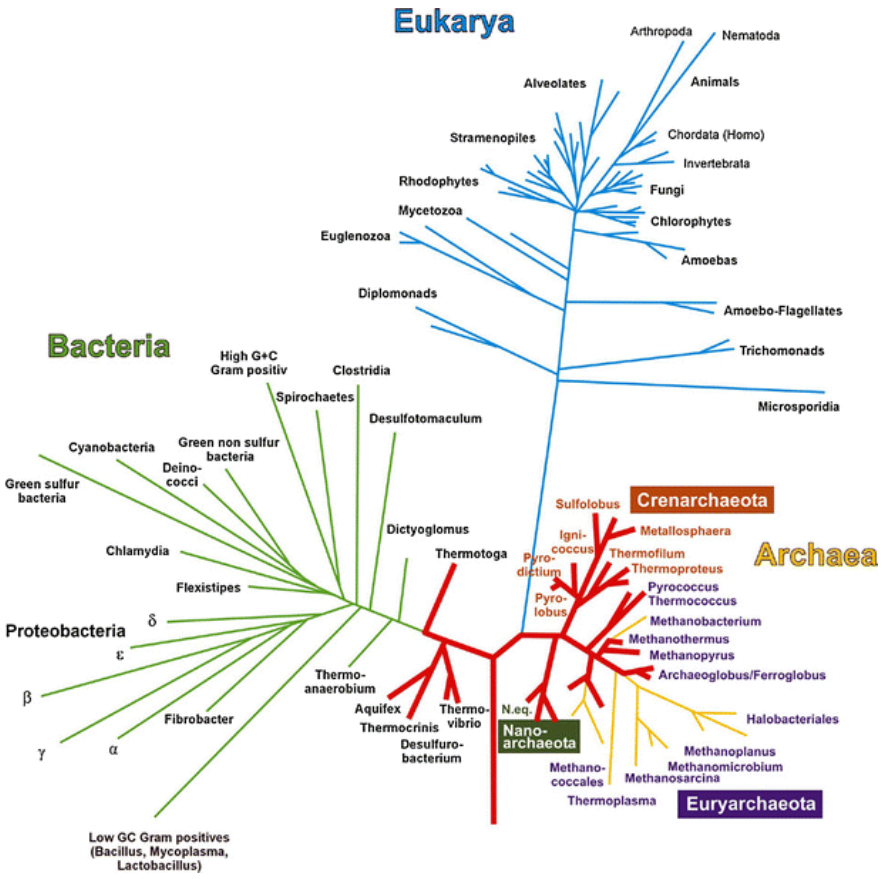

Figure 1.7 Phylogenetic tree of life including Eukaryotes, Bacteria and Archaea, with the deepest branches highlighted in red, indicating hyperthermophiles. This figure shows that LUCA was potentially a hyperthermophile.

questions about life throughout geologic time including physical biosignatures (coccoliths, diatoms, shells etc.), stromatolites, and fossils (micro and macro), isotopic composition of various compounds, inorganic isotopic compositions (e.g., sulfur and oxygen), fatty acid chains, mineral surface modifications, and minerals that have undergone direct or indirect biological transformations. Both crystalline and amorphous minerals have been found to be important as biosignatures and will be discussed below.

1.6.2.1 Biosignatures: Direct biological impacts on minerals

Microorganisms, capable of using minerals such as iron oxides may leave behind biotically altered minerals that have the potential to be biosignatures. A multitude of biotically-formed minerals have been observed due to direct cellular control by organisms that necessitate mineral precipitation as part of their life cycle (e.g., coccoliths, shells, etc.) (*de Vrind de Jong and de Vrind, 1997*). Direct interaction with minerals has also been shown through iron oxidizing microorganisms (FeOM) that produce a filamentous biomineral that is a potential biosignature (*Chan et al., 2011*). Magnetite produced by Fe(III)-reducing microorganisms also has the potential of being a biosignature (*Lovley et al., 1987*), and this reaction plays a significant role in this dissertation. It may be challenging, however, to distinguish between abiotic and biotic minerals.

1.6.2.2 Biosignature: Indirect biological impacts on minerals

Minerals associated with microorganisms can also be indirectly affected and leave behind a mineral biosignature. Some microbial metabolisms modify the redox state of aqueous ions in their local environments, and due to the production of either organic and/or inorganic complexes, may also impact their surroundings through a change in liquid and/or gas composition, pH, etc., that may induce changes in minerals. Microbial cell surface environments and by-products created by microbes may form biosignatures as mineral solubility changes and minerals precipitate (*Gadd, 2004*). Examples include mackinawite formation from corrosion of iron by sulfate-reducing bacteria (*Rickard, 1969*) and ferromagnetic greigite formation from bacteria (*McNeil, 1990*). Understanding transformations of minerals and microbial impact on these

processes requires in-depth knowledge of local environments and redox conditions that are important impacting factors.

1.6.3 Mars: Biosignatures

The study of biogenically-produced minerals as potential biosignatures has many applications, the most significant one being the ability to identify past or present life and/or potential for life's existence. The exploration and study of Mars started with telescopes and have extended to modern-day rovers on the Martian surface. Mars is the best candidate for the development of life beyond Earth in the Solar System. Early Mars and early Earth had similar physical and chemical surface properties (*McKay and Davis, 1991*). Hotspots for potential life on early Mars are similar to those on early Earth and include volcanic regions, areas of extreme UV radiation, and hydrothermal vents (*Rothschild, 1990*); environments where life has been found on Earth.

Impact hydrothermal systems on Mars form from impact cratering proximal to an aqueous environment and have been implicated as potential sites for life on early Mars. They could have been hydrothermally active anywhere from 8,000 to 4 billion years ago (*Pope et al., 2006*). Crystallization of carbonates and silicates within these systems, which can fossilize and preserve microbial life forms and their biosignatures, makes impact craters places where evidence of Martian life would likely be found (*Pope et al., 2006*). The surface of Mars has gone through many significant changes throughout geologic time. It initially had liquid water on its surface, a thick CO_2 atmosphere, and redox energy and other essential elements for life (*Olsson-Francis and Cockell, 2010*). Once Mars lost its protective atmosphere, atmospheric pressures and temperatures dropped and life may have retreated below the surface. Any evidence of such life forms would likely be found in rocks and polar ice caps on the Martian surface (*Pope et al., 2006*).

Of the 16,000 meteorite samples found on Earth, approximately 120 have been identified as Martian based on their elemental and isotopic compositions. One of these Martian meteorites, ALH84001, has distinctive properties. ALH84001 was formed when there was liquid water on the Martian surface and ejected from Mars approximately 16 Ma. It contains polycyclic aromatic hydrocarbons, magnetite, and small ovoid and tubular structures. It contains nanometer-size

magnetite (Fe_3O_4) crystals within carbonate globules that were suggested to be biotically formed (*Thomas-Keprta et al., 2000*; *2001*). Iron oxides with similar properties have only otherwise been found to be formed by magnetotactic bacteria. The full range of magnetites found within this Martian sample cannot be explained by any singular biotic or abiotic process. Suggested mechanisms for magnetite formation have included precipitation from hydrothermal fluid, decomposition of environmental minerals, and extracellular transformation by dissimilatory Fe-reducing prokaryotes. Reports on the ALH84001 sample have been controversial at best and a larger sample needs to be obtained and studied. Libraries of iron standards and biogenically transformed iron are also needed in order to accurately compare extraterrestrial samples. This dissertation has started to achieve this by demonstrating the significance of studying different types of hyperthermophilic iron reducers and their mineral products.

1.7 Summary and Research Approach

This dissertation explores the interactions and correlations between microbes and the minerals within their surrounding habitats. This dissertation also looks at habitability and microbial distribution patterns based on those interactions and correlations. This work aims to elucidate and classify abiotic vs. biotic processes that affect mineral patterns which in turn determine microbial community patterns, using specific organisms that metabolize certain minerals in a known environment: the Endeavour Segment of the Juan de Fuca Ridge. This research project began with sampling of three distinct hydrothermal chimney deposits for multiple analyses. The first set of analyses was done using mineral spectroscopic techniques to identify the minerals found within these hydrothermal chimneys. The second set of analyses determined the microbial community composition of each deposit using both molecular and culture-based techniques. Next, the growth characteristics of two novel hyperthermophilic iron reducers were characterized under varying conditions such as temperature, pH, and NaCl concentrations. Identification and classification of mineral starting and end products were performed from these cultures. The last portion of this dissertation taxonomically characterized these two hyperthermophilic iron reducers using phylogenetic and phenotypic traits and the complete genome sequence analysis of one of the strains.

Interdisciplinary studies like this one, are crucial to further understand and model environments such as deep-sea hydrothermal vents. In order to study microbial community patterns and metabolisms in hydrothermal systems, biogeochemical studies need to be carried in parallel. Compilation and interpretation of linked data sets will further develop models on the biogeochemistry and biosignatures within hydrothermal vent systems (Fig. 1.8).

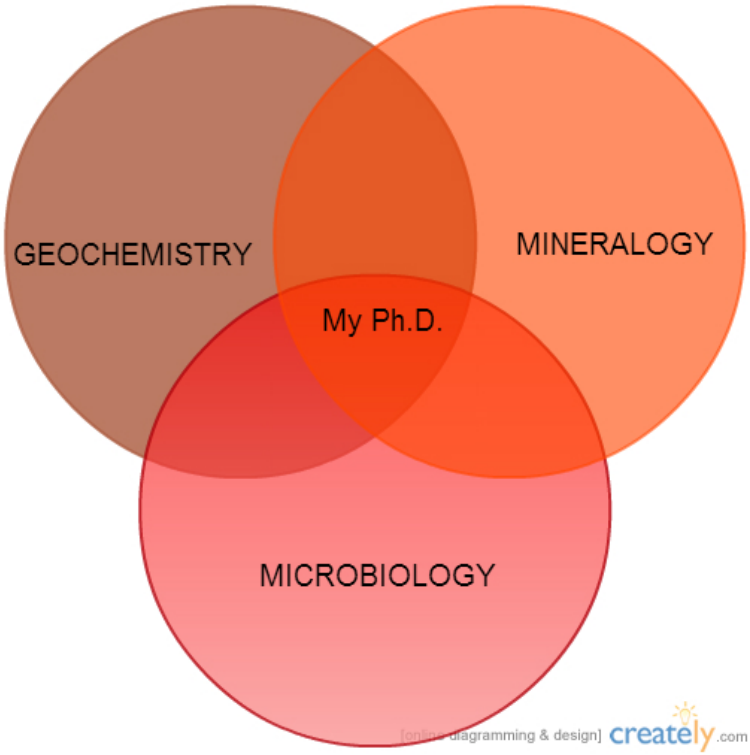

Figure 1.8. Interdisciplinary research will allow for compilation and interpretation of linked data sets that will further develop models on biogeochemistry and biosignatures within hydrothermal vents and beyond.

CHAPTER 2

MINERALOGICAL AND MICROBIAL DESCRIPTION OF THE INTERIOR HABITABLE ZONES OF THREE ACTIVE HYDROTHERMAL CHIMNEYS FROM THE ENDEAVOUR SEGMENT, JUAN DE FUCA RIDGE

2.1 Abstract

Three active hydrothermal chimneys and their associated high-temperature fluids were collected from the Endeavour Segment, Juan de Fuca Ridge to evaluate the linkages among mineralogy, fluid chemistry, and microbial community composition within the chimneys. To identify mineralogy, Mössbauer, mid-infrared thermal emission, and VNIR spectroscopies were used for the first time on vent chimneys, in addition to thin-section petrography, x-ray diffraction (XRD) and elemental analyses. A chimney from the Bastille edifice was rich in Fe-sulfide and composed primarily of chalcopyrite, marcasite, sphalerite, and pyrrhotite (i.e., type I chimney) while chimneys from the Dante and Hot Harold edifices were rich in anhydrite (type II-III chimneys). Bulk emissivity and reflectance spectroscopies corroborated petrography, XRD, and elemental analyses, demonstrating the potential of these techniques for future shipboard analysis. The microbial community within the Bastille chimney was most closely related to mesophilic and thermophilic anaerobes of the deltaproteobacteria, especially sulfate reducers, and anaerobic hyperthermophilic archaea. Microbes within the Dante and Hot Harold chimneys were most closely related to mesophilic and thermophilic aerobes of the beta-, gamma- and epsilonproteobacteria. Numerical modeling of energy availability from redox reactions in vent fluids suggests that aerobic oxidation of sulfide and methane should be the predominant autotrophic microbial metabolisms at 25°C and 55°C and that anaerobic oxidation of methane should prevail at 80°C. While the microbial community compositions of all three chimneys show aerobic sulfide-oxidizing epsilonproteobacteria, the predominance of mesophilic sulfate reducers in the Bastille chimney suggests that type I chimneys may promote anaerobic metabolisms.

2.2 Introduction

Hydrothermal vent fluids form as subseafloor seawater exchanges cations in reactions with hot rock, which results in the loss of some dissolved chemical components (O_2, Mg^{2+}, SO_4^{2-}) and gain in others (H_2, CH_4, CO_2, H_2S, reduced metals, SiO_2) (*Von Damm, 1995*). Deep-sea hydrothermal chimneys form on the seafloor when metal sulfides and silicates precipitate out of the vent fluid upon cooling, accompanied by precipitation of sulfate minerals out of heated seawater (*Goldfarb et al., 1983*; *Haymon, 1983*). Newly-formed chimneys are often porous and permit the exchange of hydrothermal fluid and seawater in their interiors, creating temperature and chemical gradients between the hot hydrothermal fluids emitted from the interior and the cool surrounding seawater (*Tivey and Singh, 1997*). The resulting chemical disequilibria between the reduced chemical species in the hydrothermal fluid and the relatively oxidized surrounding environment are slowly driven back to equilibrium through abiotic redox reactions. Microbes living within and on the exterior of hydrothermal chimneys accelerate these reactions and capture the energy released for their growth (*McCollom and Shock, 1997*; *Tivey, 2004*). This paper examines the inter-relationships among the varying mineral assemblages, hydrothermal fluids, and microbial communities within chimneys.

Hydrothermal venting along the Endeavour Segment of the Juan de Fuca Ridge in the northeastern Pacific Ocean results in the formation of massive metal sulfide-sulfate-silica deposits up to 45 m tall and 50 m wide (*Delaney et al., 1992*; *Robigou et al., 1993*; *Kelley et al., 2001*; *2012*). In general, the venting chimneys are highly porous and composed primarily of Fe-bearing sulfide minerals. A typical cross-section through a chimney contains a 2-5 cm thick sulfide zone near the outer margin with abundant late stage amorphous silica, and an anastomosing, discontinuous network of tortuous channels through a sponge-like matrix of amorphous silica, sulfide, sulfate, and clay minerals resulting from seawater ingress, outflow of warm fluids and conductive cooling (*Tivey and Delaney, 1985*; *1986*; *Kristall et al., 2006*). Hydrothermal fluids at the Endeavour Segment are ammonia-rich (0.64-0.95 mM), causing higher than normal pH of the fluid due to ammonia-ammonium buffering (*Lilley et al., 1993*; *Butterfield et al., 1994*). As a result, deposition of sulfide minerals, amorphous silica, and clay minerals is enhanced, leading to the formation of large edifices (*Tivey and Delaney, 1986*; *Tivey et al., 1999*; *Kristall et al., 2006*).

Studies that relate the mineralogy of hydrothermal chimneys to their endemic microbial community compositions are limited for Endeavour (*Schrenk et al., 2003*; *Zhou et al., 2009*) and elsewhere (e.g., *Takai et al., 2001*; *Kormas et al., 2006*; *Pagé et al., 2008*; *Olins et al., 2013*). Generally, they show that the cooler exterior regions of hydrothermal deposits contain a mix of bacteria and archaea with a shift to predominantly archaea towards the hotter interior regions of the deposits (*Hedrick et al., 1992*; *Schrenk et al., 2003*; *Pagé et al., 2008*). The archaea in these hotter regions are primarily hyperthermophiles (i.e., organisms with optimal growth above 80°C) typically belonging to the Thermococcales, Desulfurococcales, Methanococcales and Archaeoglobales (*Takai et al., 2001*; *Schrenk et al., 2003*; *Kormas et al., 2006*; *Pagé et al., 2008*; *Zhou et al., 2009*). Epsilonproteobacteria, usually related to autotrophic sulfur oxidizers, are ubiquitous in cooler regions (*Kormas et al., 2006*; *Zhou et al., 2009*; *Olins et al., 2013*). Attachment to mineral grains via biofilms is observed for all types of cells (*Schrenk et al., 2003*). These microbes are found in hydrothermal deposits that range from mostly metal sulfides and silicates (*Schrenk et al., 2003*; *Kormas et al., 2006*; *Zhou et al., 2009*) to predominantly anhydrite ($CaSO_4$) (*Pagé et al., 2008*; *Olin et al., 2013*).

In this study, three diverse and actively venting hydrothermal chimneys and their associated fluids were sampled in 2008 from the Endeavour Segment. One chimney was composed predominantly of Fe-sulfides and formed from the rapid focused discharge of high temperature fluids (i.e., type I, [*Koski et al., 1994*]). The second was a bulbous "beehive" chimney produced from unfocused and sluggish discharge of high-temperature fluid mixed with local seawater (type II-III). The third was from a "candelabra" proto-chimney formed atop a vigorously venting high-temperature edifice (type II-III). The goal was to use mineral spectroscopic techniques (Mössbauer, thermal emission, visible-near infrared, or VNIR) for the first time to characterize the mineralogy of the interior of these chimneys in tandem with more common techniques for hydrothermal chimney characterization (thin-section petrography, elemental analyses, x-ray diffraction). Emphasis was placed on characterizing the soft, porous course-grain material in the interior of these chimneys, which was previously shown to be a source of anaerobic, hyperthermophilic microorganisms for culturing (*Ver Eecke et al., 2009*; *2012*). The microbiology of this interior mineral matrix was determined through molecular analysis of the 16S rRNA genes present, culture-dependent abundance analysis for various metabolic types of hyperthermophiles, and numerical modeling of Gibbs energies for various

redox reactions at different mixing ratios of hydrothermal fluids and seawater. The goal of this study was to improve our understanding of the mineral and microbial nature of the habitable zone within active hydrothermal mineral deposits and the possible relationships among minerals, hydrothermal fluids and microbes.

2.3 Geologic Setting

The Juan de Fuca Ridge is an intermediate spreading rate mid-ocean ridge that strikes 020° and forms the boundary between the Pacific and Juan de Fuca tectonic plates in the northeastern Pacific Ocean. The Endeavour Segment is a 90 km segment near the northern end of the ridge. Its most prominent feature is an axial valley 500-1,000 m wide with walls up to 200 m in height and water depths of 2,050 mbsl in its center and a maximum depth of >2,700 mbsl to the north and south of the central high (*Delaney et al., 1992*; *Kelley et al., 2012*). Within the central 15 km of the axial valley are five major active high-temperature hydrothermal fields that are 2-3 km apart and host a myriad of focused- and diffuse-flow vent sites (*Kelley et al., 2012*), and are underlain by a series of discontinuous seismic reflectors 2.2-3.3 km below the seafloor (*Van Ark et al., 2007*; *Carbotte et al., 2012*). Based on the absence of recent lava flows, the segment currently appears to be largely in a period of fault-controlled extension (*Riddihough, 1984*; *Goldstein et al., 1991*; *Volpe and Goldstein, 1993*; *Johnson et al., 2000*; *Proskurowski et al., 2004*). However, seismic swarms within the axial valley in 1999-2000, 2003-2004, and 2005 were attributed to shallow diking events that altered hydrothermal vent fluid temperatures, fluxes, and chemistries, suggesting that some volcanic influences remain at the segment (*Davis et al., 2001*; *Lilley et al., 2003*; *Seyfried et al., 2003*; *Bohnenstiehl et al., 2004*; *Wilcock et al., 2009*; *Hooft et al., 2010*).

There are over 800 individual active or extinct hydrothermal chimneys within the central 15 km portion of the Endeavour Segment (*Clague et al., 2008*). Most of the active chimneys are located within the five major hydrothermal fields named (from north to south) Sasquatch, Salty Dawg, High Rise, Main Endeavour and Mothra. Hydrothermal venting has been ongoing at Sasquatch, High Rise, and Main Endeavour for at least 1,450, 850, and 2,300 years, respectively, based on ^{226}Ra/Ba dating of hydrothermal barite (*Jamieson et al., 2013*). Focused, high-temperature venting in the High Rise, Main Endeavour, and Mothra vent fields typically

originates from several point sources on large, steep-sided hydrothermal edifices. These sources flow from chimneys primarily on the top of the edifices and from horizontal outcrops called 'flanges' that pool high temperature hydrothermal fluids beneath them that spills upwards around their edges (*Delaney et al., 1992*; *Robigou et al., 1993*; *Kelley et al., 2001*).

2.4 Materials and Methods

2.4.1 Sample Collection

Actively venting hydrothermal chimneys and their hydrothermal fluids were sampled in August and September of 2008 using the deep-sea research submersible *Alvin*, operating from the R/V *Atlantis*. Samples were collected from the Bastille and Dante edifices in the Main Endeavour Field at depths of 2,193 and 2,186 mbsl, respectively; and from the Hot Harold edifice in the Faulty Towers hydrothermal complex in the Mothra Field at a depth of 2,271 mbsl, approximately 2 km south of the Main Endeavour Field. At each sampling site, the hydrothermal edifices were surveyed for actively-venting hydrothermal chimneys that were ~0.5 m tall and could be readily recovered by *Alvin* to bring back to the surface. When a suitable chimney was found, photographs were taken of the undisturbed chimneys on the seafloor. The maximum temperature of the exiting hydrothermal fluid was measured using the submersible's high temperature probe, either prior to or after removal of the chimneys. The maximum temperatures of the fluids emitted by the chimneys at Bastille, Dante, and Hot Harold were 282°C, 300°C, and 321°C, respectively. The chimneys were broken off near their bases using the submersible's manipulator arms and placed into PVC boxes with sealable lids in the front basket of the submersible to minimize damage to the chimney during surface recovery. Hydrothermal fluids were collected from the orifices left after the chimneys were recovered using titanium syringe major samplers, the Hydrothermal Fluid and Particle Sampler (HFPS), and titanium gas-tight syringes.

Once shipboard, the recovered chimneys were photographed as multiple fragments of the original chimney. Larger fragments were selected and cracked open using a hammer and chisel and by pulling the pieces apart without direct contact with the interior. The mineralogy of the interior and exterior regions of the chimneys was described visually with the aid of a hand lens. Once exposed, 35-50 g of the soft and porous minerals found in the interior of the chimneys

between the central chalcopyrite-lined fluid conduit (if present) and the harder exterior of the chimney were removed using a sterile scupola and placed into sterile plastic dishes. This material was mixed by hand and divided into three portions. The first (10-15 g) was added to sterile, anoxic artificial seawater, sealed in a serum bottle with a rubber stopper, flushed with N_2 gas, and reduced with 0.025% (w/v) each of cysteine-HCl and $Na_2S•9H_2O$ as previously described (*Ver Eecke et al., 2009*; *2012*). This was used to inoculate media for the growth of thermophilic and hyperthermophilic anaerobic microorganisms (see Section 2.4.5). The second portion (15-20 g) was placed into a sterile 50 ml Falcon tube and frozen immediately at -80°C for land-based DNA extractions (see Section 2.4.5). The third portion (10-15 g) was air dried and used for mineral spectroscopy analyses (see Section 2.4.2). Representative whole samples (i.e., those with intact interiors) were set aside for bulk sample geochemical analyses (see Section 2.4.3). These samples were soaked in fresh water overnight, then air dried for at least 24 h. Biological material was removed from the solid exterior of the samples before transport to the University of Ottawa in sealed plastic sample bags. Due to the high porosity of the samples (up to 70%), the samples were further dried in a 30°C oven for up to three weeks to remove any remaining moisture.

2.4.2 Spectroscopy

Mössbauer spectra were acquired on the dried chimney samples at temperatures ranging from 4-295 K using a source of ~40 mCi ^{57}Co in Rh on a WEB Research Co. model WT302 spectrometer equipped with a Janis closed cycle He cooling system at Mount Holyoke College. For each sample, about 80 mg were diluted with sucrose and deposited without packing into a holder backed by Kapton® polyimide film tape. Data were collected over a ± 4 mm/s (for spectra containing only doublets) or ± 10 mm/s (for spectra containing sextets) velocity range in 2048 channels with acquisition times ranging from 12 hours to 6 days depending on the Fe content of the samples. Spectra were corrected for nonlinearity via interpolation to a linear velocity scale, which is defined by the spectrum of the 25-μm Fe foil used for calibration. All data were corrected to remove the fraction of the baseline due to the Compton scattering of 122 keV gamma rays by electrons inside the detector. All Mössbauer data were posted for public use (www.mtholyoke.edu/courses/mdyar/database/).

Mid-infrared thermal emissivity spectra were acquired using a Nicolet Nexus 670 FTIR interferometric spectrometer at the Arizona State University Mars Space Flight Facility. The spectrometer has been modified for emission measurements by removal of the SiC source and placement of an enclosed glove box and folding mirrors outside the spectrometer housing to enable the energy from a heated sample in a sample chamber within the glove box to enter into the ray path for measurement. The chamber is water cooled to maintain the environmental temperature. The atmosphere is scrubbed of CO_2 and H_2O to eliminate those spectral lines from the sample data. The spectrometer is equipped with a thermoelectrically stabilized deuterated triglycine sulfate detector and a CsI beamsplitter that allows quality measurement of emitted radiation over the mid-infrared range of 2,000 to 240 cm^{-1} (5 to 42 μm) (e.g., *Ruff et al., 1997*). For each measurement, the sample was placed in a copper sample cup, painted with Aeroglaze® Z302 gloss black paint, and heated to and maintained at an 80°C set-point for the duration of the measurements. The 160 scans of each sample were acquired at ~4-cm^{-1} spectral resolution (~2-cm^{-1} spectral sampling) and the individual-scan spectra were averaged together. This resulting sample radiance spectrum was calibrated according to the procedure discussed in detail in *Ruff et al.* (1997) and converted to spectral emissivity. No additional spectral filtering was performed.

Reflectance spectra were measured for particulate samples in a horizontal sample dish using a bi-directional visible/near-infrared spectrometer and a Nicolet FTIR spectrometer at Brown University's RELAB as in past studies (*Bishop et al., 2008*). Spectra were measured relative to Halon from 0.3 to 2.5 μm under ambient conditions with 5 nm spectral sampling (e.g., *Pieters, 1983*). Infrared reflectance spectra were measured relative to a rough gold surface in a biconical configuration with 2 cm^{-1} spectral sampling from 1-50 μm in an environment purged of H_2O and CO_2 for 10-12 h. Composite, absolute reflectance spectra were prepared by scaling the FTIR data to the bidirectional data near 1.0 μm.

For x-ray diffraction (XRD) analysis, each sample was pulverized and a portion of the powder was mounted onto a standard holder. XRD analysis was performed by Activation Laboratories Ltd. (www.actlabs.com, Ancaster, Ontario, Canada) on a Panalytical X'Pert Pro diffractometer, equipped with a Cu x-ray source and an X'Celerator detector, operating at the following conditions: 40 kV and 40 mA; range 4.5-80 deg 2θ; step size 0.017 deg 2θ; time step 50.165 sec; fixed divergence slit, angle 0.25 deg; sample rotation: 1 rev/sec.

2.4.3 Petrography and Elemental Analyses

For the Bastille and Dante chimney samples, two thin sections (30 µm thickness) were cut from each whole sample for petrographic analysis. No thin section was cut from the Hot Harold chimney due to the small size of the sample. For the Bastille and Dante chimneys, each section was cut perpendicular to the long axis (and primary flow direction) of the chimney structure to maximize cross-sectional coverage from the outer wall toward the inner conduit zone. Sections were cut such that one section would be representative of the inner zone and the other would be representative of the outer zone. Due to the high porosity and fragility of the chimneys, samples were impregnated with epoxy prior to being cut with a rock saw. Cutting and grinding the soft interior mineral material was unsuccessful due to its high porosity. The sections were examined using an Olympus BX 51 polarizing microscope with an attached Olympus DP71 digital camera. Sections were observed under both transmitted and reflected light modes to observe sulfates and amorphous silica and the opaque minerals (sulfides), respectively.

Representative subsamples of each chimney were broken off and ground to powders (< 100 µm) with a swing mill for major element analysis. For each chimney, three samples were prepared for geochemical analysis: the soft porous interior material, material from the outer wall, and a representative whole rock sample. The Hot Harold chimney fragment was too small for an outer wall subsample; therefore, only interior and whole rock samples were analyzed. Elemental concentrations were determined by a combination of fusion inductively-coupled plasma mass spectrometry and neutron activation analysis at Activation Laboratories Ltd., in Ontario. Analytical uncertainties were determined from repeat analyses of laboratory standard materials. The results and analytical uncertainties are reported in concentrations of elemental and oxide weight percent (wt. %).

2.4.4 Fluid Chemistry and Redox Energy Estimates

For end-member hydrothermal fluid sampling, duplicate titanium major fluid samplers and gas-tight fluid samplers were used to collect fluids from Bastille. The Hydrothermal Fluid and Particle Sampler (HFPS) was used to collect duplicate fluids from Dante and Hot Harold. The HFPS pumped vent fluid at its maximum stable temperature through a titanium nozzle that

measured the temperature of the fluid at 1 Hz just inside the nozzle tip. HFPS fluid sample containers were either collapsible Tedlar plastic bags with valves within rigid housings, PVC piston samplers, or titanium piston samplers. All samplers have check valves to prevent the samples from leaking out or being drawn out of the containers. Sample valves were closed up on arrival on deck, and samples were stored under refrigeration until processed. Fluid samples were analyzed on board ship for pH, alkalinity, hydrogen sulfide, dissolved silica, and ammonia. Subsamples were taken directly from the collapsible bags into syringes without exposure to air for shipboard analysis of methane and hydrogen by gas chromatography. If a gas headspace was present, then the gas phase and liquid phase volume were measured, and both phases were sampled and analyzed by gas chromatography. Piston samples intended primarily for gas analyses were extracted on the same shipboard gas extraction line used for titanium gas-tight samplers, and the gases sealed for later analysis. The extraction water (acidified with sulfamic acid) was analyzed for major elements on shore. Major, minor, and trace elements in the hydrothermal fluids were analyzed at the Pacific Marine Environmental Laboratory and the University of Washington. Analytical methods for major and minor elements are described in *Butterfield et al.* (1997).

Six redox reactions were considered for microbial energy availability estimates. Three of them represent aerobic respiration of inorganic electron donors (sulfide oxidation, methane oxidation, hydrogen oxidation), and three others represent anaerobic respiration of inorganic electron donors (methanogenesis, sulfate reduction, anaerobic oxidation of methane) as previously described (*Amend et al., 2011*). The compositions of the mixed hydrothermal solutions were calculated from those of the end-member vent fluids and seawater using the REACT module in the computer code Geochemist's Workbench^{TM} as previously described (*Jin and Bethke, 2005*; *Amend et al., 2011*). All minerals were allowed to precipitate during mixing except quartz, tridymite, cristobalite, chalcedony, and hematite (*Jin and Bethke, 2005*). HS^-, $CH_{4(aq)}$, $H_{2(aq)}$ and NH_4^+ were decoupled from redox reactions, but all other redox reactions were allowed. Mineral precipitations at temperatures ranging from 8°C to 300°C were predicted from the output of the mixing model. Values of Gibbs energy (ΔG_r) for the catabolic reactions were computed using the activities of relevant species as previously described (*Amend et al., 2011*). The amount of energy available (J) from catabolic reactions at mesophilic (25°C), thermophilic (55°C), and hyperthermophilic (80°C) temperatures in a kg of mixed fluid was calculated by

multiplying the calculated Gibbs energy for the reaction at each temperature by the concentration of reactants in the mixed fluid (*Amend et al., 2011*). These took into account the stoichiometry of the reaction and the reactant that is in limiting supply.

2.4.5 Microbiology

DNA was extracted from the soft porous interior material from each chimney that had been frozen on the ship. The extraction was based on a CTAB extraction protocol (*Huber et al., 2003*). Approximately 1 g of chimney material was transferred into microfuge tubes and mixed with 0.5 ml of buffer that consisted of 200 mM NaCl, 200 mM Tris-HCl, 2 mM sodium citrate, 10 mM $CaCl_2$ and 50 mM EDTA (pH 8.0). Then 20 µl of 10% sodium pyrophosphate, 30 µl of lysozyme (100 mg/ml), and 20 µl of Poly A (10 mg/ml) were added to the suspension, and the sample was incubated at 37°C for 40 min. Next, 10 µl of 20% sodium dodecylsulfate (SDS) and 60 µl of proteinase K (20 mg/ml) were added and the sample was incubated at 50°C for 30 min. Following this, 80 µl of 5 M NaCl and 80 µl of 10% cetyltrimethyl ammonium bromide (CTAB) in 0.7 M NaCl were added. The sample was mixed well and incubated at 50°C for 30 min. Glass beads (0.1 mm diameter) were added to the tube and the sample was shaken in a Beadbeater shaker for 20 sec. The sample was mixed with 500 µl of phenol:chloroform:isoamyl alcohol (25:24:1) and spun in a centrifuge at 12,000 × *g* and 4°C for 20 min. The supernatant was then decanted into a clean microfuge tube. The previous step was repeated 1-2 times. Because of low DNA yields, the Dante and Hot Harold samples were transferred to dialysis tubing and suspended in TE buffer (10 mM Tris and 1 mM EDTA, pH 8.0) overnight at 4°C. The DNA was precipitated overnight by adding an equal volume of isopropanol and 0.1 volumes of 3 M sodium acetate. The samples were spun at 12,000 × *g* at 4°C for 20 min, the pellet was washed with 70% ethanol, and the dry pellet was re-suspended in TE buffer.

Polymerase chain reaction was performed to amplify a fragment of the 16S rRNA genes present in these samples with universal bacteria specific primers 27Fb (5′-AGA GTT TGA TCM TGG CTC AG-3′) and 1492Rb (5′-RGY TAC CTT GTT ACG ACT T-3′), and universal archaea specific primers 21Fa (5′-TTC CGG TTG ATC CYG CCG GA-3′) and 958Ra (5′-YCC GGC GTT GAM TCC AAT T-3′). Each PCR reaction contained 7 µl of ddH_2O, 2.5 µl of 20% acetamide, 12.5 µl of GoTaq Green mastermix (Promega), 0.25 µl of each primer, and 2.5 µl of

DNA (undiluted, 1/10 dilution, or 1/100 dilution from the extracted DNA). The DNA was amplified using the following program: 2 min at 94°C, followed by 30 cycles of 94°C for 50 sec, 55°C for 45 sec, and 72°C for 2 min with a final incubation at 72°C for 10 min. The PCR products were visualized on a 1% agarose gel that had been stained with ethidium bromide. Amplification products were reconditioned to minimize heteroduplexes (*Thompson et al., 2002*). Cloning was performed with a TOPO-TA cloning kit (Invitrogen) according to the manufacturer's instructions. Clones were chosen for sequencing by amplification with M13 primers as described previously (*Huber et al., 2003*) and sequenced with 519Rb (5′-GWA TTA CCG CGG CKG CTG-3′) for bacteria and 515Ra (5′-TTA CCG CGG CKG CTG RCA C-3′) for archaea.

For phylogenetic analyses, bacterial and archaeal 16S rRNA gene nucleotide sequences were aligned using ClustalX2 (*Larkin et al., 2007*) and the Greengenes reference alignment files in Mothur phylogenetic software (*Schloss et al., 2009*). Clones were checked for chimeric sequences using both the Bellerophon server (*De Santis et al., 2006*) and UChime (*Edgar et al., 2011*) within Mothur and Qiime (*Caporaso et al., 2010*). Operational taxonomic units (OTUs) were then built (*Edgar, 2010*) using a cutoff of 97% to reference sequences; both closed and open reference databases were used and the latter was chosen as the standard in Qiime. Taxonomies were assigned based on the Greengenes taxonomy and a Greengenes reference database (*McDonald et al., 2012*; *Werner et al., 2013*) and the RDP Classifier 2.2 (*Wang et al., 2007*).

Relative abundances of culturable hyperthermophilic iron reducers, methanogens and heterotrophic sulfur reducers were estimated using three-tube most-probable-number (MPN) estimates. In triplicate, 3.33 ml, 0.33 ml, and 0.03 ml of each anoxic mineral slurry were used to inoculate each media type as previously described (*Ver Eecke et al., 2009*; *2012*). After inoculation, the tubes were incubated at 85°C for up to 7 d. Growth in the tubes was confirmed by the observation of cells using phase-contrast microscopy, and the detection of CH_4 and H_2 in the head-space using gas chromatography for methanogens and heterotrophs, respectively. Elevated Fe^{2+} was quantified using a ferrozine spectrophotometric assay (*Phillips and Lovley, 1987*) to analyze ferromagnetic iron in the medium for iron reducers. The methanogen and heterotroph results were reported previously (*Ver Eecke et al., 2012*).

2.5 Results and Discussion

2.5.1 Sample Descriptions and Compositions

The Bastille sample, collected from the top of the Bastille edifice, is an active black smoker chimney (Fig. 2.1a) venting fluid from a central longitudinal fluid conduit. The recovered sample was heavily colonized by *Ridgeia* tubeworms, *Paralvinella* polychaete worms, and scale worms (Fig. 2.1d). Its interior consists of loosely-consolidated porous sulfide material and numerous interior fluid conduits with varying diameters (<5 cm) that are often lined with a ~1 mm thick rind of euhedral chalcopyrite (Fig. 2.1d). The presence of chalcopyrite indicates that the fluids flowing through the conduit were high-temperature (>300°C) and that limited mixing with local seawater had taken place prior to venting. Some conduits are also lined with a very thin (<2 mm) secondary rind of sphalerite or marcasite (Fig. 2.2a), which may indicate a decrease in venting temperature through mixing either within the chimney or in the subsurface. The highly porous interior "mush" consists of a mixture of pyrite, marcasite, chalcopyrite and sphalerite (Fig. 2.2b). The smaller crystals and complex overgrowth patterns of the sulfide minerals suggest a complex growth history controlled by variations in fluid chemistry, flux and mixing, relative to the coarser fluid conduit linings. Fluid temperatures in this zone were likely lower than those in the central, chalcopyrite-lined conduit due to mixing with local seawater and conductive cooling through the chimney walls. The exterior walls of the sample consist of a grey matrix of marcasite/pyrite, sphalerite, and silica, with minor chalcopyrite (Fig. 2.2c). The sphalerite appears to be the latest sulfide phase to precipitate in the outer wall. Late-stage, lower-temperature barite is common within outer wall pore spaces (Fig. 2.2d). The porosity of the outer wall is significantly lower than in the interior due to the higher abundance of amorphous silica that commonly coats all exposed mineral surfaces (Fig. 2.2d and e). The exterior of the chimney is coated in 5 mm of biogenic marcasite crust with minor white bacterial coating and minor red

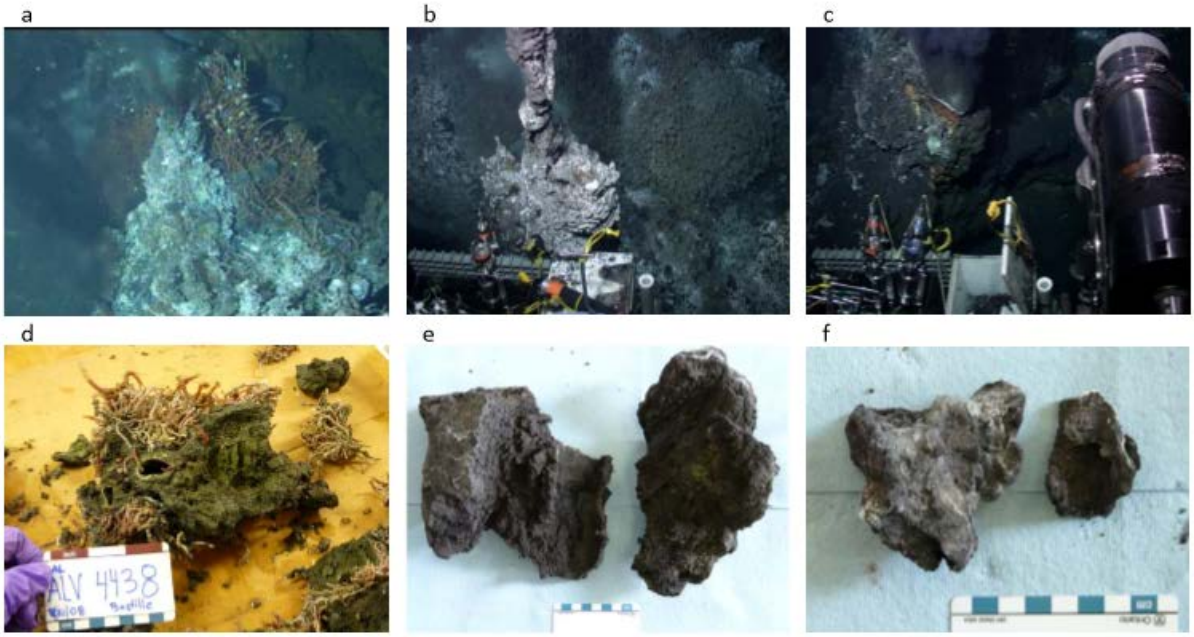

Figure 2.1. Actively venting hydrothermal chimneys as seen on the seafloor prior to collection: (a) Bastille (top left), (b) Dante and (c) Hot Harold. The hydrothermal chimney fragments as seen on board ship prior to subsampling: (d) Bastille, (e) Dante and (f) Hot Harold.

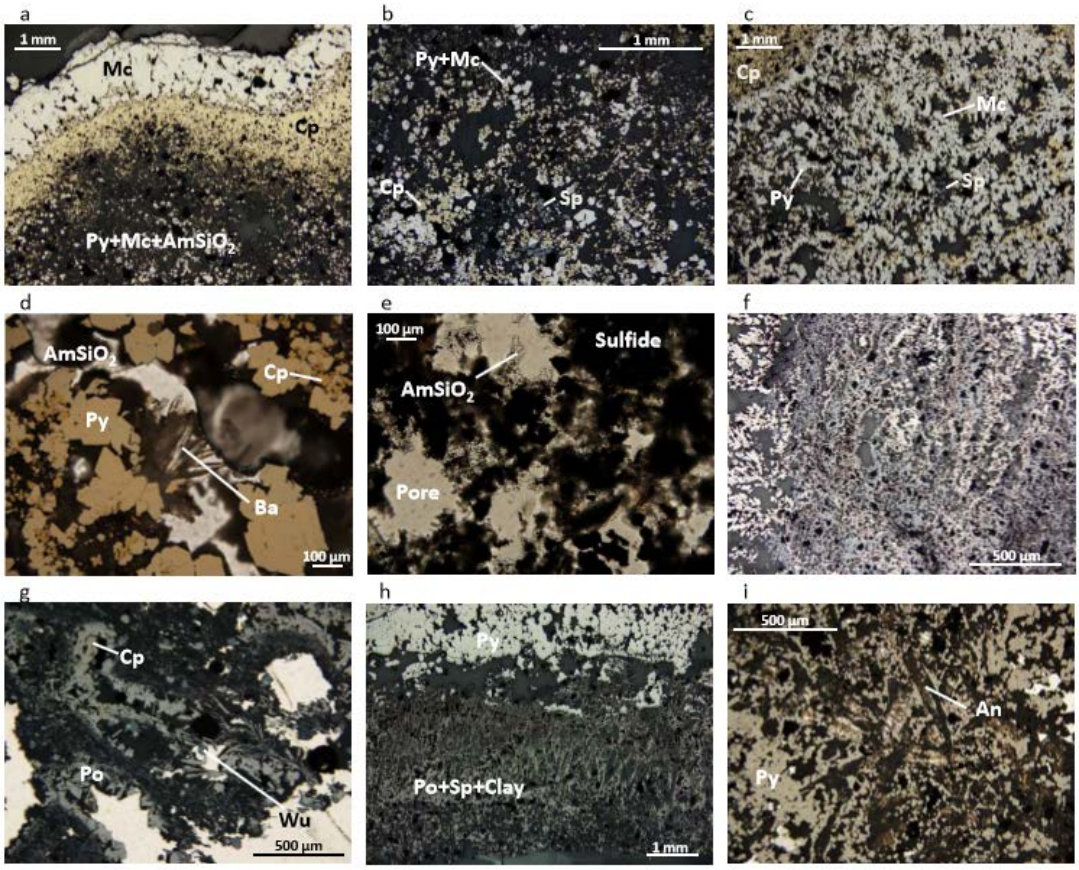

Figure 2.2. (a) Bastille: Reflected light photomicrograph (RLP) showing concentric sulfide layering of two phases of marcasite (Mc) and chalcopyrite (Cp) lining an open conduit (top), and a gradational shift to a typical lower temperature porous assemblage of pyrite (Py), marcasite and amorphous silica ($AmSiO_2$). (b) Bastille: RLP of typical mineral assemblage of porous interior "mush zone", with blocky pyrite/marcasite, chalcopyrite, and sphalerite. (c) Bastille: RLP of a mid- to high-temperature mineral assemblage consisting of blocky and dendritic marcasite and minor pyrite, with lesser, later stage chalcopyrite followed by sphalerite. (d) Bastille: Combined reflected and transmitted light photomicrograph (RLP/TLP) of late-stage bladed barite (Ba) growing off of pyrite in a pore space in the outer layer. Late stage amorphous silica coats all sulfide phases. (e) Bastille: Transmitted light photomicrograph (TLP) of amorphous silica coating sulfide minerals in pore spaces in the outer layer. (f) Dante: RLP of typical pyrite- and sphalerite-rich mush in the interior. (g) Dante: RLP/TLP of bladed pyrrhotite, hexagonal wurtzite, minor chalcopyrite (yellow), and fine sphalerite in a dark grey clay matrix. (h) Dante:

RLP of sharp contact with inner pyrite (top) and outer pyrrhotite (Po) with clay minerals and sphalerite. (i) Dante: RLP/TLP of semi-massive colloform pyrite with interstitial anhydrite.

oxidizing coating. The temperature-dependent mineralogical distribution within the sample, with a high-temperature chalcopyrite-rich core and lower temperature sphalerite-rich exterior, is corroborated by the elevated and lower concentrations of Cu (in chalcopyrite) and Zn (in sphalerite), respectively, within the core, relative to the exterior (Table 2.1).

The Dante sample, collected from the top of the Dante edifice, is a beehive-like chimney that was diffusely venting clear fluid (Fig. 2.1b). The interior is a black/brown, highly porous fluid conduit fill (Fig. 2.1e), composed primarily of pyrite and sphalerite (Fig. 2.2f). The high CaO content within the interior also suggests a high abundance of anhydrite (Table 2.1). Primary flow channels are defined by a high-temperature mineral assemblage of euhedral chalcopyrite, pyrrhotite and wurtzite (Fig. 2.2g). Dark brown to black bladed crystals (up to 3 mm long) of pyrrhotite occur within the interior and have a preferential alignment that may be related to fluid flow direction. The mineral distribution shows a clear concentric layering of pyrite and pyrrhotite-sphalerite-rich layers within the sample (Fig. 2.2h). A 7 mm pyrite/marcasite crust is the outermost layer, and contains late-stage white anhydrite that has significantly reduced the porosity of the outer walls and represents ingress of seawater through the chimney walls (Fig. 2.2i). The exterior is grey with white bacterial mat and Fe-staining and a few *Paralvinella* polychaete worms. Low-temperature amorphous silica coating of sulfide grains increases towards the exterior of the sample.

The Hot Harold sample, collected from the side of the Hot Harold edifice on the larger Faulty Towers complex, is a candelabra-like chimney that was vigorously venting black smoker fluid from a >10 cm orifice at the base of the chimney (Fig. 2.1c). The sample had a number of small (<14 mm) fluid conduits. The sample is dominated by fine dark grey/black pyrite and sphalerite with abundant bladed (<2 mm long) anhydrite. Bacterial mats stain the exterior of the sample (Fig. 2.1f). The distribution of Cu and Zn within the sample suggests a similar temperature-controlled sulfide mineral distribution as the Bastille sample (Table 2.1).

2.5.2 Mineral Spectroscopy

A comparison of all of the mineral identifications using various techniques is provided in Table 2.2. XRD analysis of the interior material used for mineral spectroscopy and

Table 2.1. Major element concentrations of rock samples, divided into analyses of material from the inner fluid conduits (used for microbial culturing), outer chimney walls and total bulk composition.

	Bastille			Dante			Hot Harold	
	inner	outer	bulk sample	inner	Outer	bulk sample	inner	bulk sample
Fe%	33.00	33.10	31.50	0.73	38.60	3.86	19.10	0.91
Cu%	10.00	2.18	4.64	0.11	0.48	1.18	0.33	0.09
Zn%	2.03	6.31	3.33	0.68	0.44	0.20	0.83	1.29
S%	40.2	43.4	40.2	25.7	40.5	27.4	34.1	25.6
SiO_2%	4.62	6.93	3.29	0.24	0.26	0.19	< 0.02	0.90
Ba%	0.48	0.42	0.40	0.09	0.01	0.03	0.04	0.07
Al_2O_3%	1.47	0.34	0.45	0.02	0.06	0.02	< 0.02	0.02
Pb%	0.03	0.06	0.04	0.01	0.03	0.00	0.02	0.01
CaO%	0.10	<0.01	4.88	39.46	7.82	37.22	24.91	38.90
MgO%	0.05	< 0.02	0.02	0.15	0.18	0.07	< 0.02	0.5
Na_2O%	0.53	0.08	0.22	0.67	0.89	0.27	0.47	0.54

Table 2.2. Comparison of analytical results for mineralogy

Technique	Scale	Bastille	Dante	Hot Harold
Petrography	Microscale, All	Marcasite, pyrite, chalcopyrite, sphalerite, silica, barite, anhydrite	Anhydrite, pyrite, pyrrhotite, sphalerite, wurtzite, iron oxide	Not available due to small sample size
Elemental analysis	Bulk, All	Relatively abundant Fe, Cu, Zn, Al_2O_3, SiO_2, Ba	Relatively abundant CaO, MgO; Fe high in outer wall	Relatively abundant CaO, MgO
X-ray diffraction	Bulk, interior	Pyrite, chalcopyrite, marcasite gypsum	Gypsum, anhydrite, pyrite, sulfur	Gypsum, anhydrite
VNIR reflectance spectroscopy	Bulk, interior	Chlorophyll-*a*, mica, orthopyroxene, chalcopyrite and/or pyrite	Gypsum, anhydrite, chlorophyll-*a*, chalcopyrite and/or pyrite	Anhydrite, gypsum, sphalerite and/or pyrite, possibly sulfur
Thermal emission spectroscopy	Bulk, interior	Chalcopyrite and/or pyrite	Gypsum, pyrite	Anhydrite
Mössbauer spectroscopy	Bulk, interior	Chalcopyrite (sextet), possible pyrite, sphalerite, marcasite (doublet)	Possible pyrite, sphalerite, marcasite (doublet), possible ferricopiapite, lepidocrocite, maybe schwertmannite (sextets)	Too little Fe to ID minerals

microbiological analyses showed that the Bastille chimney sample contained pyrite, chalcopyrite, and marcasite plus gypsum in one of the two replicates; the Dante chimney sample contained gypsum, anhydrite, lepidocrocite, pyrite, and sulfur; and the Hot Harold chimney sample contained gypsum and anhydrite.

Visible/near-infrared (VNIR) reflectance spectra of all three samples are very dark, consistent with the presence of pyrite, chalcopyrite, and sphalerite that were identified using other techniques (Fig. 2.3). Two broad bands observed near 1 and 2 μm in spectra of the Bastille samples are characteristic of Fe^{2+} excitations in pyroxene and pyrite (Fig. 2.3a). The wavelength positions of these bands are highly dependent on mineral chemistry (*Burns, 1993*) and the band centers near 0.90 and 1.80 μm are most consistent with orthopyroxene, although these features could also be due to pyrite with a composition different from that available in spectral libraries. The sharp bands at 2.73-2.75 μm are due to OH stretching vibrations and are characteristic of phyllosilicates. A broadening of the 0.9 μm Fe^{2+} band towards 0.85 μm for both Bastille samples is attributed to a Fe^{3+} electronic transition, as found in iron oxide minerals such as hematite or Fe^{3+} in some clays and sulfates. A small amount of mica containing some Fe^{3+} such as zinnwaldite is present in this sample. The sharp band at 0.662 μm is due to chlorophyll *a*, while the additional sharp band at 0.87 μm is due to bacteriochlorophyll *a* (e.g., *Pierson et al., 1987; Hubas et al., 2011*). Another sharp weak band near 0.975 μm may also be due to an anoxic pigment as it is narrower than typically observed for Fe transitions.

The dominant features in the spectra of the Dante and Hot Harold samples (Fig. 2.3b) are H_2O and SO_4 bands characteristic of Ca sulfates (*Bishop et al., 2014*). The Hot Harold spectrum exhibits a suite of sharp bands from 4.2-5 μm that indicate the presence of anhydrite. The broader bands near 4.5 and 4.7 μm in the spectrum of Dante are consistent with a mixture of gypsum and anhydrite. A H_2O stretch plus bend combination band near 1.94 μm is present in the spectra of both Dante and Hot Harold, indicating that both samples are hydrated (note that the anhydrite lab spectrum also contains this band but that is not due to anhydrite (*Bishop et al., 2014*). Due to the presence of this H_2O band, Hot Harold likely contains some gypsum as well as anhydrite, although anhydrite is spectrally dominant. The Dante spectrum also contains a weak chlorophyll band at 0.662 μm. A rather unusual reflectance maximum is observed near 0.58 μm for Bastille and Dante. It could be caused by a mixture of chalcopyrite and pyrite or it could also be consistent with the sulfate coquimbite (max at 0.47 μm) mixed with other minerals; however,

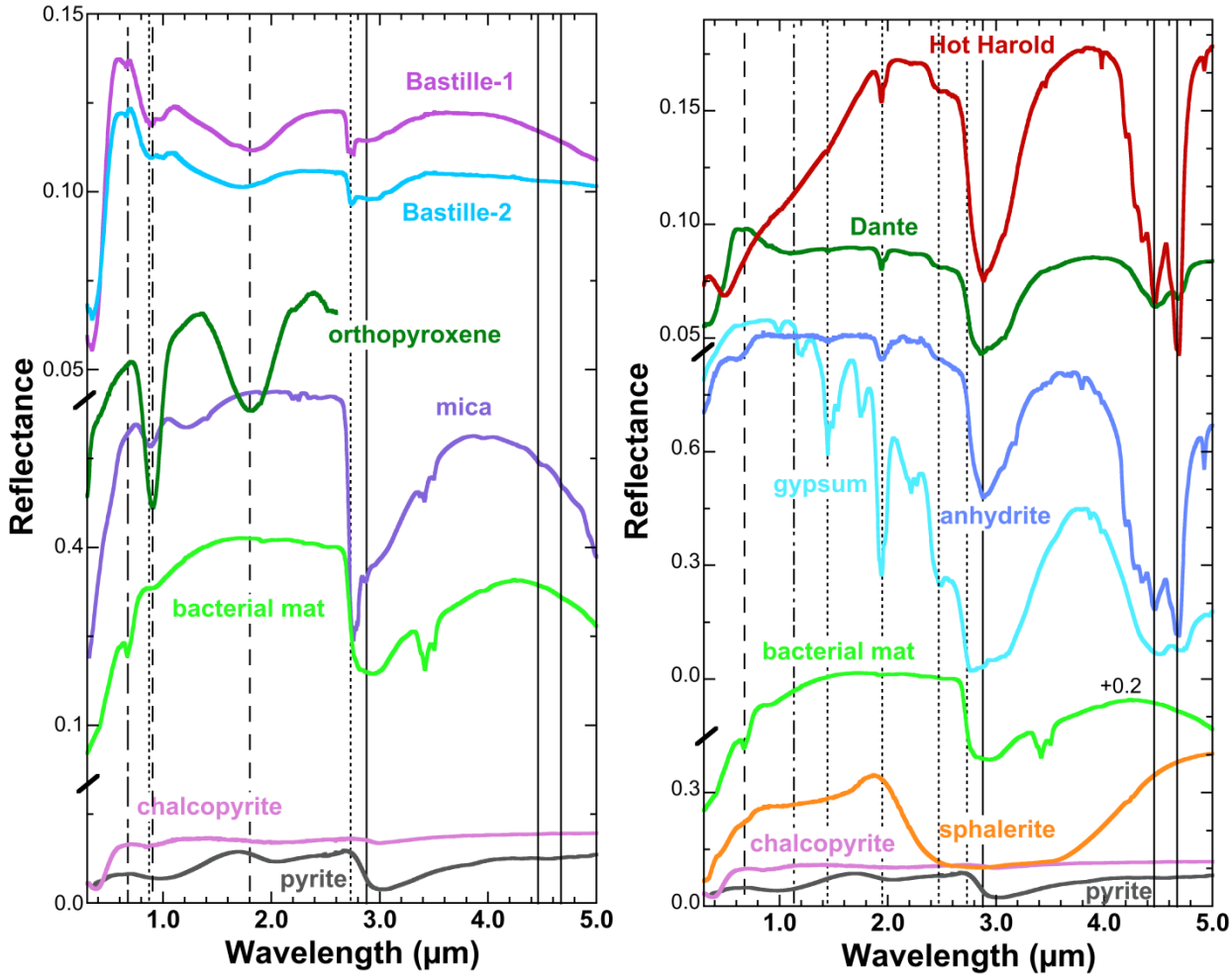

Figure 2.3. Reflectance spectra are shown from 0.35-5 μm for the Bastille, Dante, and Hot Harold samples together with spectra of likely minerals present in the samples. (a) VNIR spectra of Bastille-1, Bastille-2, orthopyroxene DL064 (*Klima et al., 2007*), zinnwaldite mica JB729 (*Bishop et al., 2008*), JB205, a chlorophyll-bearing bacterial mat from beneath Lake Hoare in the Antarctic Dry Valleys (*Bishop et al., 2001*), chalcopyrite HS431 (*Clark et al., 2007*), and pyrite GDS483 (*Clark et al., 2007*). (b) VNIR spectra of Hot Harold, Dante, anhydrite GDS42 (*Clark et al., 2007*), gypsum JB567 (*Bishop et al., 2014*), chlorophyll-bearing mat JB205, sphalerite HS136 (*Clark et al., 2007*), chalcopyrite HS431, and pyrite GDS483.

the latter has not been identified with other techniques so is less likely to be present. The increasing spectral slope observed for Hot Harold is attributed to a mixture of a Fe^{2+} phase with the other minerals. The difference in spectral shape from 0.5-1.8 μm in the Hot Harold spectrum compared to spectra of the other samples in the study could be explained by the presence of sphalerite instead of chalcopyrite as the darkening agent. The spectrum of sulfur also exhibits a minimum near 0.4 μm (*Clark et al., 2007*), but is spectrally too bright in the NIR to be a major component of this sample.

The thermal emission spectra (Fig. 2.4) do not show any evidence of the hydrated iron sulfates suggested by VNIR, but are very much consistent with the Fe-rich sulfide phases identified by Mössbauer (below). The emissivity spectra are fairly simple spectroscopically, thus mineralogically. In fact, the mineralogy of the samples was very easily determined from the emissivity spectra because each spectrum was dominated by single mineral phases and complex mineral mixtures were not present. Laboratory spectra of pure mineral sulfide and sulfate species (*Lane, 2007*; *2008*) are shown in Figure 2.4 for comparison to the Endeavour chimney samples. Both Bastille sample spectra clearly indicate iron sulfide (chalcopyrite and/or pyrite), but no sulfate. Gypsum was found in Dante, with a possible small amount of pyrite. Anhydrite is seen clearly in Hot Harold. There is no evidence for carbonate in any of the sample spectra.

Mössbauer data for the chimney samples and several sulfide and sulfate standards are shown in (Fig. 2.5), with spectra normalized to 1% absorption. Room-temperature spectra of Bastille contain a central doublet and sextet consistent with that seen in the chalcopyrite sample. The relative increase in the area of the central doublet in Bastille as compared to chalcopyrite is likely due to contribution from pyrite, marcasite, or sphalerite. This doublet broadens but does not split at 4K, ruling out ferricopiapite, fibroferrite, schwertmannite, lepidocrocite, and hematite as possible constituents. Dante spectra are also dominated by a doublet that persists to 4K, again consistent with pyrite, marcasite, or sphalerite. Several sextet distributions are observed in Dante at 4K. They are poorly defined but overlap with sextet distributions of ferricopiapite, lepidocrocite, and possibly schwertmannite. Hot Harold contains little iron (< 0.5% absorption with an undiluted sample) and any iron-bearing minerals present cannot be identified by Mössbauer spectroscopy. The Mössbauer data do not show any evidence for phases such as gypsum that do not contain Fe.

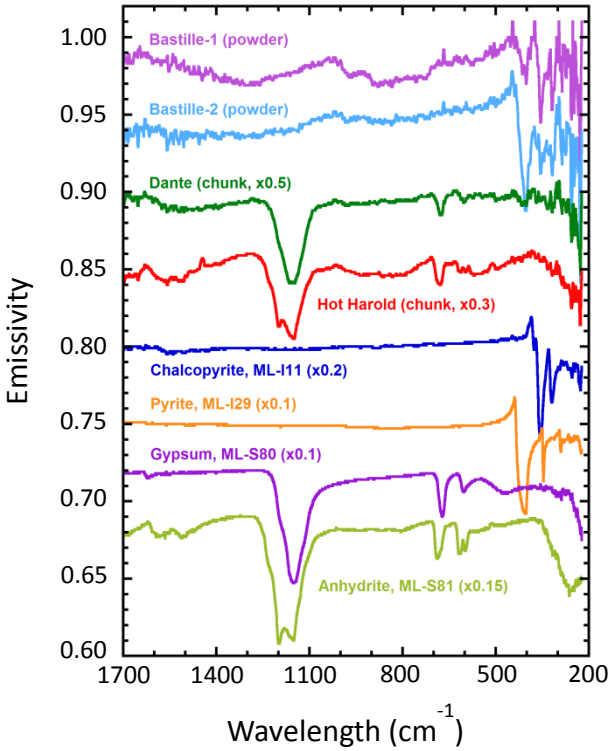

Figure 2.4. Thermal emissivity spectra of the Endeavour hydrothermal chimney samples and four laboratory mineral spectra for comparison (sulfide spectra are from Lane, 2008; sulfate spectra are from Lane, 2007). Spectra are offset for clarity.

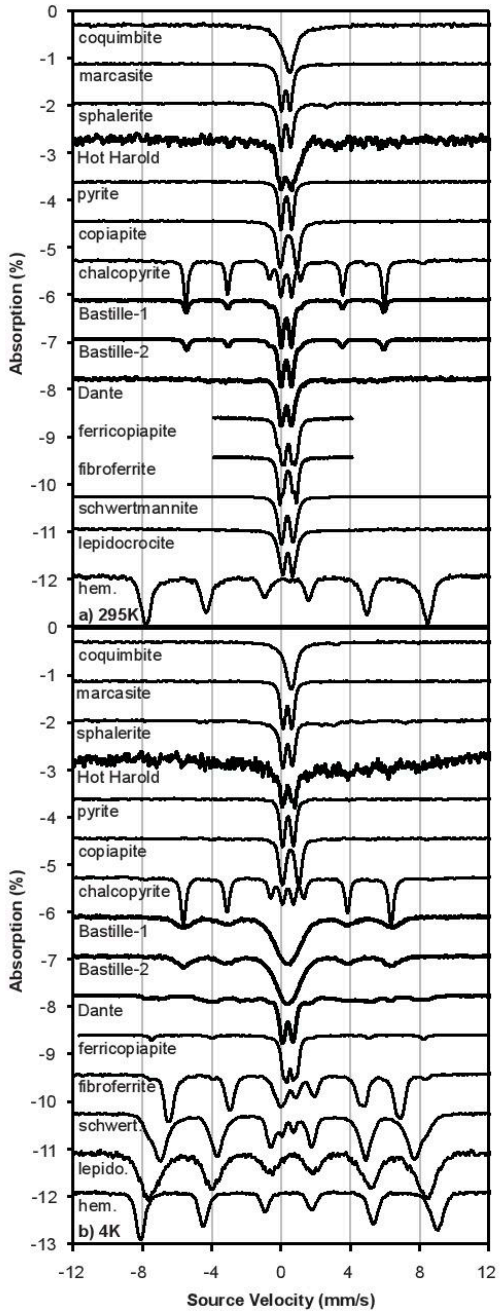

Figure 2.5. Mössbauer data acquired at 295 K (top panel) and 4K (bottom panel). Hydrothermal samples are shown with similar minerals. The spectra of Bastille consist of a chalcopyrite sextet and a doublet that could be pyrite, sphalerite, or marcasite. The Dante spectra contain a doublet that could represent pyrite, sphalerite, or marcasite and a sextet that could be ferricopiapite, lepidocrocite, or schwertmannite. The Hot Harold sample had too little Fe to produce an interpretable Mössbauer spectrum.

2.5.3 Fluid Chemistry

Most of the calculated end-member chemical concentrations for the hydrothermal fluids emanating from Bastille, Dante and Hot Harold (Table 2.3) fall within the range of previously measured values for the Main Endeavour Field on the Endeavour Segment (*Lilley et al., 1993*; *Butterfield et al., 1994*; *Lilley et al., 2003*). Generally, the chemistries of the three fluids were very similar to one another. The pHs of the fluids were mildly acidic at 25°C with ranges of pH 4.0-4.5. H_2 concentrations were slightly low to normal relative to historical values for Endeavour, while CH_4 and NH_3 concentrations were typical for Endeavour but highly elevated relative to global mid-ocean ridge hydrothermal systems. Concentrations of ΣH_2S and SiO_2 were within the range of previously measured values for Endeavour. The Cl^- concentrations of Bastille and Dante were below that of seawater, suggesting that they were in the vapor phase of phase separation while the Cl^- concentration of Hot Harold was above that of seawater and likely in the mineral phase (*Von Damm et al., 1995*; *Butterfield et al., 1997*). However, the Fe^{2+} concentration in Hot Harold fluids was considerably lower than in Bastille and Dante.

Reaction energetics for the six microbial catabolic processes were evaluated for Bastille, Dante and Hot Harold and plotted for seawater:hydrothermal fluid mixtures representing a kg of mixed fluid at 25°C, 55°C and 80°C (Fig. 2.6). The reaction energetics do not vary significantly between sites at any of the modeled temperatures. At 25°C, aerobic sulfide oxidation and methane oxidation provide the largest amount of redox energy for microbial catabolism. They are both limited by the availability of O_2 in seawater, and thus the energy available for these reactions decreases 30-50% with increasing temperature. The energy available for the anaerobic oxidation of methane increased roughly four-fold from 25°C to 80°C and exceeded the energy available for aerobic sulfide and methane oxidations at 80°C at all three vents. Reaction energies for aerobic H_2 oxidation, hydrogenotrophic sulfate reduction, and methanogenesis increased with temperature due to the increased availability of H_2, but were substantially lower than the energy available at 80°C for the other three reactions. Anhydrite, pyrite, and various iron oxides such as hematite, goethite and magnetite reach their saturation states during the mixing of hydrothermal fluid and seawater and form minerals in the system. These have only a minor impact on the availability of reactants.

Table 2.3. Chemical composition of end-member hydrothermal vent fluids extrapolated to zero-Mg^{2+}(± standard error) from this study and seawater for modeling purposes

	Bastille	Dante	Hot Harold	Seawater[a]
Temp., max	282°C	300°C	321°C	2°C
pH at 25°C	4.00 ± 0.05	4.25 ± 0.05	4.51 ± 0.05	7.8
SiO_2 (mmol/kg)	16.97 ± 0.20	17.13 ± 0.20	16.10 ± 0.01	0.13
ΣH_2S (mmol/kg)	3.34 ± 0.26	4.00 ± 0.30	4.30 ± 0.11	0
H_2 (µmol/kg)	28.8	87.6	90.0	0
CH_4 (µmol/kg)	1,884	1,546	1,500	0
ΣCO_2 (mmol/kg)	10.8	13.1	7.0	2.2
O_2 (µmol/kg)	0	0	0	123
NH_3 (µmol/kg)	498.2 ± 6.1	452.8 ± 18.3	426.0 ± 2.0	0
Cl^- (mmol/kg)	440.3 ± 9.7	507.8 ± 2.3	655.1 ± 0.7	550
SO_4^{2-} (mmol/kg)	0	0	0	27.9
Na^+ (mmol/kg)	358.4 ± 8.1	399.6 ± 3.4	501.3 ± 0.2	441
Mg^{2+} (mmol/kg)	0	0	0	54.5
K^+ (mmol/kg)	21.2 ± 0.2	27.5 ± 0.8	39.0 ± 0.0	9.8
Ca^{2+} (mmol/kg)	27.7 ± 0.7	38.2 ± 1.2	51.6 ± 0.2	10.7
Fe^{2+} (µmol/kg)	562.6 ± 27.1	442.7 ± 69.3	139.9 ± 1.5	-
PO_4^{3-} (µmol/kg)	0.64 ± 0.25	0.53 ± 0.47	0.90 ± 0.05	-
Li (µmol/kg)	253.1 ± 27.3	368.1 ± 35.4	516.4 ± 4.1	-
Rb (µmol/kg)	20.1 ± 0.7	27.6 ± 1.1	42.6 ± 0.5	-
Sr^{2+} (µmol/kg)	101.7 ± 1.6	141.8 ± 24.0	198.0 ± 1.4	-
Ba^{2+} (µmol/kg)	-	1.4 ± 0.4	5.6 ± 0.2	-
B (µmol/kg)	608.2 ± 47.8	646.4 ± 37.4	591.5 ± 15.1	-
Al^{3+} (µmol/kg)	7.2 ± 1.3	6.1 ± 1.5	6.1 ± 0.5	-
Mn^{2+} (µmol/kg)	163.7 ± 3.3	189.3 ± 21.9	292.9 ± 3.5	-
Cu^+ (µmol/kg)	11.3 ± 4.0	13.8 ± 0.4	-	-
Zn^{2+} (µmol/kg)	27.7 ± 3.6	17.5 ± 8.2	11.7 ± 6.4	-
Cs (nmol/kg)	246.8 ± 6.7	349.4 ± 27.4	532.5 ± 5.6	-
Pb (nmol/kg)	112.6 ± 19.1	127.3 ± 97.4	-	-
Tl (nmol/kg)	31.8 ± 3.5	21.1 ± 17.7	41.8 ± 2.9	-
Mo (nmol/kg)	24.2 ± 11.8	6.8 ± 22.1	0.6 ± 2.5	-
W (nmol/kg)	2.2 ± 0.9	1.9 ± 0.3	2.7 ± 0.2	-

[a]Seawater composition from *Amend et al.* (2011), except the O_2 concentration which is from *Von Damm et al.* (1985).

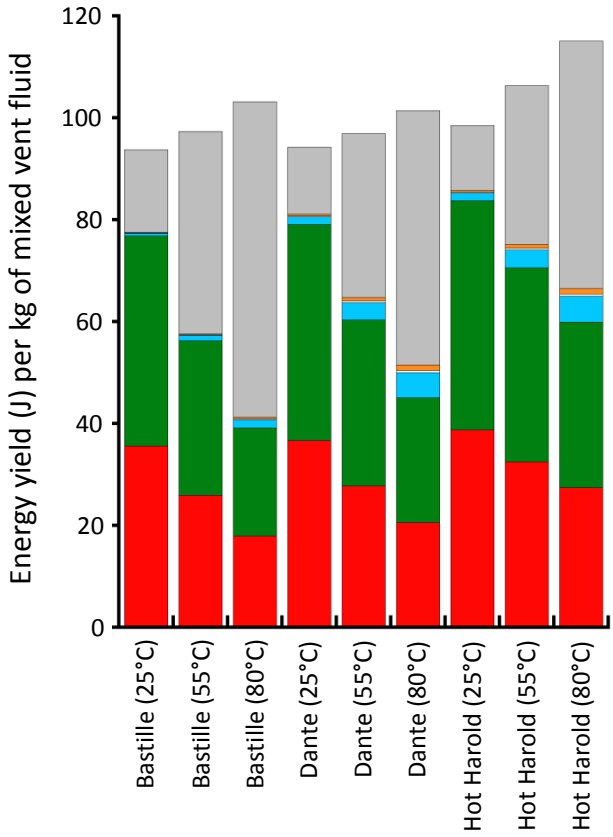

Figure 2.6. Predicted catabolic energies (in J per kg of mixed fluid) available for anaerobic oxidation of methane (grey), hydrogenotrophic sulfate reduction (orange), hydrogenotrophic methanogenesis (white), aerobic hydrogen oxidation (blue), aerobic methane oxidation (green), and aerobic sulfide oxidation (red) at 25°C, 55°C and 80°C in mixed abiotic hydrothermal-seawater solutions flowing from Bastille, Dante and Hot Harold.

2.5.4 Microbiology

To compare microbial community compositions among the three hydrothermal chimneys, bacterial 16S rRNA gene clone libraries were constructed and resulted in 68, 74 and 62 clone sequences for the chimneys from the Bastille, Dante and Hot Harold edifices, respectively (Table 2.4). All of the bacterial clone libraries were largely dominated by Proteobacteria (Fig. 2.7), but distributions within subclasses of this phylum varied widely. Deltaproteobacteria were found almost exclusively in the Bastille chimney and represented 48% of the total OTUs in that sample. Of these, 45% were most closely related (87-91% identity) to *Desulfobulbus mediterraneus* and 24% were most closely related (84-91% identity) to *Desulfobacterium indolicum* and *Desulfobacterium aniline*. These are mesophilic, obligately anaerobic sulfate reducers. Another 15% of the deltaproteobacteria sequences were most closely related (82-91% identity) to other mesophilic, obligately anaerobic sulfate reducers, and 9% were most closely related (80-86% identity) to the thermophilic, anaerobic iron reducer *Geothermobacter ehrlichii*. Alpha-, gamma-, and epsilonproteobacteria were also present at low abundances, along with representatives of the Bacteroidetes, Chloroflexi, Deinococcus-Thermus, Firmicutes and Planctomycetes. The majority of the sequences in the Bastille chimney (74%) were most closely related to mesophilic and thermophilic anaerobes and microaerophiles.

Within the Dante and Hot Harold chimneys, betaproteobacteria dominated with contributions of 58% and 45%, respectively (Fig. 2.7). Sequences most closely related to *Roseateles depolymerans* comprised 44% and 89% of the betaproteobacteria in Dante (90-99% identity) and Hot Harold (97-98% identity), respectively. Also, 23% of the betaproteobacteria in Dante were most closely related (99% identity) to *Delftia acidovorans*, 12% were most closely related (99-100% identity) to *Ralstonia pickettii*, and 5% were most closely related (99% identity) to *Cupriavidus metallidurans*. These latter three betaproteobacteria are mesophilic aerobes that are highly resistant to heavy metals. Epsilonproteobacteria comprised 32% of the bacterial sequences in Hot Harold, 15% in Bastille, and 7% in Dante. Sequences most closely related (88-95% identity) to *Sulfurimonas autotrophica* and *Sulfurimonas paralvinella* comprised 60% of the epsilonproteobacteria in Hot Harold. These are mesophilic, autotrophic sulfur-oxidizing aerobes. Alpha-, gamma-, and deltaproteobacteria were also present at much lower percentages along with representatives of Actinobacteria and Cyanobacteria in Dante and Aquificae and Firmicutes

Table 2.4. Distribution of representative bacterial and archaeal 16S rRNA gene phylotypes in the interior of the actively venting hydrothermal chimneys

	Number of clones		
	Bastille	Dante	Hot Harold
Bacteria			
Alphaproteobacteria	6	5	1
Betaproteobacteria	0	43	28
Gammaproteobacteria	5	18	9
Deltaproteobacteria			
Desulfobacterales	25	0	1
Desulfuromonadales	4	0	0
Desulfovibrionales	2	1	0
Other Deltaproteobacteria	2	0	0
Epsilonproteobacteria			
Campylobacterales	8	4	16
Nautiliales	0	0	1
Other Epsilonproteobacteria	2	1	3
Actinobacteria	0	1	0
Aquificae	0	0	2
Bacteroidetes	5	0	0
Chloroflexi	3	0	0
Cyanobacteria	0	1	0
Deinococcus-Thermus	1	0	0
Firmicutes	2	0	1
Planctomycetes	3	0	0
Archaea			
Thermococcales	13	-	-
Methanococcales	3	-	-
Korarcheales	2	-	-
Desulfurococcales	1	-	-
Thermoproteales	1	-	-
Other Euryarchaeota	2	-	-
Other Crenarchaeota	1	-	-

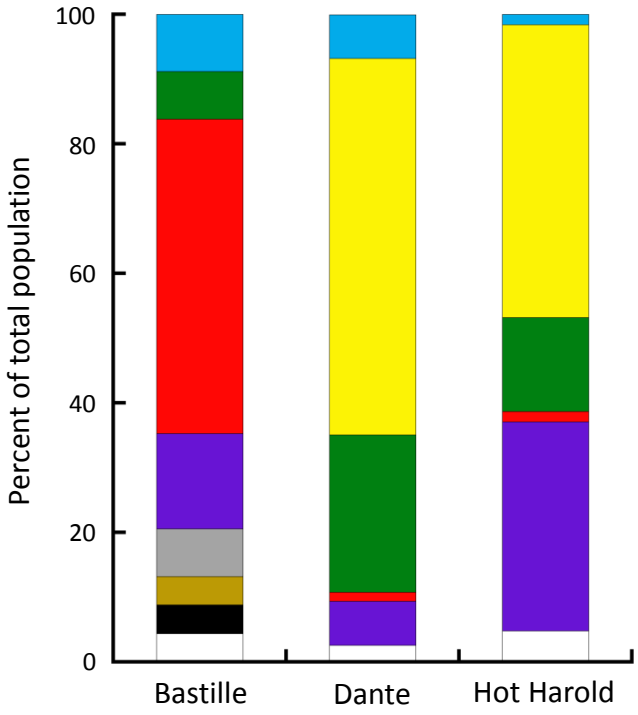

Figure 2.7. Relative abundances of bacterial orders observed in Bastille, Dante and Hot Harold hydrothermal vent deposits. The orders are alphaproteobacteria (blue), betaproteobacteria (yellow), gammaproteobacteria (green), deltaproteobacteria (red), epsilonproteobacteria (purple), Bacteriodetes (grey), Chloroflexi (brown), Planctomycetes (black), and white is other. The phylogenetic groupings were determined from BLAST analyses.

in Hot Harold. The majority of the sequences from Dante and Hot Harold were most closely related to mesophilic and thermophilic aerobes.

Chao1, Shannon index, and Observed Species diversity indices were calculated in Qiime for bacterial clone libraries from all three samples (Table 2.5). These indicated that both Bastille and Dante had relatively higher diversity than Hot Harold in all three diversity indices calculated. However, rarefaction curves suggested that complete saturation of the environment was not reached and therefore no trends in alpha-diversity could be identified. Across samples, the relative distances measured between communities (beta-diversity) using UniFrac and Weighted UniFrac (*Lozupone et al.,2005*) indicated that Dante and Hot Harold were closer in relative taxa seen than either of these with Bastille. Taken together, the community structures in the Dante and Hot Harold chimneys seem to be more similar to each other than to those in the Bastille chimney.

Twenty-three archaeal 16S rRNA gene clone sequences were retrieved from the Bastille chimney and were primarily related to hyperthermophilic anaerobes (Table 2.4). Despite repeated attempts, no archaeal clones could be recovered from either the Dante or Hot Harold chimneys, most likely due to the generally low DNA yield from these samples. Thermococcales contributed 57% of the total archaeal clones in the Bastille chimney with additional contributions from Methanococcales (13%), Korachaeoles (9%), Desulfurococcales (4%), and Thermoproteales (4%). The Thermococcales were most closely related (85-87% identity) to *Thermococcus* spp., which are hyperthermophilic, heterotrophic sulfur reducers and H_2 producers. The Methanococcales were most closely related (88%) to *Methanocaldococcus* spp., hyperthermophilic methanogens. In general, the interior mineral sample from the Bastille chimney contained higher numbers of culturable hyperthermophiles than the interior mineral samples from the Dante and Hot Harold chimneys based on MPN estimates (Table 2.6). Heterotrophic sulfur reducers were at least ten-fold more abundant in the samples than either iron reducers or methanogens, mirroring the pattern observed with the archaeal clone library from the Bastille chimney. All sequences are deposited in GenBank under accession numbers KF578145-KF578374.

Table 2.5. Diversity indices for the Bastille, Dante and Hot Harold hydrothermal chimneys used in this study

	Bastille	Dante	Hot Harold
α Diversity			
Chao1[a]	15.13	18.34	11.20
Shannon index[b]	3.75	3.57	2.84
Observed Species	15.0	16.2	11.0
β Diversity			
UNiFRac			
Bastille	0.0	0.7336	0.6684
Dante		0.0	0.3715
Hot Harold			0.0
Weighted UNiFRac			
Bastille	0.0	0.5926	0.5634
Dante		0.0	0.1963
Hot Harold			0.0

[a]Chao1 richness estimator (*Chao, 1987*)

[b]Shannon diversity index (*Shannon, 1948*)

Table 2.6. Most-probable-cell estimates of various hyperthermophilic anaerobes per gram of hydrothermal mineral material. Enrichments were incubated at 90°C

Sample	Most-probable-number estimates		
	Iron reducers	Methanogens[a]	Heterotrophs[a]
Bastille	108	34	3,470
Dante	13	4	511
Hot Harold	106	ND	1,061

[a]Results previously reported in *Ver Eecke et al.* (*2012*)

2.6 Summary and Concluding Remarks

Our study used for the first time reflectance and emission spectroscopic techniques such as Mössbauer, VNIR and thermal emissivity to analyze the minerals in actively-venting deep-sea hydrothermal chimneys. Each of these techniques has its own advantages and disadvantages.

Mössbauer is the gold standard for identification of Fe oxides, but it cannot be done shipboard, and it cannot uniquely distinguish sulfide, sulfate, or silicate phases, though it can constrain them (*Dyar et al., 2014*). Mössbauer data can resolve questions relating to the bioproducts and reactants of Fe-reducing microorganisms, albeit at bulk scales. Reflectance spectroscopy from the visible to the mid-IR can be done on hand samples at sea using relatively inexpensive portable spectrometers, and these techniques are non-destructive. Mineral identification from the reflectance techniques depends on the availability of matching software and spectral databases containing end-member mineral spectra, but these exist in public libraries, largely assembled for remote sensing of planetary surfaces. For example, sulfate spectra have been extensively characterized by coauthors on this paper, and are reported in *Lane et al*. (2007 and submitted). Those data have become part of the Arizona State University Thermal Emission Spectral Library (http://speclib.asu.edu) and the Reflectance Experiment Laboratory (RELAB) facility at Brown University (http://www.planetary.brown.edu/relab).

These spectroscopic techniques show enormous promise. In this study, TIR analyses rapidly and accurately identified the major mineral components in samples from all three chimneys in agreement with the major phases found by XRD. Gypsum and anhydrite were readily identified in the Dante and Hot Harold samples using VNIR reflectance spectra. Spectra of all samples were very dark, consistent with the presence of sulfides such as chalcopyrite, pyrite, sphalerite, but these could not be uniquely identified. Minor amounts of mica were detected in the NIR spectra of the Bastille samples that were not detected by XRD or TIR spectra. However, NIR spectra are generally more sensitive to the presence of clays than other techniques. The VNIR spectral analyses indicated the presence of chlorophyll *a* in the Bastille and Dante samples and bacteriochlorophyll *a* in the Bastille samples. While the presence of chlorophyll is seemingly inconsistent with the deep-sea source of the samples, the Bastille 16S rRNA gene clone library contained two *Chlorobaculum*-like sequences and three Chloroflexi sequences (anaerobic, green sulfur and non-sulfur photosynthetic bacteria, respectively) and the

Dante sample contained one Cyanobacteria sequence (aerobic, oxygenic photosynthetic bacteria) thus supporting the detection of chlorophyll in the samples. No chlorophyll or photosynthetic bacteria were found in the Hot Harold sample. The chlorophyll spectra match a bacterial mat spectrum from an anoxic mat in pyrite-rich sediments growing 34 m deep in an Antarctic lake below 3 m of ice (*Bishop et al., 2001*). The green photosynthetic bacteria in Bastille are anaerobes, consistent with the other organisms found in the sample, and may be growing chemosynthetically on H_2 and sulfur compounds but possess some basal level of photosynthetic pigments. Shipboard measurement of the VNIR spectra could provide fast and nondestructive analysis for photosynthetic pigments to ensure that the samples collected represent the desired communities. In the future, shipboard analyses can also be acquired with hyperspectral imaging, providing an understanding of the spatial distribution of major phases present at smaller than cm-scale resolution.

The focus of this study was the habitable zone in the interiors of active chimneys. Several studies have examined the microbial community composition in diffuse hydrothermal vent fluids along the Juan de Fuca Ridge (*Huber et al., 2002*; *2003*; *2007*; *Opatkiewicz et al., 2009*; *Anderson et al., 2012*; *Ver Eecke et al., 2012*; *Akerman et al., 2013*; *Meyers et al., 2013*). Only a few studies have correlated microbial community compositions with the mineralogy of actively venting chimneys from the Juan de Fuca Ridge (*Shrenk et al., 2003*; *Zhou et al., 2009*; *Olins et al., 2013*). This study combined for the first time detailed mineralogy, fluid chemistry, redox reaction energetics, molecular microbial community analyses, and culture-dependent estimates of hyperthermophiles of active chimneys from the Endeavour Segment to assess the nature of their habitable interior zones. We found evidence that suggests mineralogy or venting type (e.g., type I or II), in addition to fluid chemistry, can have a significant impact on the types of microorganisms and microbial processes present.

The chimney from the Bastille edifice contained primarily mesophilic, thermophilic and hyperthermophilic anaerobes, mostly deltaproteobacteria. The chimneys from the Dante and Hot Harold edifices contained microbial communities that were similar to each other and composed primarily of mesophilic and thermophilic aerobes, mostly beta- and epsilonproteobacteria, although an equal proportion of epsilonproteobacteria was also present in the Bastille chimney. The differences observed in microbial community compositions despite close similarities in fluid

chemistry for all three samples indicates that additional factors influence the types of microbes and microbial processes present within a chimney.

There are several possible explanations for the different bacterial community composition in the Bastille chimney. First, the anaerobes in Bastille use sulfur and iron compounds as terminal electron acceptors and may be dependent upon the oxidized weathering products of Fe-sulfide minerals for growth. Second, temperature is known to shape microbial communities in vent samples with anaerobes more prevalent at higher temperatures and aerobes more prevalent at lower temperatures (*McCollum and Shock, 1997*; *Tivey, 2004*; *Amend et al., 2011*). The Bastille chimney sample may have been hotter than either the Dante and Hot Harold chimney samples. However, all three samples showed mesophiles to hyperthermophiles in their clone libraries, with mostly mesophilic bacteria present in all three chimneys. Therefore, temperature does not appear to be a large factor in these samples. Finally, the outer surface of the Bastille chimney may be more conducive to the growth of macrofauna and microbial mats, perhaps due to heat flow patterns, which might have generated sources of organic compounds that were drawn into the chimney by seawater ingress. These organics could be consumed by aerobic heterotrophs, which would decrease the O_2 concentration and provide reactants for anaerobic growth. The reduced minerals in the chimney may also aid in decreasing the O_2 concentration in the chimney's interior. Anaerobic, H_2-generating heterotrophs, such as the *Thermococcus* spp. identified in the Bastille chimney but not in the Dante and Hot Harold chimneys, could then generate sufficient H_2 to support hydrogenotrophic autotrophs that are otherwise H_2 limited for growth through syntrophy. Both molecular and culture-dependent analyses show that Thermococcales were the most abundant hyperthermophilic archaea present in the Bastille chimney.

The aerobes in the Bastille, Dante and Hot Harold chimneys are largely dependent upon the aqueous chemical species in hydrothermal fluids, such as H_2S, and the O_2 in seawater for their growth. The presence and predominance of betaproteobacteria in the Dante and Hot Harold chimneys is unusual; however, they have been found in other molecular analyses from the Endeavour Segment (*Zhou et al., 2009*; *Anderson et al., 2012*). The betaproteobacteria in our samples show some distant similarity to known metal oxidizing bacteria such as *Leptothrix* and heavy metal tolerant bacteria such as *Delftia* and may have similar functions. However, while our controls were negative, we also cannot rule out the possibility that our high homology (>99%

identity) betaproteobacteria are contaminants in these samples with low DNA concentrations, as previously observed (*Zeigler Allen et al., 2011*).

This study brings together the diverse perspectives of marine geoscience, microbiology, mineral spectroscopy, and geochemistry to directly address issues with new technological approaches to understand the nature and limits of life in rock. Hydrothermal vents are among the most productive regions in the deep ocean and represent an ideal starting point for modeling life in the ocean crust and the subsurface in general. Many questions remain to be addressed. Are microbes from deep-sea vents selective for specific mineral types for attachment and growth? Are these accompanied by morphological changes to cells and minerals? How widespread are mineral transformations various types of microbes, and are they diagnostic? Can mineral biosignatures be found in hydrothermal mineral deposits where these organisms grow? These remain largely open questions, especially at scales smaller than individual cell and mineral grains. However, using a holistic approach that includes mineralogy, microbiology, geochemistry and fluid dynamics can begin to address these questions and lead to a broader understanding and detection of life within rock.

CHAPTER 3

MAGNETITE FORMATION FROM FERRIHYDRITE BY HYPERTHERMOPHILIC ARCHAEA FROM ENDEAVOUR SEGMENT, JUAN DE FUCA RIDGE HYDROTHERMAL VENT CHIMNEYS

3.1 Abstract

Hyperthermophilic iron reducers are common in hydrothermal chimneys found along the Endeavour Segment in the northeastern Pacific Ocean based on culture-dependent estimates. However, information on the availability of Fe(III) (oxyhydr)oxides within these chimneys, the types of Fe(III) (oxyhydr)oxides utilized by the organisms, rates and environmental constraints of hyperthermophilic iron reduction, and mineral end products are needed to determine their biogeochemical significance and are addressed in this study. Thin-section petrography on the interior of a hydrothermal chimney from the Dante edifice at Endeavour showed a thin coat of Fe(III) (oxyhydr)oxide associated with amorphous silica on the exposed outer surfaces of pyrrhotite, sphalerite and chalcopyrite in pore spaces, along with anhydrite precipitation in the pores that is indicative of seawater ingress. The iron sulfide minerals were likely oxidized to Fe(III) (oxyhydr)oxide with increasing pH and E_h due to cooling and seawater exposure, providing reactants for bioreduction. Culture-dependent estimates of hyperthermophilic iron reducer abundances in this sample were 1,740 and 10 cells per gram (dry weight) of material from the outer surface and the marcasite-sphalerite-rich interior, respectively. Two hyperthermophilic iron reducers, *Hyperthermus* sp. Ro04 and *Pyrodictium* sp. Su06, were isolated from other active hydrothermal chimneys on the Endeavour Segment. Strain Ro04 is a neutrophilic (pH_{opt} 7-8) heterotroph while strain Su06 is a mildly acidophilic (pH_{opt} 5), hydrogenotrophic autotroph, both with optimal growth temperatures of 90-92°C. Mössbauer spectroscopy of the iron oxides before and after growth demonstrated that both organisms form nanophase (<12 nm) magnetite [Fe_3O_4] from laboratory-synthesized ferrihydrite [$Fe_{10}O_{14}(OH)_2$] with no detectable mineral intermediates. They produced up to 40 mM Fe^{2+} in a growth-dependent manner while all abiotic and biotic controls produced < 3 mM Fe^{2+}. Hyperthermophilic iron reducers may have a growth advantage over other hyperthermophiles in

hydrothermal systems that are mildly acidic where mineral weathering at elevated temperatures occurs.

3.2 Introduction

Hydrothermal vents along the Endeavour Segment of the Juan de Fuca Ridge in the northeastern Pacific Ocean form massive mineral deposits up to 45 m tall and 50 m wide (*Delaney et al., 1992; Robigou et al., 1993; Kelley et al., 2001; Kelley et al., 2012*). In general, these deposits are coarse grained and highly porous with Fe-sulfide rich interiors, amorphous silica rich exteriors, and zones of sulfate and clay minerals due to seawater ingress (*Tivey & Delaney, 1986; Kristall et al., 2006*). H_2 concentrations in hydrothermal fluids vary significantly between global sites (see *Holden et al., 2012* for a review), which may be a key driving factor for the variations observed in microbial community compositions (*Takai & Nakamura, 2010; Flores et al., 2011; Ver Eecke et al., 2012*). At sites with low H_2 in hydrothermal vent fluids, like the Endeavour Segment (*Lilley et al., 2003; Ver Eecke et al., 2012*), microorganisms such as microaerophiles and dissimilatory iron reducers are likely to play a more prominent ecological role than organisms that prefer highly reduced conditions for growth (*Flores et al., 2011; Hentscher & Bach, 2012*). At Endeavour, hyperthermophilic iron reducers are commonly found in hydrothermal chimneys while hyperthermophilic methanogens are either absent or less abundant (*Ver Eecke et al., 2009; Zhou et al., 2009; Ver Eecke et al., 2012*).

Fe(III) (oxyhydr)oxides are abundant terminal electron acceptors for microbial respiration in mildly-reducing anoxic habitats (*Lovley et al., 2004*). While most studies on microbial dissimilatory iron reduction have focused on proteobacteria (*Weber et al., 2006*), which typically grow best at 20-45°C, the process is also catalyzed by hyperthermophilic archaea (*Vargas et al., 1998*). Specifically, several species of *Pyrobaculum* can reduce either the mineral ferrihydrite [$Fe_{10}O_{14}(OH)_2$] or soluble Fe^{3+}-citrate (*Kashefi & Lovley, 2000; Feinberg & Holden, 2006; Feinberg et al., 2008*), with magnetite [Fe_3O_4] formed as the end-product of ferrihydrite reduction (*Kashefi et al., 2008*). *Ferroglobus* and *Geoglobus* species couple the oxidation of H_2, acetate, and organic compounds with the dissimilatory reduction of ferrihydrite (*Tor & Lovley, 2001; Tor et al., 2001; Kashefi et al., 2002*). A member of the Desulfurococcales (strain 121) couples formate oxidation with ferrihydrite reduction at temperatures up to 121°C (*Kashefi &*

Lovley, 2003). Hyperthermophilic iron-reducing archaea are found at deep-sea hydrothermal vents (*Kashefi et al., 2002; Kashefi & Lovley, 2003; Ver Eecke et al., 2009*), but our understanding of these organisms, the ecological constraints on their growth in vent environments, the sources of Fe(III) (oxyhydr)oxide for reduction, and the end products of growth is nascent.

In this study, a petrographic context for hyperthermophilic iron reducers was established using most-probable-number estimates to determine the location and abundances of the organisms in an active hydrothermal chimney and thin-section photomicrography of the same chimney to identify possible sources of Fe(III) (oxyhydr)oxides for iron reduction. This was performed on a hydrothermal chimney collected from the Dante edifice in the Main Endeavour vent field that was venting 336°C fluid at the time of collection. We also report the characteristics of ferrihydrite reduction catalyzed by two hyperthermophilic archaea, *Hyperthermus* sp. Ro04 and *Pyrodictium* sp. Su06, isolated from two actively venting hydrothermal chimneys (Roane in 2004 from the Mothra vent field and Sully in 2006 from the Main Endeavour vent field) at Endeavour. Specifically, we measured growth rates on laboratory-synthesized ferrihydrite and estimated cell yields based on Fe^{2+} production and cell-specific rates of Fe^{2+} production at varying temperatures, pHs and chlorinities. We identified the mineral end product of ferrihydrite reduction by our model organisms using Mössbauer spectroscopy. These data are needed to model the habitability of chimneys for hyperthermophilic iron reducers and the potential biogeochemical impact of these organisms in hydrothermal systems.

3.3 Materials and Methods

3.3.1 Field studies

In order to put the growth of hyperthermophilic iron reducers into an environmental context, a hydrothermal chimney (~30 cm tall) that was actively venting 336°C hydrothermal fluid was recovered in 2009 from the Dante edifice within the Main Endeavour vent field using the deep-sea research submarine *Alvin*. The number of culturable hyperthermophilic iron reducers per gram of sample material was determined by incubating material subsampled from the interior and exterior of the sulfide at 90°C in modified DSM 1210 medium (see below) using the most-probable-number (MPN) technique as described previously (*Ver Eecke et al., 2009*).

The major mineral phases present in the Dante chimney were determined by cutting thin sections (30 µm thick) from the parts of the chimney adjoining the portions used for growth enrichments. The samples were first strengthened by impregnation with an epoxy prior to being cut with a rock saw due to the highly porous and fragile nature of the chimney. Sections were cut perpendicular to the long axis (and primary flow direction) of the chimney in order to maximize the cross-sectional coverage from the outer wall towards the inner flow channel. The thin sections were examined using an Olympus BX 51 polarizing petrographic microscope with an attached Olympus DP71 digital camera. Sections were observed under both transmitted and reflected light modes, in order to observe the textural and paragenesis relationships between both the mineral phases that transmit light (Fe(III) (oxyhydr)oxides, sulfates, amorphous silica) and the opaque minerals (sulfides).

3.3.2 Organisms used

Hyperthermus sp. Ro04 and *Pyrodictium* sp. Su06 were from the Holden lab hyperthermophile culture collection. They were isolated, but minimally characterized, from active hydrothermal chimneys from the Endeavour Segment as previously described (*Ver Eecke et al., 2009*). *Hyperthermus butylicus* DSM 5456 and *Pyrodictium abyssi* DSM 6158 were purchased from the Deutsche Sammlung von Mikroorganismen und Zellkulturen (DSMZ; Braunschweig, Germany) for comparison.

3.3.3 Growth conditions

The growth medium for strains Ro04 and Su06 and the MPN estimates was based on DSM Medium 1210 (*Kashefi et al., 2002*) except that acetate was omitted, yeast extract was increased from 0.01% to 0.02% (wt/vol), and cysteine-HCl was increased from 0.25 mM to 0.5 mM. The carbon and energy sources for strains Ro04 and Su06 were the 0.02% yeast extract present in the medium and the H_2-CO_2 present in the headspace, respectively. The terminal electron acceptor was 100 mmol/l ferrihydrite and was synthesized as previously described (*Lovley & Phillips, 1986*). Fe^{3+}-citrate (20 mM), 10 mM $Na_2S_2O_3$, 10 mM KNO_3 and 0.1% (wt/vol) elemental sulfur were also tested as terminal electron acceptors, along with growth

without an added electron acceptor. The medium was pH balanced to 6.80 ± 0.05 (room temperature), or as specified for the pH range experiment, at the outset of the experiment. The cysteine-HCl mentioned above was added as the reducing agent to remove any residual O_2. The headspace was 2 atm of N_2-CO_2 (80%:20%) for strain Ro04 and 2 atm of H_2-CO_2 (80%:20%) for strain Su06 and the MPNs. *H. butylicus* and *P. abyssi* were incubated in modified DSM Medium 1210 with 100 mmol/l ferrihydrite at pH 6.8 and pH 5.5, respectively, with 2 atm of H_2-CO_2 in the headspace. *H. butylicus* was also grown fermentatively at pH 6.8 without an added terminal electron acceptor, and *P. abyssi* was grown at pH 5.5 with 10 mM $Na_2S_2O_3$ substituted for iron as the electron acceptor.

The effect of chlorinity on growth was determined by varying the NaCl concentration from 4.5 g/l to 45 g/l. For the pH experiment only, media were pH balanced at pH 5.0 and 6.0 using 5 mM MES (morpholineethanesulfonic acid) buffer, at 7.0 and 8.0 using 20 mM PIPES [piperazine-*N*,*N*′-bis(2-ethanesulfonic acid)] buffer, and at 8.5 and 9.0 using 30 mM $NaHCO_3$ buffer (*Feinberg et al., 2008*). There was less than 0.5 pH unit shift in the pH of the media following incubation. Otherwise, only 30 mM $NaHCO_3$ was used to buffer the medium at pH 6.8 for all other experiments. All media were sterilized by heating the complete medium in their containers at 95°C for 1-2 h prior to inoculation.

For kinetic experiments, cultures were grown in 10 ml of medium contained within Balch tubes, and incubated in a forced-air oven at 90°C unless otherwise stated. A logarithmic growth-phase culture grown and transferred on a particular medium at least three times was used to inoculate 12 Balch tubes simultaneously. At various time points over a 20-30 h period, a pair of Balch tubes was permanently removed from incubation. An aliquot from each tube was preserved with 2% (vol/vol) formaldehyde and mixed 1:1 in an oxalate solution (28 g/l ammonium oxalate and 15 g/l oxalic acid) to dissolve the iron. The concentration of cells in each tube was determined by epifluorescence microscopy (*Hobbie et al., 1977*). Cells were filtered onto a 0.2-µm-pore-size membrane filter prestained with Irgalan black (Sterivex), stained with 0.1% (wt/vol) acridine orange for 2 min, and counted with a Nikon eclipse E400 microscope (including a 0.5-1.25 100× oil iris). The specific growth rate (k) of the culture was determined by a best-fit curve through the logarithmic portion of the growth data. Fe^{2+} concentration was determined spectrophotometrically using the ferrozine assay method (*Phillips & Lovley, 1987*). Errors for epifluorescence cell counts were ± 9% and for Fe^{2+} were ± 8%. Growth yield based on

Fe^{2+} production (*Y*) was determined by assuming a linear relationship between cell and Fe^{2+} concentrations during growth, and from the slope of cell concentration versus Fe^{2+} concentration for each time point in each growth experiment for the logarithmic phase data points. Statistical significance of each growth rate and cell yield was determined by using linear regression analysis ($\alpha = 0.1$). The cell specific rate of Fe^{2+} production was determined by dividing the specific growth rate (*k*) by the product of $0.693 \times Y$ (*Ver Eecke et al., 2013*).

Uninoculated media with the various pH buffers were incubated for up to 24 h at 92°C to test for abiotic iron reduction. Uninoculated media containing 0.05% (wt/vol) each of sodium acetate, sodium propionate, and maltose, and 0.05% (vol/vol) each of ethanol, butyric acid, and *n*-butanol, were individually incubated for 24 h as further controls representing possible metabolites secreted by the cells that could potentially reduce the iron (0.6 mM acetate and < 0.05 mM ethanol were measured in spent growth medium). Spent growth medium was filter sterilized, added to fresh ferrihydrite, and incubated anaerobically at 92°C for 24 h as another abiotic test condition.

3.3.4 Electron microscopy

To examine the interaction between cells and insoluble iron, 10 ml of culture within a sealed Balch tube were fixed by adding 0.2 ml of 50% glutaraldehyde (EM-grade) with gentle agitation and incubation at room temperature for 1 h. Samples with non-dissolved iron were taken from the bottom of the Eppendorf tubes and applied to plasma-treated carbon films (ca. 0.5 nm thickness) on 400 mesh copper grids and incubated in a moist chamber for 5 min. Grids were then rinsed by 2 cycles of incubation with a drop of 3% (wt/vol) NH_4OH, drained on filter paper, incubated for 15 sec with a drop of 2% (wt/vol) aqueous uranyl-acetate (pH 4), and drained onto filter paper. Once air dried, the grids were viewed with a JEOL-100S transmission electron microscope.

3.3.5 Mineral analyses

Transformation of iron oxide minerals was determined for both abiotic and biotic conditions using the 1 mol/l ferrihydrite stock solution, uninoculated and unincubated DSM 1210

medium with 100 mmol/l ferrihydrite, uninoculated medium that was incubated at 92°C for 24 h, and inoculated growth medium that was incubated at 92°C until the culture reached late logarithmic growth phase. These were dried at room temperature in an anoxic chamber on glass Petri plates, ground down using a mortar and pestle, and sealed in anoxic serum bottles with a N_2 headspace for transport and storage. The resultant samples were roughly 1% oxide by volume and 99% halite from the evaporated growth medium based on visual inspection under a petrographic microscope.

For x-ray diffraction (XRD) analysis, samples were analyzed by Activation Laboratories Ltd. (Ancaster, Ontario, Canada). Each sample was pulverized and a portion of the powder mounted onto a standard holder. The XRD analysis was performed on a Panalytical X'Pert Pro diffractometer, equipped with a Cu x-ray source and an X'Celerator detector, operating at the following conditions: 40 kV and 40 mA; range 4.5-80 deg 2θ; step size 0.017 deg 2θ; time per step 50.165 sec; fixed divergence slit, angle 0.25 deg; sample rotation: 1 rev/sec. The XRD procedure detects crystalline materials that are present in amounts more than 3% of the total sample volume.

For Mössbauer spectroscopy, samples were mounted into holders backed by Kapton® polyimide film tape. For reacted samples, which are low in Fe, about 300 mg was used to completely fill the sample holder volume. Fe oxides were mounted using ~20 mg of sample and 280 mg of table sugar to thin the sample and optimize spectral acquisition. Spectra were acquired at temperatures ranging from 4-295 K using a source of ~40 mCi ^{57}Co in Rh on a WEB Research Co. model WT302 spectrometer (Mount Holyoke College) equipped with a Janis closed cycle He cooling system. Data were collected at 295K over a ± 4 mm/s velocity range and at 4K over a ± 10 mm/s velocity range in 2048 channels with acquisition times ranging from 12 hours to 6 days depending on the Fe content of the samples. Spectra were corrected for nonlinearity via interpolation to a linear velocity scale, which is defined by the spectrum of the 25 μm Fe foil used for calibration. All data were corrected to remove the fraction of the baseline due to the Compton scattering of 122 keV gamma rays by electrons inside the detector. All Mössbauer data were posted for public use (www.mtholyoke.edu/courses/mdyar/database/).

All spectra were fit using Mexdisd (*De Grave & van Alboom, 1991*). The program uses a line-shape-independent model for fitting the spectra and solves the full hyperfine-interaction Hamiltonian, producing a distribution of values for the hyperfine field and using quadrupole

shift, center shift, and line width as adjustable parameters. It does not presume any particular shape of the distribution. Isomer shifts (IS), and quadrupole splittings (QS), and areas of the doublets and sextets were allowed to vary, with widths of both peaks in each doublet or all peaks in a sextet coupled to vary in unison (i.e., one width for each doublet/sextet, but every doublet/sextet independent). The area of the peaks that make up each doublet or sextet is proportional to the percentage of Fe in that site. Errors (accuracy) of peak areas are roughly ± 3% absolute, on Mössbauer parameters are ± 0.03 mm/s, and on B_{hf} ~± 0.2 Tesla for individual sextets or doublets.

Although 295K data were collected for all samples, they were not useful because some of the Fe oxides were too fine-grained to be magnetically ordered at that temperature. Such superparamagnetism has been observed in both biogenic and synthetic magnetite at particle sizes below ~13 nm, often manifested as a doublet in room temperature Mössbauer spectra (*Hassett et al., 1980; Vali et al., 2004; Weiss et al., 2004; Ambashta et al., 2005; Kalska-Szostko et al., 2006; Bandhu et al., 2009; Li et al., 2009; Marquez-Linares et al., 2011; Starowicz et al., 2011; Zajac et al., 2011*). The magnetic field of superparamagnetic nanoparticles varies in direction faster than the inverse lifetime of the ^{57}Fe nuclear excited state (on the order of 10^7/sec). Net magnetization appears to be zero when measured over the time scale of ^{57}Fe Mössbauer spectroscopy, and a quadrupole-split doublet is observed at room temperature despite a large magnetization of the material (*Hassett et al., 1980*).

So 4K data were collected for all samples to slow down the superparamagnetic relaxations of the small particles and produce magnetic ordering (e.g., *Murad, 1992*), resulting in superimposed sextets, each of which is described by the Mössbauer parameters. For those sextets, isomer shift is the center of gravity of the six peaks. Quadrupole splitting for a sextet is defined as $(l_6 - l_5) - (l_2 - l_1)$, where l_i is line position with peaks numbered from left to right, if the electric quadrupole interaction is small. The combination of IS and QS parameters (along with B_{hf} in the case of magnetically ordered phases) is usually sufficient to identify the valence state and site occupancy of Fe in a given site and individual mineral.

However, at 4K the Mössbauer spectral features are broad because Fe oxides may have multiple non-unique sextets arising from subtle variations in the coordination polyhedra around Fe atoms. For example, Murad (1992) notes that “no unique set of Mossbauer parameters can be given for ferrihydrite at 4.2K” and Murad and Johnston (1988) and Berry *et al.* (1998) report that

the lowest temperature Mössbauer measurements of magnetite can be modeled with up to five sextets. Thus numerous acceptable fits could be obtained for each spectrum using from 3-5 sextet distributions, and the parameters of the individual sextets are not very helpful in discerning the oxide that is present. To aid in the comparison between the unknown samples and nano-phase iron oxide standards, and to mediate possible bias from arbitrary fitting of a specific number of distributions, an average sextet IS, QS, and B_{hf} were calculated for each spectrum. The average was described by the sum of the products of the fit parameter of an individual sextet and the relative contribution of that individual sextet to the total sextet area of the spectrum, as follows:

Average $IS_{sextet} = IS_{sextet1} * (Area_{sextet1} / \text{Total } Area_{sextet}) + \ldots + IS_{sextetn} * (Area_{sextetn} / \text{Total } Area_{sextet})$.

The average sextet IS, QS, and B_{hf} are effectively the parameters that would result if the spectrum were fit with just one sextet, but total fit (as indicated by a χ^2 goodness of fit test) improves with the inclusion of multiple distributions. Use of average fit parameters for characterization eliminates bias in fit parameters of individual sextets related to the total number of distributions used to fit each spectrum. It is possible that the use of average sextet fit parameters masks some contribution of unused growth media to the spectrum. All 4K spectra were fit multiple times with varying numbers of sextet distributions, and the resulting average fit parameters were consistent within a precision of ± 0.05 mm/s for IS, ± 0.03 mm/s for QS, and ± 3.7 kOe for B_{hf} across fits for a single sample.

3.4 Results

3.4.1 Petrography of Dante chimney

The petrography of the hydrothermal chimney collected from the Dante edifice on the Endeavour Segment was carefully examined to understand the nature of the chimney habitat and the sources of potential terminal electron acceptors for hyperthermophilic iron reduction. Based on thin section photomicrography, the mineralogy of the chimney is dominated by white (with some minor pink) anhydrite ($CaSO_4$, >50%) with light grey, sphalerite (ZnS)/wurtzite ($Zn,Fe^{2+}S$). An outer 2 mm dark green/grey marcasite ($Fe^{2+}S_2$) crust occurred around a single sphalerite/wurtzite-rich, sulfate-poor secondary flow channel that occurred outside of the primary fluid conduit. Distribution of sulfide versus sulfate minerals is irregular, with areas of

100% sulfate minerals and others that were void of sulfate. A weak mineralogical repeating concentric zonation occurs between sulfate- and sulfide-rich zones (each zone ~5 mm thick). The porosity of the sample was visually estimated by hand lens to be ~40% near the exterior to up to 70% in the interior. A single irregular primary flow channel ~2 cm in diameter is lined with pink/grey fine anhydrite peppered with 0.5 mm euhedral chalcopyrite ($Cu,Fe^{2+}S_2$) crystals. Several minor secondary flow channels with thin chalcopyrite rinds are also present. From thin section observations, the exterior margins of the sample consist of blocky and dendritic marcasite with minor, late-stage sphalerite (Fig. 3.1a). A sharp mineralogical contact separates this outer layer from an inner sphalerite-rich layer with minor pyrrhotite ($Fe^{2+}_{0.8\text{-}0.9}S$) and very minor chalcopyrite. Another sharp boundary separated this layer from the innermost, high-temperature zone containing abundant bladed pyrrhotite with minor sphalerite. This zone also contains abundant interstitial anhydrite. Late stage Fe(III) (oxyhydr)oxide-stained amorphous silica coats sulfide minerals in all zones (Fig. 3.1b).

3.4.2 Hyperthermophilic iron reducer abundances in the Dante chimney

Based on MPN enrichments, it was estimated that there were 1,740 hyperthermophilic iron reducers per gram (dry weight) of sample on the exterior surface of the Dante chimney, and 10 hyperthermophilic iron reducers per gram in the soft marcasite-sphalerite-rich interior. All of the most-probable-number incubations that showed growth contained coccoid-shaped cells that produced Fe^{2+} based on the ferrozine assay and black iron that was strongly attracted to a magnet.

3.4.3 Biogenic iron reduction

Hyperthermus sp. strain Ro04 and *Pyrodictium* sp. strain Su06 each showed exponential growth on ferrihydrite with concomitant Fe^{2+} production (Fig. 3.2). The end-product of ferrihydrite reduction following growth was black and strongly magnetic. The maximum cell concentrations reached by both strains were 6×10^7 cells/ml. There was a linear relationship between cell concentration and Fe^{2+} concentration throughout logarithmic growth. Uninoculated, incubated media showed a small (< 3 mM) initial abiotic reduction of iron within the first 30 min

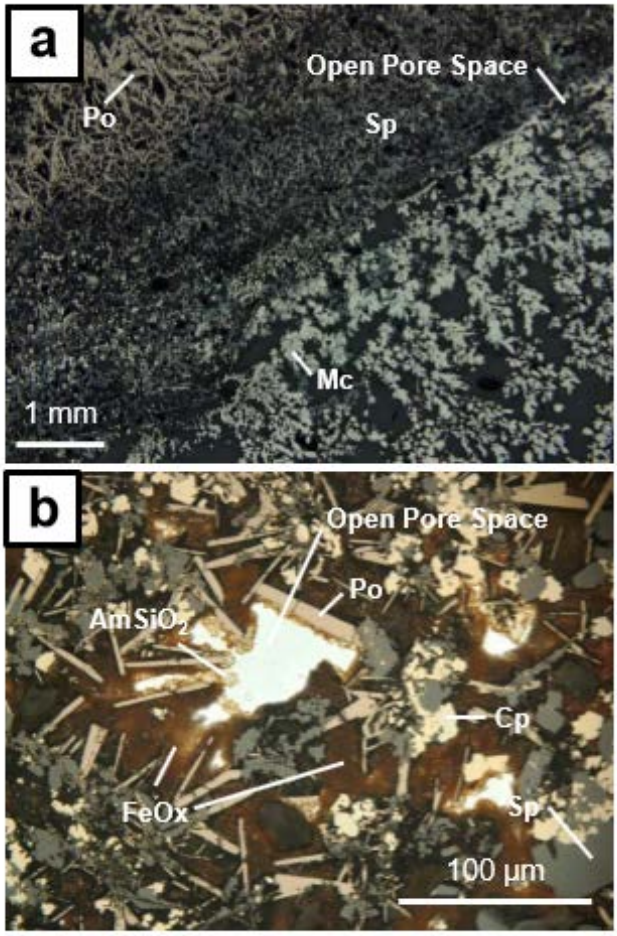

Figure 3.1. (a) Reflected light photomicrograph of the Dante hydrothermal mineral sample showing mineralogical zonation from low-temperature marcasite (Mc)-rich exterior (bottom right) through a sphalerite (Sp)-rich zone to a high-temperature bladed pyrrhotite (Po)-rich zone (top left). (b) Reflected and transmitted light photomicrograph showing Fe(III) (oxyhydr)oxides (FeOx) stained amorphous silica ($AmSiO_2$) coatings on pyrrhotite, sphalerite, and chalcopyrite (Cp) minerals in an otherwise porous zone.

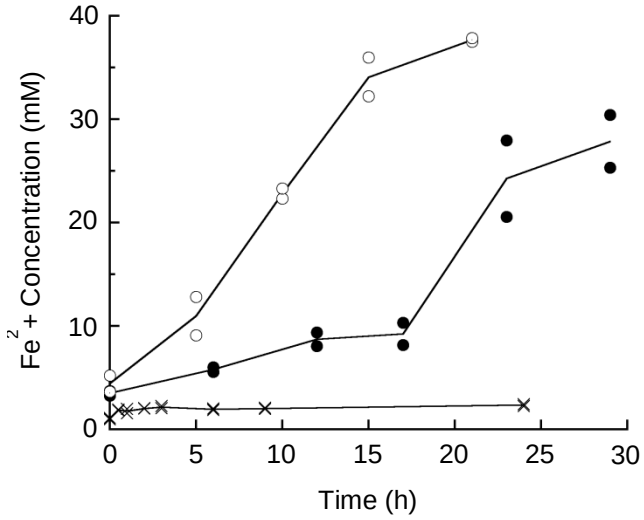

*Figure 8*Figure 3.2. Fe^{2+} concentrations in the growth medium during growth of *Hyperthermus* sp. Ro04 (●) and *Pyrodictium* sp. Su06 (○), and in uninoculated medium that was incubated at 92°C with 30 mM $NaHCO_3$ at pH 6.8 (×).

of incubation without any further iron reduction over a 24 h period (Fig. 3.2), and the material was neither black nor magnetic. This was the case for all abiotic media tested, including the pH experiment where MES and PIPES were used as buffers. There also was < 3 mM abiotic reduction of iron when acetate, propionate, butyrate, maltose, ethanol, *n*-isobutanol or sterile spent medium were separately added to the medium and incubated at 92°C for 24 h. There was no ferrihydrite reduction when strain Ro04 and strain Su06 were incubated at room temperature, nor was there any ferrihydrite reduction by the cells at 92°C in the absence of carbon and energy sources. Neither strain grew on Fe^{3+}-citrate, $Na_2S_2O_3$ or elemental sulfur or in the absence of an added terminal electron acceptor. Only strain Su06 grew on KNO_3.

For both strain Ro04 and strain Su06, growth on ferrihydrite was observed between 82°C and 97°C with an optimum of 90-92°C (Fig. 3.3a), between pH 5.0 and 9.0 with optima of pH 8.0 for strain Ro04 and pH 5.0 for strain Su06 (Fig. 3.3b), and between 254 mM and 716 mM chloride with optima of 425 mM to 562 mM chloride (Fig. 3.3c). Growth yields varied between 0.5×10^{12} cells/mol Fe^{2+} and 5×10^{12} cells/mol Fe^{2+} for both organisms and all growth conditions tested, except at superoptimal temperatures for strain Su06 (Fig. 3.3d-f). The cell-specific rate of Fe^{2+} production for strain Ro04 ranged from 0.03 to 0.23 pmol Fe^{2+}/cell/h for all conditions, while the rate for strain Su06 ranged from 0.05 to 0.54 pmol Fe^{2+}/cell/h for all conditions except at superoptimal temperatures where activities were up to 1.81 pmol Fe^{2+}/cell/h (Fig. 3.3g-i). These data are summarized in Tables S1 and S2.

Hyperthermus butylicus was grown at 95°C in modified DSM 1210 medium with and without the addition of 100 mmol/l ferrihydrite. Its growth rate without an added terminal electron acceptor (0.173 h^{-1} ± 0.031 h^{-1} [90% CI]) was not significantly different than the rate with added ferrihydrite (0.153 h^{-1} ± 0.010 h^{-1}). When *H. butylicus* was grown with ferrihydrite, Fe^{2+} concentrations increased exponentially in direct proportion to cell concentrations, but the iron did not turn black and was not magnetic. The *H. butylicus* growth yield (*Y*) was 5.15×10^{12} cells/mol Fe^{2+} ± 1.23×10^{12} cells/mol Fe^{2+} (90% CI) and the cell-specific Fe^{2+} production rate was 0.03 pmol/cell/h ± 0.01 pmol/cell/h. The *Y* of *H. butylicus* was significantly higher than the *Y* of strain Ro04 at its optimal growth temperature (2.70×10^{12} cells/mol Fe^{2+} ± 0.46×10^{12} cells/mol Fe^{2+}), and the Fe^{2+} production rate was significantly lower than that of strain Ro04 (0.08 pmol/cell/h ± 0.02 pmol/cell/h). This suggests that the iron reduction by *H. butylicus* was a byproduct of growth by other means. There was no growth of *Pyrodictium abyssi* at 95°C on 100

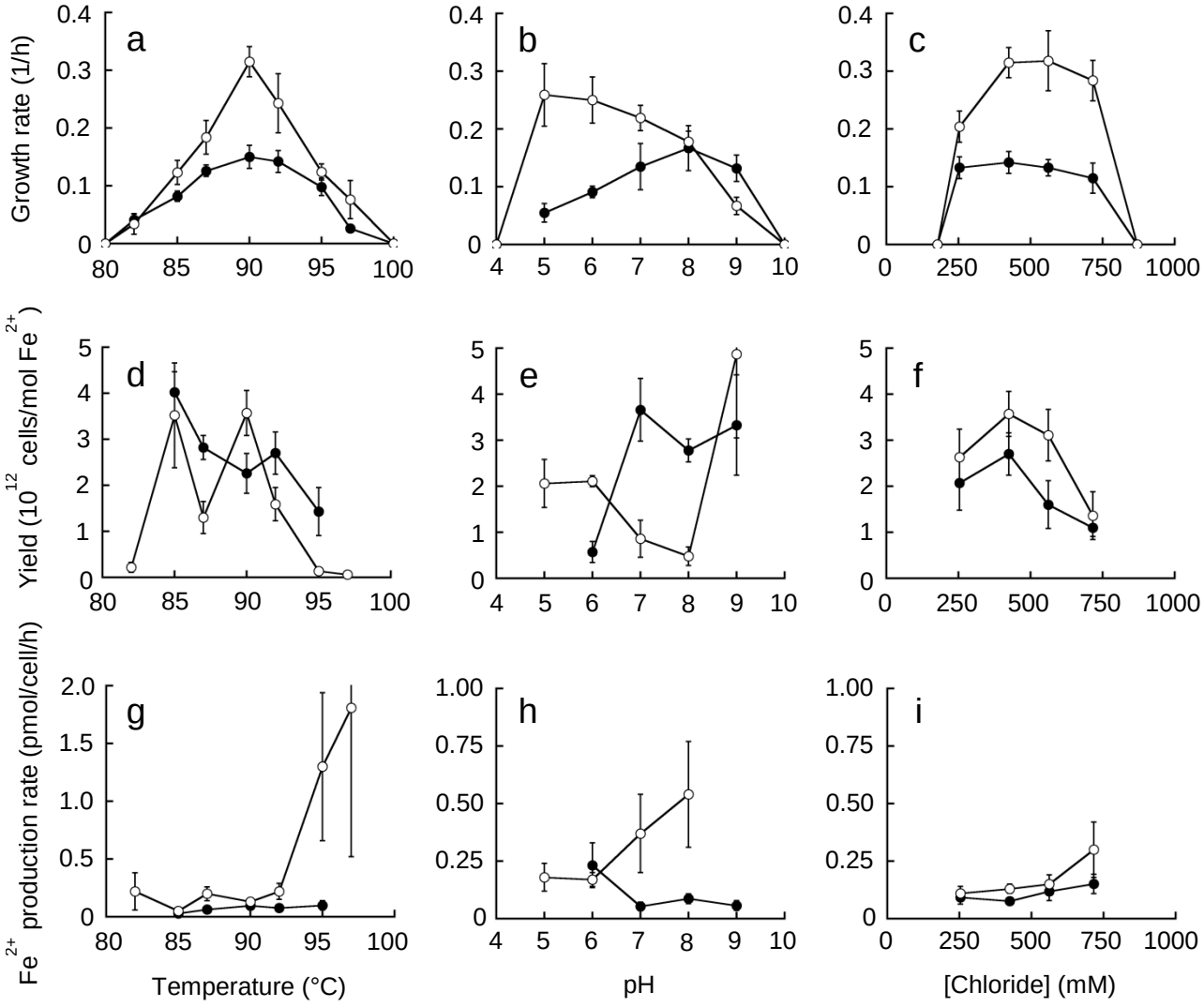

*Figure 9*Figure 3.3. Growth rates (a-c), cell yields (Y) based on Fe^{2+} production (d-f), and cell-specific Fe^{2+} production rates (g-i) for *Hyperthermus* sp. Ro04 (●) and *Pyrodictium* sp. Su06 (○) across their growth range of temperature (a, d, g), pH (b, e, h), and chloride concentration (c, f, i). The error bars represent 90% confidence intervals.

mmol/l ferrihydrite after three consecutive transfers, which did grow when 10 mM $Na_2S_2O_3$ was substituted as the terminal electron acceptor.

3.4.4 Mössbauer spectroscopy and XRD analyses

Mössbauer spectra were acquired at 295 and 4 K from the iron oxide stock solution, the growth medium before and after incubation without cells, and the growth medium after the growth of strains Ro04 and Su06 to late logarithmic growth phase. Fit parameters for room temperature spectra are unaveraged (Table 3.1) and represent individual doublet distributions (Fig. 3.4b). These 295K data were not useful in identifying the iron oxide present because so many iron oxides exhibit a doublet structure with IS ~ 0.36 mm/s and QS ~ 0.65 mm/s at room temperature (Table 3.1) due to fine grain sizes as noted above. So the oxides are all indistinguishable in 295K Mössbauer spectra.

The 4K spectra have broad features but are far more diagnostic of individual species because they include multiple, albeit superimposed, sextet distributions (Fig. 3.4a). The average fitted IS, QS, and B_{hf} parameters for the iron oxide stock solution and the growth media without inoculation before and after incubation for 24 h at 90°C are all consistent with those of the nanophase ferrihydrite standard (Table 3.1). The hyperfine field of their spectra is so low that any significant contributions from Fe in other Fe oxides can be ruled out above 1% of the total iron. The 4 K spectra for the samples where strains Ro04 and Su06 were incubated to late logarithmic growth phase exhibit average sextet parameters of IS = 0.52 and 0.55 mm/s, QS = -0.02 and -0.08 mm/s, and B_{Hf} of 511.0 and 508.6 kOe, respectively. When these parameters are compared to those of other phases listed in Table 3.1, it is apparent that they most closely match those of the 12-nm magnetite standard. Because averaged parameters are being used, it is possible that the reacted samples might represent a mixture of other phases with higher (maghemite) and lower (ferrihydrite) B_{hf}. However, the isomer shift of the bioreduced oxide is significantly higher than all the other oxides we tested, and this could not be achieved by mixing spectra of, for example, ferrihydrite and maghemite. Moreover, the Ro04 and Su06 samples are strongly attracted to a magnet at room temperature. A very limited number of minerals exhibit such behavior, so at least one of them must be present: magnetite, maghemite, greigite (Fe_3S_4), and pyrrhotite ($Fe_{1-x}S$). Maghemite would be a possibility but its isomer shift is significantly

Table 3.1. Mössbauer spectra fit parameters for various experimental samples, iron oxide and sulfide standards at 295K and 4 K

Sample	4K				295K			
	IS (mm/s)	QS (mm/s)	B_{hf} (kOe)	Area (%)	IS (mm/s)	QS (mm/s)	B_{hf} (kOe)	Area (%)
Fe oxide and oxyhydroxide standards*:								
nanoferrihydrite 1GOE 03/2010 Julian Bosch	0.46	-0.02	489.6	100	0.35	0.67	n/a	100
nanoakaganeite 1GOE 07/2010 Julian Bosch	0.49	-0.15	482.2	100	0.36	0.54	n/a	100
nanogoethite C1 Nicholas Tosca	0.50	-0.23	507.2	100	0.37	-0.24	312.3	100
nanohematite Alfa Aesar 22-30 nm	0.45	-0.01	525.9	100	0.33	0.00	489.9	100
lepidocrocite HMM 81159 Zlaté Hory	0.50	-0.21	501.8	100	0.39	0.57	n/a	100
nanomaghemite VI.4 12-nm Ilona Nyiro-Kosa	0.44	-0.05	523.5	100	0.33	-0.05	472.6	84
					0.33	0.91	n/a	16
magnesioferrite 775 John Parise	0.42	0.00	524.5	100	0.30	0.00	469.3	100
nanomagnetite I.1 12-nm Ilona Nyiro-Kosa	0.51	-0.04	512.1	100	0.45	0.01	468.9	87
					0.35	0.71	n/a	13
greigite (Chang *et al.*, 2008)	0.38		319		0.29		312	
	0.66		327		0.53		315	
This study:								
iron oxide stock solution	0.47	-0.02	486.5	100	0.35	0.74	n/a	100
uninoculated, unincubated medium	0.47	-0.04	479.3	100	0.35	0.58	n/a	100
uninoculated medium incub ated at 90°C	0.46	-0.04	487.7	100	0.36	0.52	n/a	100
strain Ro04 logarithmic growth	0.52	-0.02	511.0	100	0.34	0.76	n/a	100
strain Su06 logarithmic growth	0.55	-0.08	508.6	93	0.34	0.72	n/a	67
	1.22	2.77	n.a	7	0.58	2.09	n/a	33
H. butylicus logarithmic growth	0.46	-0.04	488.3	100	0.36	0.62	n/a	100

*data from Breves & Dyar, in preparation. n/a = not applicable

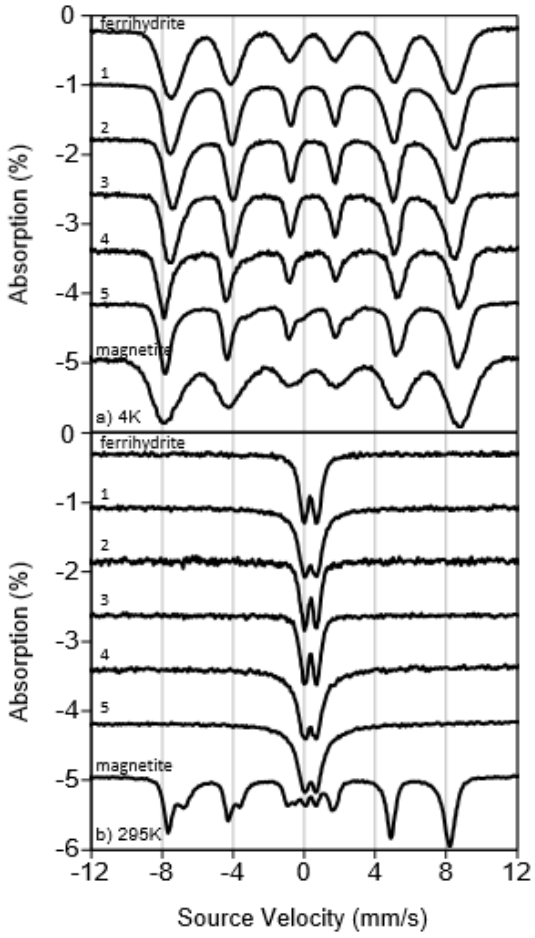

Figure 3.4. Mössbauer spectra at 4 K (a) and room temperature (b) of the iron oxide starting material (1), uninoculated growth medium before (2) and after (3) incubation at 90°C for 24 h, the medium following growth of *Hyperthermus* sp. Ro04 (4) and *Pyrodictium* sp. Su06 (5) to late logarithmic growth phase, along with nanophase ferrihydrite and magnetite standards.

lower than that of magnetite or the reacted samples. Greigite forms under anoxic, sulfate-reducing conditions (*Roberts & Weaver, 2005*) and is isostructural with magnetite but distinguishable because it lacks a low-temperature transition. However, it did not appear in the XRD refinements and its hyperfine field is significantly lower than that of magnetite (*Chang et al., 2008*). The Mössbauer spectrum of nanophase $Fe_{1-x}S$ produces a sextet at 295K (*Lyubutin et al., 2011*) and a hyperfine field averaging 300 bOe at 80K, so the possibility that our reaction products could also be pyrrhotite can be ruled out. For all these reasons, the Mössbauer spectra of the reacted samples are assigned to represent magnetite.

At 295K, Su06 also produced a doublet that is heavily overlapped with magnetite so its area and parameters cannot be accurately determined. However, it is clearly resolved at 4K, where its peak area is 7% of the total Fe (Table 3.1). Because this phase does not magnetically order, it is unlikely to be Fe oxide. The growth medium contains both NaCl and KH_2PO_4, so the best assignment of this doublet is to a phase containing either Cl or PO_4. Cl is usually associated with Fe^{3+} (e.g., the mineral molysite, $Fe^{3+}Cl_3$), but there are many Fe^{2+}-bearing phosphate minerals with analogous parameters found here as extrapolated from 295K spectra reported in Dyar *et al.* (submitted), such as vivianite ($Fe^{3+}(PO_4)_2 \bullet 8(H_2O)$). So this extra doublet is assigned to an Fe phosphate mineral that likely does not participate in the bioreduction process.

The x-ray diffraction patterns of the iron oxide material following growth of strains Ro04 and Su06 were indistinguishable from those of the abiotic control sample, which only showed halite. We presume that the unreacted and reacted iron oxides are too fine-grained and poorly crystalline to be detected by XRD. Thus the XRD results can neither support nor refute the identification of magnetite by Mössbauer spectroscopy.

3.4.5 Electron microscopy

Strain Ro04 and strain Su06 cells were regular to irregular coccoids 0.5-0.8 μm in diameter and were found mostly as singlets or doublets. Transmission electron micrographs show attachment of the cells to electron dense iron particles in the medium (Fig. 3.5).

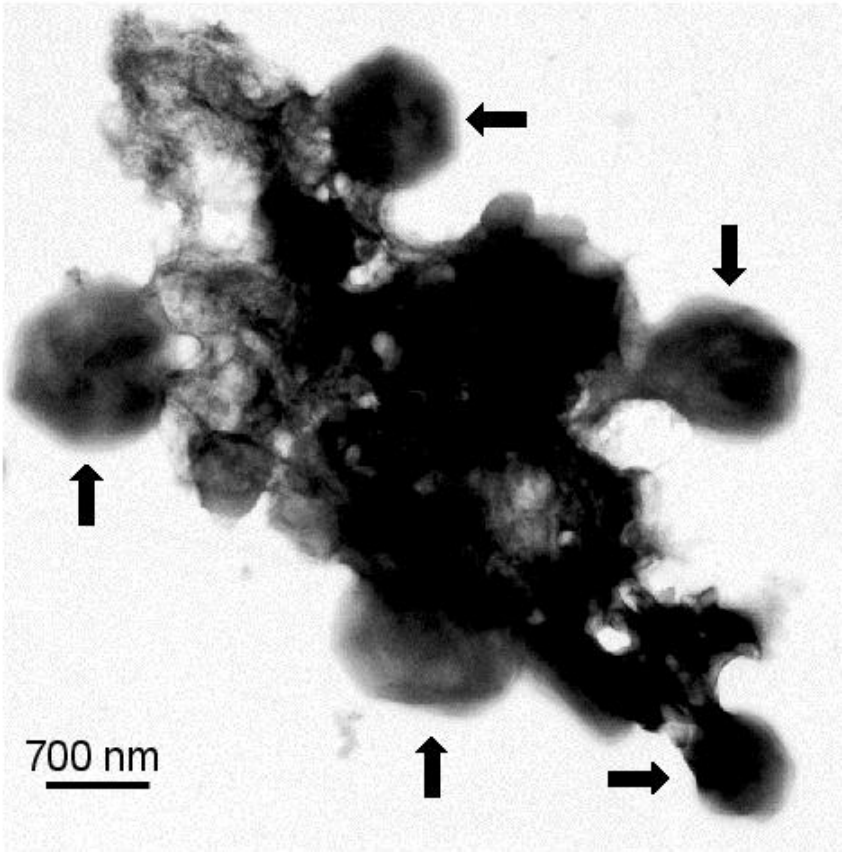

Figure 3.5. Negative-stain transmission electron microscopy of *Hyperthermus* sp. Ro04 with attachment to iron oxide particles. The arrows indicate the locations of the coccoid cells.

3.5 Discussion

Hyperthermus strain Ro04 and *Pyrodictium* strain Su06 grow in direct contact with ferrihydrite. They do not reduce Fe^{3+}-citrate, $Na_2S_2O_3$ or elemental sulfur, or grow purely by fermentation, although strain Su06 will grow by nitrate reduction. They grow over a narrow temperature range (82-97°C), but within pH and chlorinity ranges expected to be found within Endeavour Segment hydrothermal sulfide deposits (*Tivey, 2004*). Hydrogenotrophic strains such as Su06 may provide a slow-growing alternative to fast-growing methanogens at hyperthermophilic temperatures in hydrothermal systems that are H_2 limiting for methanogenesis. The primary constraint for the growth of hyperthermophilic iron reducers may be the availability of ferrihydrite. However, Fe(III) (oxyhydr)oxide, which may contain ferrihydrite in the less acidic conditions at Endeavour, appears to be available in the interior and exterior of hydrothermal chimneys as an oxidized weathering product of the iron sulfide minerals in pore spaces present in the deposits. The microbial end-product of ferrihydrite reduction appears to be nanophase (< 12 nm) magnetite. Magnetite formation is not universal among *Hyperthermus* and *Pyrodictium* species as neither *H. butylicus* nor *P. abyssi* could perform the reaction.

This study was the first to measure growth yield and Fe^{2+} production kinetics for hyperthermophilic iron reducers. These data are necessary to begin modeling the ecology of hyperthermophiles in hydrothermal systems and their biogeochemical impacts across their temperature, pH and chlorinity ranges of growth. Cell yields based on Fe^{2+} production and Fe^{2+} production rates were largely consistent for strains Ro04 and Su06, although Su06 grew faster than Ro04 under most conditions. Similar kinetics data were collected for the hyperthermophilic methanogen *Methanocaldococcus* sp. strain JH146 (*Ver Eecke et al., 2013*). When normalized to moles of electrons transferred to form either Fe^{2+} or CH_4, the rates of metabolite produced for both groups of organisms are comparable. However, cell yields per mole of electron transferred are significantly lower for the methanogen relative to the iron reducers, which may reflect the lower Gibbs energy available for methanogenesis relative to iron reduction. Both strain Su06 and strain JH146 showed a dramatic increase in the rate of metabolite production at superoptimal temperatures, which may be due to higher energy demands of the cells during thermal stress. While more kinetics data are needed from other microorganisms before broad ecological

conclusions can be drawn, the data presented herein demonstrate their utility for future modeling efforts.

Strains Ro04 and Su06 both grew over a pH range of pH 5 to 9. At hydrothermal vents along the Endeavour Segment, the estimated pH of a seawater-hydrothermal fluid mixture at 90°C is ~ pH 6 (*Butterfield et al., 1994*) due to high NH_4^+ concentrations in the hydrothermal fluids that yield a higher fluid pH than is typically found in deep-sea hydrothermal vents (*Tivey et al., 1999*). This may promote the growth of hyperthermophilic iron reducers at Endeavour relative to many other hydrothermal systems where the estimated pH of the fluid at 90°C is below pH 5.

The hydrothermal mineral deposits that form along the Endeavour Segment contain a coarse-grained, highly porous iron-sulfide-rich interior and a thick zone (2-5 cm) near the outer margin that is dominated by amorphous silica (*Tivey & Delaney, 1986; Tivey et al., 1999; Kristall et al., 2006*). Strain Ro04 was isolated in 2004 from an active sulfide chimney that was growing from the top of the Roane sulfide spire within the Mothra vent field, the southernmost known active vent field along the Endeavour Segment. In 1998, the top 2 m of the Roane spire was removed and analyzed for its mineralogy and petrography (*Kristall et al., 2006*). Using thin-section photomicrography, the study showed extensive mineral replacement in the spire and evidence of significant mixing of seawater and hydrothermal fluids in the highly porous outer portions of the structure that led to increased deposition of Fe(III) (oxyhydr)oxide phases a few microns thick that locally form continuous growths that enclose sulfide grains. As reported herein, a similar thin coat of Fe(III) (oxyhydr)oxide was found coating the interior pore spaces of iron sulfide minerals within zones where hyperthermophilic iron reducers had been detected through MPN estimates. This thin coat of Fe(III) (oxyhydr)oxide most likely contains the terminal electron acceptor for hyperthermophilic iron reducers. The outer surface of the Roane sulfide structure was colonized with macrofauna and bacterial mat with fossilized worm tubes penetrating into the outer margin of the deposit. These may be the source of the organic material used by strain Ro04 for growth, which is drawn into the interior of the structures through seawater ingress.

A 16S rRNA gene survey of a hydrothermally active chimney from the Dante edifice within the Main Endeavour Field showed that 47% of the archaeal clones were members of the Desulfurococcales (a third of which were closely related to *Pyrodictium* and *Hyperthermus* spp.)

and 20% were hyperthermophilic heterotrophs (Thermococcales), with a complete absence of any methanogen genes (*Zhou et al., 2009*). Archaeal clones that show high sequence similarity (> 95%) to the 16S rRNA genes from strains Ro04 and Su06 are found in shallow and deep marine hydrothermal environments around the planet (e.g., *Takai et al., 2001; Takai et al., 2004; Nakagawa et al., 2005; Kato et al., 2010; Price et al., 2013*). However, since *Pyrodictium*, *Hyperthermus* and *Pyrolobus* species show more than 97% 16S rRNA gene sequence identity and catalyze different metabolic reactions (autotrophy and heterotrophy; sulfur, nitrate and iron reduction), it is not possible to predict the biogeochemical impact of hyperthermophilic iron reducers based solely on phylogenies.

A culture-dependent survey of seven hydrothermal sulfide deposits from Endeavour showed the presence of hyperthermophilic iron reducers (22-99 cells per g [dry weight] of mineral material) in each deposit (*Ver Eecke et al., 2009*). No hyperthermophilic methanogens were detected in this survey. The abundance of hyperthermophilic iron reducers was much higher (1,740 cells per g [dry weight] of mineral material) on the outer surface of the chimney from the Dante edifice where mineral oxidation by seawater is more likely to occur. Hyperthermophilic methanogens were only found in one of three MPNs from the same sample at a much lower concentration (14 cells per g) (*Ver Eecke et al., 2012*). Like strains Ro04 and Su06, the cells in the iron reducer MPNs in this study were coccoids that grew at 90°C and produced Fe^{2+} that was black and attracted to a magnet. However, it is not known if the organisms in the MPNs were *Pyrodictium* or *Hyperthermus* species or other hyperthermophilic iron reducers. Rather, the results indicate the capacity for microbial iron reduction at hyperthermophile temperatures in this system.

In conclusion, hyperthermophilic iron reducers may be more prevalent than other hyperthermophiles in iron-rich, circumneutral, mildly-reducing environments like those found at the Endeavour Segment. The data herein will assist in determining their ecological significance in hydrothermal systems. The production of nanoscale magnetite may provide a mineral biomarker that could aid in the detection of these organisms in past and present hydrothermal mineral deposits.

CHAPTER 4

HYPERTHERMUS HEPHAESTI Ro04 SP. NOV. AND *PYRODICTIUM DELANEYI* Su06 SP. NOV., NOVEL HYPERTHERMOPHILIC ARCHAEA THAT REDUCE POORLY CRYSTALLINE Fe(III) OXIDE TO MAGNETITE

4.1 Abstract

Two novel hyperthermophilic iron-reducing archaea, designated strain Ro04^T and strain Su06^T, were isolated from actively venting hydrothermal sulfide deposits on the Endeavour Segment, Juan de Fuca Ridge. Strain Ro04^T grew on peptides, reduced poorly-crystalline iron oxide to black ferromagnetic magnetite and produced acetate and minor amounts of ethanol. It did not grow on any other terminal electron acceptor or purely by fermentation. Strain Su06^T also catabolized peptides but only when H_2 was present and reduced poorly crystalline iron oxide to magnetite and nitrate to N_2. They both grew between 82°C and 97°C (T_{opt} 90-92°C) and pH 5.0 and 9.0, but strain Ro04^T had a pH optimum of 8.0 while strain Su06^T had a pH optimum of 5.0. 16S rRNA gene sequence similarity analysis indicated they are 98.4% identical to each other and are most closely related (>98%) to *Hyperthermus butylicus* DSM 5456^T, *Pyrodictium abyssi* DSM 6158^T, *Pyrodictium occultum* DSM 2709^T and *Pyrodictium brockii* DSM 2708^T. The complete genome for Strain Su06 was obtained and genome comparisons done *in silico* between Strain Su06^T against *Hyperthermus butylicus* and *Pyrolobus fumarii,* revealed ANI (average nucleotide identity) scores below 65, TETRA scores above 93, and a 0% probability that the DNA-DNA hybridizations were > 70%, which confirms that it is a novel species. Strain Ro04^T had growth characteristics most similar to *H. butylicus* while strain Su06 was more similar to *P. abyssi*. However, the ability of the strains to reduce iron and their inability to reduce sulfur compounds clearly distinguished them from all of their closest relatives. Phylogenetic, genomic and phenotypic data indicate that strain Ro04^T is novel species of *Hyperthermus* and strain Su06^T is a novel species of *Pyrodictium*. The name *Hyperthermus hephaesti* is proposed for strain Ro04^T and *Pyrodictium delaneyi* is proposed for Su06^T.

4.2 Introduction

The family Pyrodictiaceae, proposed by Burggraf *et al.* (1997), is a group of marine hyperthermophilic members of the Crenarchaeota that consists of five fully characterized species: *Pyrodictium brockii* DSM 2708^T (*Stetter et al., 1983*), *Pyrodictium occultum* DSM 2709^T (*Stetter et al., 1983*), *Pyrodictium abyssi* DSM 6158^T (*Pley et al., 1991*), *Hyperthermus butylicus* DSM 5456^T (*Zillig et al., 1990*) and *Pyrolobus fumarii* DSM 11204^T (*Blöchl et al., 1997*). 16S rRNA gene sequence analysis of these strains shows that they are >97% identical to one another (Fig. 4.1); therefore, their differentiation is based largely on phenotypic traits (Table 4.1). *P. abyssi* and *H. butylicus* are strict peptide heterotrophs that can grow fermentatively or reduce sulfur compounds with concomitant production of short-chain organic acids and alcohols. Their growth is stimulated by H_2. *P. occultum*, *P. brockii* and *P. fumarii* are strict autotrophs that reduce sulfur compounds. *P. fumarii* also reduces nitrate. *P. occultum*, *P. brockii* and *P. fumarii* grow optimally at 105-108°C while *P. abyssi* and *H. butylicus* grow optimally at 97°C and 95-105°C, respectively. The three *Pyrodictium* species and *P. fumarii* grow optimally at pH 5.5 while *H. butylicus* grows optimally at pH 7.0.

Fe(III) oxide is an abundant terminal electron acceptor for microbial respiration in mildly-reducing anoxic habitats. While most studies on microbial dissimilatory iron reduction have focused on mesophilic Proteobacteria, this form of respiration is also found in hyperthermophilic archaea. For example, several species of *Pyrobaculum* can reduce poorly crystalline Fe(III) oxide or soluble Fe^{3+}-citrate (*Kashefi and Lovley, 2000; Feinberg and Holden, 2006; Feinberg et al., 2008*), with magnetite formed as the end-product (*Kashefi et al. 2008*). *Ferroglobus* and *Geoglobus* species couple the oxidation of H_2, acetate, and organic compounds with the dissimilatory reduction of poorly crystalline Fe(III) oxide (*Tor et al., 2001; Tor and Lovley, 2001; Kashefi et al., 2002*). A member of the Desulfurococcales (strain 121) couples formate oxidation with reduction of poorly crystalline Fe(III) oxide at temperatures up to 121°C (*Kashefi and Lovley 2003*).

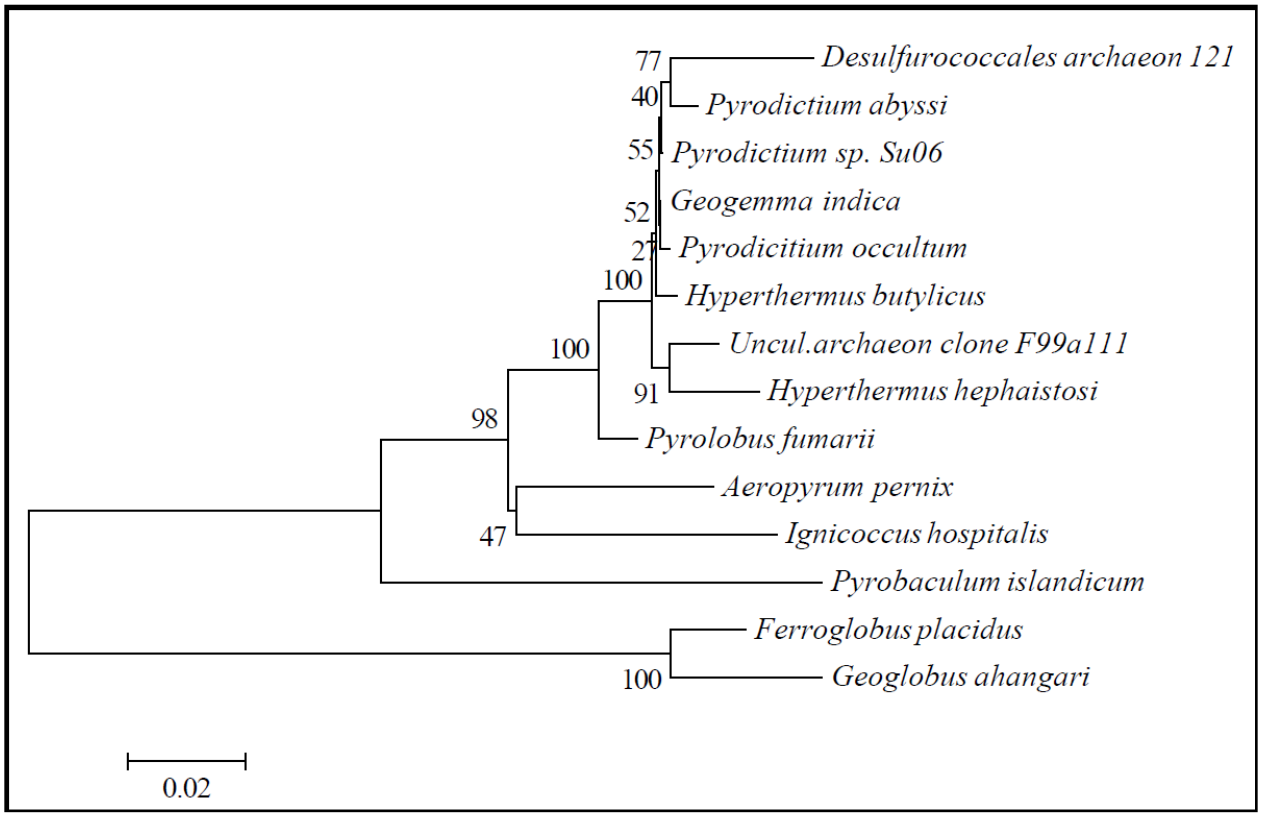

Figure 4.1 Neighbor-joining tree (Tamura et al., 2011) based on almost-complete 16S rRNA gene sequences showing the positions of strain *Hyperthermus* sp. Ro04 (*Hyperthermus hephaistosi*) and strain *Pyrodictium* sp. Su06T amongst its phylogenetic neighbors. *Geoglobus ahangari* and *Ferroglobus placidus* were used as outgroups. Numbers at nodes indicate the levels of bootstrap support (%).Bar, 0.01 substitutions per site.

Table 4.1. Phenotypic characteristics that differentiate strain Ro04^T and strain Su06^T from related type strains in the family Pyrodictiaceae Strains: 1, Ro04^T; 2, Su06^T; 3, *Hyperthermus butylicus* DSM 5456^T (*Zillig et al., 1990*); 4, *Pyrodictium abyssi* DSM6158^T (*Pley et al., 1991*); 5, *Pyrodictium occultum* DSM 2709^T (*Stetter et al., 1983*); 6, *Pyrolobus fumarii* DSM 11204^T (*Blöchl et al., 1997*); and 7, Desulfurococcales strain 121 (*Kashefi & Lovley, 2003*). ND, not determined.

Characteristic	1	2	3	4	5	6	7
Temperature (optimum)	82-97°C (90-92°C)	82-97°C (90-92°C)	>75-108°C (95-106°C)	80-110°C (97°C)	80-110°C (105°C)	90-113°C (106°C)	85-121°C (106-108°C)
pH (optimum)	5.0-9.0 (8.0)	5.0-9.0 (5.0)	(7.0)	4.7-7.1 (5.5)	4.5-7.2 (5.5)	4.0-6.5 (5.5)	ND[a]
NaCl concentration (optimum)	0.9-3.6% (1.9%)	0.9-3.6% (1.9%)	< 3.0% (1.7%)	0.7-4.2% (~2%)	0.2-12% (1.5%)	1-4% (1.7%)	ND
Carbon & energy Sources	strict heterotroph, yeast extract, tryptone, peptone	autotroph, stimulated by yeast extract	strict heterotroph, tryptone	strict heterotroph, protein, acetate, formate, carbohydrate	strict autotroph, stimulated by yeast extract	strict autotroph	formate
Growth stimulated by H_2	No	Required	yes, with S°	Yes	Required	required	ND
Electron acceptors	Fe(III) oxide	Fe(III) oxide, NO_3^-	S°, fermentation	S°, $S_2O_3^{2-}$ (with H_2), fermentation	S°, $S_2O_3^{2-}$	NO_3^-, $S_2O_3^{2-}$, low O_2	Fe(III) oxide
End products	magnetite, acetate, propionate, isobutyrate, isovalerate, ethanol, isopropanol, isobutanol,	magnetite, N_2	H_2S, CO_2, acetate, propionate, phenylacetate, 1-butanol	H_2S, CO_2, isovalerate, isobutyrate, butanol	H_2S	NH_4^+, H_2S	magnetite

Accession numbers: *Hyperthermus hephaesti*, JX227922.1; *Hyperthermus butylicus*, NC_008818.1; uncultured archaeon clone F99a111, DQ228526; *Desulfurococcales* strain 121, AY216935.1; *Geogemma indica*, DQ492260.1; *Pyrodictium occultum*, NR_025933.1; *Pyrodictium abyssi*, KC145153; *Pyrolobus fumarii*, NC_015931.1; *Ignicoccus hospitalis*, NR_028955.1; *Aeropyrum*

pernix, NC_000854.2; *Pyrobaculum islandicum*, NC_008701.1; *Geoglobus ahangari*, NR_041788.1; *Ferroglobus placidus*, NC_013849.1.

4.3 Results and Discussion

Strains Ro04^T and Su06^T were isolated on DSM medium 1210 (*Kashefi et al., 2002*) except that acetate was omitted and the headspace was 2 atm of 80% H_2 and 20% CO_2. They were incubated at 90-95°C for 7 days from actively venting deep-sea hydrothermal sulfide chimneys collected from the Endeavour Segment, Juan de Fuca Ridge in the northeastern Pacific Ocean (*Ver Eecke et al., 2009*). After three successive transfers with evidence of iron reduction, the strains were purified by three successive dilution-to-extinction incubations at 95°C. The last tube in the third dilution series to show growth was used as the source of the strain.

Strain Ro04^T grew equally well when the headspace was replaced with 2 atm of 80% N_2 and 20% CO_2. With an N_2:CO_2 headspace, it grew on 0.02% yeast extract only and on 0.5% (w/v) peptone only, but did not grow on any other carbon sources tested. Strain Su06^T did not grow when its headspace was replaced with N_2:CO_2. It was unable to grow heterotrophically on any organic substrate tested, but its growth with H_2:CO_2 was stimulated by 0.02% (w/v) yeast extract (Difco, vitamin B_{12} fortified) and peptides.

For both strains, the poorly crystalline Fe(III) oxide was reduced to a black ferromagnetic form of iron that was shown by x-ray diffraction to consist of magnetite (Chapter 3). Fe^{2+} concentration was determined following Phillips and Lovley (1987). Strain Ro04^T and strain Su06^T produced up to 40 mM Fe^{2+} produced up to 40 mM Fe^{2+}, both in a growth-dependent manner. Uninoculated growth media showed <2 mM Fe^{2+} production following 24 h of incubation at 92°C that occurred within the first 30 min of incubation. Less than 3 mM Fe^{2+} was produced when anoxic cell-free spent supernatant was incubated at 92°C for 24 h with fresh poorly crystalline Fe(III) oxide, and less than 3 mM Fe^{2+} was produced when 0.02% (v/v) each of ethanol and butanol and 0.02% (w/v) each of maltose and glucose were separately added to uninoculated medium and incubated at 92°C for 24 h. Therefore, the reduction of poorly crystalline Fe(III) oxide to magnetite was biogenic. Neither strain grew when the poorly crystalline Fe(III) oxide was replaced with goethite, hematite, maghemite, lepidocrocite, Fe(III)-citrate, elemental sulfur, thiosulfate or O_2, and neither strain grew in the absence of an electron acceptor. Strain Su06^T did grow when NO_3^- was used as an electron acceptor but strain Ro04^T did not. Gas chromatography showed that N_2 was produced by strain Su06^T, and the washed

insoluble protein fraction contained dissimilatory nitrate reductase activity using the enzyme activity assay of Afshar *et al.* (1998).

Specific growth rates were measured by determining cell concentrations at various growth time points during growth. Samples were preserved with 2% (v/v) formaldehyde, mixed 1:1 in an oxalate solution (28 g/l ammonium oxalate and 15 g/l oxalic acid) to dissolve the iron, stained with 0.1% (wt/vol) acridine orange for 2 min, and counted using epifluorescence microscopy following Hobbie *et al.* (1977). The growth temperature ranges for strain Ro04^T and Su06^T were both 82-97°C with optimal growth temperatures of 90-92°C. Both strains grew between pH 5.0 and pH 9.0. The optimal growth pH for strain Ro04^T was pH 8.0 and for strain Su06^T was pH 5.0. Both strains grew uniformly well between 0.9% and 3.6% NaCl.

Strain Ro04^T and strain Su06^T were regular to irregular coccoids 0.5-0.8 µm in diameter and were found mostly as singlets or doublets. They were fixed with 1% (v/v) electron microscopy-grade glutaraldehyde and negatively stained with 2% (w/v) aqueous uranyl acetate (pH 4). The grids were viewed with a JEOL-100S transmission electron microscope, which showed lophotrichous flagellation of the cells.

Genomic DNA was extracted using a Power Soil DNA isolation kit (MoBio^{TM}). The 16S rRNA gene sequence was amplified by PCR using archaeal primers 4aF (5′-TCC GGT TGA TCC TGC CRG-3′) and 1391R (5′-GAC GGG CRG TGW GTR CA-3′) (Hugenholtz and Goebel, 2001) using PCR mixtures following Murray *et al.* (1996). Sequencing was performed at the University of Massachusetts Amherst Sequencing Facility. The resulting sequences were aligned using ClustalW in BioEdit (v. 7.1.3.0, Hall 1999) and compared to sequences in GenBank using BLAST (*Altschul et al., 1990*). The evolutionary history was inferred using the Neighbor-Joining method (*Saitou & Nei, 1987*). The bootstrap consensus tree inferred from 1000 replicates (*Felsenstein, 1985*) is taken to represent the evolutionary history of the taxa analyzed. The evolutionary distances were computed using the Maximum Composite Likelihood method (*Tamura et al., 2004*) and are in the units of the number of base substitutions per site. There were a total of 1254 positions in the final dataset. Phylogenetic analyses were conducted in MEGA4 (*Tamura et al., 2007*).

It is evident from the phylogenetic tree based on the neighbor-joining algorithm that strain Ro04^T and strain Su06^T formed a cluster with *Pyrodictium abyssi* DSM 6158^T, *Pyrodictium occultum* DSM 2709^T, *Pyrodictium brockii* DSM 2708^T and *Hyperthermus*

butylicus DSM 5456^T within the family Pyrodictiaceae (Fig. 4.1.). Strain Ro04^T and Strain Su06^T each showed highest 16S rRNA gene similarity with *Pyrodictium abyssi* DSM 6158^T (98.5% and 99.9%, respectively). Strain Ro04^T also showed high similarity values with strain Su06^T (98.4%), *Hyperthermus butylicus* DSM 5456^T (98.3%), *Pyrodictium occultum* DSM 2709^T (98.3%) and *Pyrodictium brockii* DSM 2708^T (98.2%). Strain Su06^T showed high similarity values with *Pyrodictium occultum* DSM 2709^T (99.8%), *Pyrodictium brockii* DSM 2708^T (99.7%) and *Hyperthermus butylicus* DSM 5456^T (99.7%).

Due to the high 16S rRNA sequence similarity between the entire genus (>98%) and the development of rapid and cost-effective next-generation sequencing technologies, whole genome comparisons *in silico* between Strain Su06^T and the two only other completed genomes: *Hyperthermus butylicus* and *Pyrolobus fumarii* were performed. *In silico* genome comparisons were done as previously described (*Konstantinidis et al., 2006* and *Chun and Rainey, 2014*). One output of the comparison is the so-called 'average nucleotide identity' (ANI) of two complete genomes. An ANI score of 95% has been shown to correspond to 70% DNA-DNA homology, which is the threshold for defining a new species (*Brenner et al., 2000*). The ANI scores for comparisons of strain Su06^T with *H. butylicus* and *P. fumarii* were both below 65 yielding a 0% likelihood that strain Su06^T is the same organism as either *H. butylicus* or *P. fumarii*. The whole genome sequences for strain Ro04^T and *Pyrodictium abyssi* are currently being sequenced and will provide further genomes for comparison in the near future.

Based on the phenotypic differences of strains Su06^T and Ro04^T with other *Pyrodictium* and *Hyperthermus* species, and the in silico genome comparison results with strain Su06^T, we propose that both organisms are novel species.

4.3.1 Description of *Hyperthermus hephaesti* sp.nov.

Hyperthermus hephaesti (he.phae.sti Gr. masc. n.; named for the Greek god Hephaestus of fire, volcanoes, and metallurgy).

Obligately anaerobic, regular to irregular cocci 0.5 to 0.8 µm in diameter, lophotrichous flagellation. Growth at 82-97°C (optimum 90-92°C), at pH 5.0-9.0 (optimum pH 8.0), and at 0.9-3.6% NaCl (optimum 1.9%). Minimal doubling time, 4.1 h. Strictly heterotrophic growth by

anaerobic oxidation of yeast extract, peptone and tryptone. Individual amino acids, sugars, formate, butyrate, malate and succinate were not used. Poorly crystalline Fe(III) oxide is reduced to magnetite, with some production of organic acids and alcohols. No stimulation of growth by H_2, and no growth on S°, $S_2O_3^{2-}$, NO_3^-, O_2, goethite, hematite, maghemite or lepidocrocite, or purely by fermentation.

The type strain, Ro04^T was isolated from an active hydrothermal vent sulfide chimney (Roane), Endeavour Segment, Juan de Fuca Ridge.

4.3.2 Description of *Pyrodictium delaneyi* sp.nov.

Pyrodictium delaneyi (de.lan.ey.i; named for Dr. John R. Delaney, hydrothermal vent researcher).

Obligately anaerobic, regular to irregular cocci 0.5 to 0.8 µm in diameter, lophotrichous flagellation. Growth at 82-97°C (optimum 90-92°C), at pH 5.0-9.0 (optimum pH 5.0), and at 0.9-3.6% NaCl (optimum 1.9%). Minimal doubling time, 2 h. Autotrophic growth by H_2 oxidation and CO_2 fixation, but growth stimulated by yeast extract. Individual amino acids, sugars, formate, butyrate, malate and succinate were not used. Poorly crystalline Fe(III) oxide is reduced to magnetite and NO_3^- is reduced to N_2, with some production of organic acids and alcohols. No growth on S°, $S_2O_3^{2-}$, O_2, goethite, hematite, maghemite or lepidocrocite, or purely by fermentation.

The type strain, Su06^T was isolated from an active hydrothermal vent sulfide chimney (Sully), Endeavour Segment, Juan de Fuca Ridge.

CHAPTER 5

DISCUSSION

This dissertation has presented three research projects with the goal of 1) determining whether environmental factors such as fluid chemistry and mineral composition influence microbial community composition within Endeavour hydrothermal chimneys with particular attention given to hyperthermophilic iron reducers, 2) characterizing the growth and metabolite production rates and constraints of two novel hyperthermophilic iron reducers, and 3) determining the mineral end-products of these iron reducers using mineral spectroscopic techniques that have not been used previously with hyperthermophiles. The dissertation is the result of extensive collaborations with mineralogists, petrologists, geochemists, and molecular ecologists. None of the analyses herein could have been accomplished by one researcher (Fig 1.8).

The first research project described hydrothermal vent chimney environments of different types in terms of their mineral compositions and fluid chemistry and then correlated these with the microbial community compositions found within the chimneys. We found that mineralogically diverse hydrothermal chimneys host different types of microorganisms. Chimneys with more reduced minerals were dominated by anaerobes while chimneys rich in oxidized minerals were dominated by aerobes. This project was also the first to use mineral techniques such as Mössbauer, thermal emission, and visible/near-infrared spectroscopy to identify the minerals present within hydrothermal chimneys. This opens the door to using some of these techniques in a non-destructive manner while at sea and also creates new avenues for modeling microbe-mineral interactions and biogenic mineral transformations.

The second research project was the first to characterize the growth and metabolite production rates and constraints of hyperthermophilic iron reducers. In most hydrothermal vent environments, methanogens and sulfur reducers are considered to be the major primary producers at thermophilic temperatures. At the Endeavour Segment, hydrogen concentrations are thought to be too low to support the growth of methanogens. It was suggested that hyperthermophilic iron reducers might be more prominent primary producers at this site (*Ver Eecke et al., 2009*). Understanding growth characteristics of hyperthermophilic iron reducers will

increase our knowledge on biogeochemical cycling and habitability within this and similar environments and

explain why Endeavour may be partial to iron reducers. This project also determined the mineral end-products produced by these iron-reducers using mineral spectroscopic techniques that had not been used previously with hyperthermophiles. Both organisms produced nanophase (<12 nm) magnetite [Fe_3O_4] from laboratory-synthesized ferrihydrite [$Fe_{10}O_{14}(OH)_2$] with no detectable mineral intermediates. These results help to define biosignatures and start to build spectroscopic libraries that can be used to detect similar life in deep-sea hydrothermal vents, in ancient rock formations, and at sites beyond Earth.

The third research project fully characterized two novel hyperthermophilic iron reducers: *Hyperthermus hephaesti* Ro04 and *Pyrodictium delaneyi* Su06. Very little is known about hyperthermophilic iron reducers, especially those from deep-sea hydrothermal vents. Characterization of these organisms opens the door to further ecological end physiological studies to better understand where, how and when these organisms grow and transform minerals.

Habitability of hydrothermal vent chimneys, particularly by hyperthermophilic iron reducers, was the central theme of this dissertation. The many facets of habitability are important for understanding distribution patterns and growth requirements and limitations. The implications of this dissertation range from better understanding microbe-mineral interactions and the effects of minerals on primary production in vent environments.

REFERENCES

Afshar S, Kim C, Monbouquette HG & Schröder I. **(**1998**)** Effect of tungstate on nitrate reduction by the hyperthermophilic archaeon *Pyrobaculum aerophilum*. *Applied Environmental Microbiology* **64**, 3004–3008.

Akerman NH, Butterfield DA, Huber JA (2013) Phylogenetic diversity and functional gene patterns of sulfur-oxidizing subseafloor Epsilonproteobacteria in diffuse hydrothermal vent fluids. *Frontiers in Microbiology* **4**, 185.

Altschul SF, Gish W, Miller W, Myers EW, Lipman DJ (1990) Basic local alignment search tool. *Journal of Molecular Biology* **215**, 403-410.

Ambashta RD, Yusuf SM, Mukadam MD, Singh S, Wattal PK, Bahadur D (2005) Physical and chemical properties of nanoscale magnetite-based solvent extractant. *Journal of Magnetism and Magnetic Materials* **293**, 8-14.

Amend JP, McCollom TM, Hentscher M, Bach W (2011) Catabolic and anabolic energy for chemolithoautotrophs in deep-sea hydrothermal systems hosted in different types. *Geochimica et Cosmochimica Acta* **75**, 5736-5748.

Anderson RE, Beltran MT, Hallam SJ, Baross JA (2013) Microbial community structure across fluid gradients in the Juan de Fuca Ridge hydrothermal system. *FEMS Microbiology Ecology* **83**, 324-339

Baas-Becking LGM (1934) Geobiologie of inleiding tot de milieukunde. The Hague, The Netherlands.

Baker ET, German CR, Elderfield H (1995) Hydrothermal plumes over spreading-center axes: Global distributions and geological inferences, pp. 47-71. In *Seafloor Hydrothermal Systems:Physical, Chemical, Biological, and Geological Interactions*, Humphris S, Zierenberg R, Mullineaux L, Thomson R (eds.), Geophysical Monograph 91, American Geophysical Union, Washington, D.C.

Baker ET, Edmonds HN, Michael PJ, Bach W, Dick HJB, Snow JE, Walker SL, Banerjee NR, Langmuir CH (2004) Hydrothermal venting in magma deserts: The ultraslow-spreading Gakkel and Southwest Indian Ridges. *Geochemistry Geophysics Geosyst*ems **5**, Q08002.

Balashova VV, Zavarzin GA (1979) Anaerobic reduction of ferric iron by hydrogen bacteria. *Mikrobiologia* **48**, 773-775.

Bancroft GM (1973) *Mössbauer Spectroscopy: An Introduction for Inorganic Chemists and Geochemists*. Van Nostrand Press, London.

Bandhu A, Mukherjee S, Acharya S, Modak S, Brahma SK, Das D, Chakrabarti PK (2009) Dynamic magnetic behavior and Mössbauer effect measurements of magnetite nanoparticles prepared by a new technique in the co-precipitation method. *Solid State Communications* **149**, 1790-1794.

Benner SA, Ellington AD (1991) RNA World. *Science* **252**, 1232-1232

Berry FJ, Skinner S, Thomas MF (1998) Fe-57 Mossbauer spectroscopic examination of a single crystal of Fe_3O_4. *Journal of Physics: Condensed Matter* **10**, 215-220.

Beveridge TJ, Meloche JD, Fyfe WS, Murray RGE (1983) Diagenesis of metals chemically complexed to bacteria: laboratory formation of metal phosphate, sulfide, and organic condensates in artificial sediments. *Applied Environmental Microbiology* **45**, 1094-1108.

Beveridge TJ, Murray RGE (1976) Uptake and retention of metals by cell walls of *Bacillus subtilis*. *Journal of Bacteriology* **127**, 1502-1518.

Bishop JL, Lane MD, Dyar MD, Brown AJ (2008) Reflectance and emission spectroscopy study of four groups of phyllosilicates: Smectites, kaolinite-serpentines, chlorites and micas *Clay Minerals*, **43**, 35-54.

Bishop JL, Lane MD, Dyar MD, King SJ, Brown AJ, Swayze G (2014) Spectral properties of Ca-sulfates: Gypsum, bassanite and anhydrite. *American Mineralogist* (in revision)

Blöchl E, Rachel R, Burggraf S, Hafenbradl D, Jannasch HW, Stetter KO (1997) *Pyrolobus fumarii*, gen. and sp. nov., represents a novel group of archaea, extending the upper temperature limit for life to 113°C.

Bohnenstiehl DR, Dziak RP, Tolstoy M, Fox CG, Fowler M (2004) Temporal and spatial history of the 1999-2000 Endeavour Segment seismic series, Juan de Fuca Ridge. *Geochemistry Geophysics Geosyst*ems **5**, Q09003.

Brazelton WJ, Schrenk MO, Kelley DS, Baross JA (2006) Methane- and sulfur-metabolizing microbial communities dominate the Lost City hydrothermal field ecosystem. *Applied and Environmental Microbiology* **72**, 6257-6270.

Brenner D, Staley J, Krieg N. (2000) Classification of prokaryotic organisms and the concept of Bacterial speciation. Springer; New York: *Bergey's manual of systematic bacteriology*.

Burggraf S, Huber H, Stetter KO (1997) Reclassification of the crenarchaeal orders and families in accordance with 16S rRNA sequence data. *International Journal of Systematic and Evolutionary Microbiology* **47**, 657–660.

Burns R (1993) Mineralogical Applications of Crystal Field Theory, Second Edition, *Cambridge University Press*, Cambridge, 551p

Butterfield DA, McDuff RE, Mottl MJ, Lilley MD, Lupton JE, Massoth GJ (1994) Gradients in the composition of hydrothermal fluids from the Endeavour segment vent field: phase separation and brine loss. *Journal of Geophysical Research* **99**, 9561-9583.

Butterfield DA, Jonasson IR, Massoth GJ, Feely RA, Roe KK, Embley RE, Holden JF, McDuff RE, Lilley MD, Delaney JR (1997) Seafloor eruption and evolution of hydrothermal fluid chemistry, *Philosophical Transactions of the Royal Society of London A* **355**, 369-386.

Caccavo F, Coates JD, Roseello-Mora RA, Ludwig W, Schleifer KH, Lovley DR, McInerney MJ (1996) *Geovibrio ferrireducens*, a phylogenetically distinct dissimilatory Fe(III)-reducing bacterium. *Archives of Microbiology* **165**, 370-376.

Caporaso JG, *et al.* (2010) QIIME allows analysis of high-throughput community sequencing data, *Nature Methods* **7**, 335-336.

Carbotte SM, Canales JP, Nedimovic MR, Carton H, Mutter JC (2012) Recent seismic studies at the East Pacific Rise 8° 20′-10° 10′ N and Endeavour Segment: Insights into mid-ocean ridge hydrothermal and magmatic processes. *Oceanography* **25**, 100-112.

Chan CS, Fakra SC, Emerson D, Fleming EJ, Edwards KJ (2011) Lithotrophic iron-oxidizing bacteria produce organic stalks to control mineral growth: implications for biosignature formation. *ISME J* **5**, 717–727

Chang L, Roberts AP, Tang Y, Rainford BD, Muxworthy AR, Chen Q (2008) Fundamental magnetic parameters from pure synthetic greigite (Fe_3S_4). *Journal of Geophysical Research* **113**, B06104.

Chao A (1987) Estimating the population size for capture-recapture data with unequal catchability. *Biometrics* **43**, 783-791.

Childers SE, Clufo S, Lovley DR (2002) *Geobacter metallireducens* accesses insoluble Fe(III) oxide by chemotaxis. *Nature* **416**, 767-769.

Chun J, Rainey FA (2014) Integrating genomics into the taxonomy and systematics of the *Bacteria* and *Archaea*. *International Journal of Systematic and Evolutionary Microbiology* **64**, 316-324

Clague DA, Caress DW, Thomas H, Thompson D, Calarco M, Holden JF, Butterfield D (2008) Abundance and distribution of hydrothermal chimneys and mounds on the Endeavour Ridge determined by 1-m resolution AUV multibeam mapping surveys. *Eos Transactions AGU* **89**, Fall Meeting Supplement, Abstract V41B-2079.

Clark RN, Swayze GA, Wise R, Livo E, Hoefen T, Kokaly R and Sutley SJ (2007) USGS digital spectral library splib06a. *U.S. Geological Survey, Digital Data Series* 231.

Coates JD, Ellis DJ, Gaw CV, Lovley DR (1999) *Geothrix fermentans* gen. nov., sp. nov., a novel Fe(III) reducing bacterium from a hydrocarbon contaminated aquifer. *International Journal of Systematic Bacteriology* **49**, 1615-1622.

Coleman ML, Hedrick DB, Lovley DR, White DC, Pye K (1993) Reduction of Fe(III) in sediments by sulphate-reducing bacteria. *Nature* **361**, 436-438.

Corliss JB, Dymond J, Gordon LI, Edmond JM, von Herzen RP, Ballard RD, Green K, Williams D, Bainbridge A, Crane K, van Andel TH (1979) Submarine thermal springs on the Galápagos Rift. *Science* **203**, 1073-1083.

Cornell RM, Schwertmann U (2003) *The Iron Oxides: Structure, Properties, Reactions, Occurences and Uses, Second Edition*. Wiley-VCH Verlag GmbH & Co. KGaA, Weinheim.

Davis EE, Wang K, Thomson RE, Becker K, Cassidy JF (2001) An episode of seafloor spreading and associated plate deformation inferred from crustal fluid pressure transients. *Journal of Geophysical Research* **106**, 21,953-21,963.

DeGrave E, Van Alboom A (1991) Evaluation of ferrous Mössbauer fractions. *Physics and Chemistry of Minerals* **18**, 337-342.

Delaney JR, Kelley DS, Lilley MD, Butterfield DA, Baross JA, Wilcock WSD, Embley RW (1998) The quantum event of oceanic crustal accretion: impacts of diking at mid-ocean ridges. *Science* **281**, 222–230.

Delaney JR, Kelley DS, Mathez EA, Yoerger DR, Baross J, Schrenk MO, Tivey MK, Kaye J, Robigou V (2001) “Edifice Rex” sulfide recovery project: Analysis of a submarine hydrothermal microbial habitat. *EoS Trans* **82**, 67-73.

Delaney JR, Robigou V, McDuff RE, Tivey MK (1992) Geology of a vigorous hydrothermal system on the Endeavour Segment, Juan de Fuca Ridge. *Journal of Geophysical Research* **97**, 19,663-19,682.

DeSantis TZ, *et al.* (2006) Greengenes, a chimera-checked 16S rRNA gene database and workbench compatible with ARB. *Applied and Environmental Microbiology* **72**, 5069-5072.

De Vrind-de Jong and de Vrind (1997) Algal deposition of carbonates and silicates. In: Banfield JF, Nealson KH (eds). *Geomicrobiology: Interaction between microbe and minerals. Reviews of Mineralogy*, Washington DC: Mineralogical Society of America **35**, 267-307.

Dobbin PS, Warren LH, Cook NJ, McEwan AG, Powell AK, Richardson DJ (1996) Dissimilatory iron reduction by *Rhodobacter capsulatus. Microbiology* **142**, 765-774.

Dobbin PS, Carter JP, Garcia-Salamanca San Juan C, von Hobe M, Powell AK, Richardson DJ (1999) Dissimilatory Fe(III) reduction by *Clostridium beijerinckii* isolated from freshwater sediment using Fe(III) maltol enrichment. *FEMS Microbiology Letters* **176**, 131-138.

Davis KJ, Luttge A (2005) Quantifying the potential role of microbial surface colonization in determining the mechanism and rate of carbonate dissolution. *American Journal of Science* **305**, 727-751.

Dyar MD, Agresti DG, Schaefer MW, Grant CA, Sklute EC (2006) Mössbauer spectroscopy of earth and planetary materials. *Annual Review of Earth and Planetary Sciences* **34**, 83-125.

Dyar MD, Breves EA, Jawin E, Marchand G, Nelms M, O'Connor V, Peel S, Rothstein Y, Sklute EC, Lane MD, Bishop JL, Mertzman SA (2014) Mössbauer parameters of iron in phosphate minerals. *American Mineralogist* **98**, 1943-1965.

Edgar RC (2010) Search and clustering orders of magnitude faster than BLAST. *Bioinformatics* **26**, 2460-2461.

Edgar RC, Haas BJ, Clemente JC, Quince C, Knight R (2011) UCHIME improves sensitivity and speed of chimera detection. *Bioinformatics* **27**, 2194-2200.

Edwards KJ, Bach W, McCollom TM (2005) Geomicrobiology in oceanography: microbe-mineral interactions at and below the seafloor. *Trends in Microbiology* **13**, 449–456.

Ehrlich HL, Newman DK (2009) *Geomicrobiology*, 5th edition. CRC Press/Taylor & Francis, Boca Raton, FL.

Feinberg LF, Holden JF (2006) Characterization of dissimilatory Fe(III) versus NO_3^- reduction in the hyperthermophilic archaeon *Pyrobaculum aerophilum*. *Journal of Bacteriology* **188**, 525-531.

Feinberg LF, Srikanth R, Vachet RW, Holden JF (2008) Constraints on anaerobic respiration in the hyperthermophilic archaea *Pyrobaculum islandicum* and *Pyrobaculum aerophilum*. *Applied and Environmental Microbiology* **74**, 396-402.

Ferris FG, Beveridge TJ, Fyfe WS (1986) Iron-silica crystallite nucleation by bacteria in a geothermal sediment. *Nature* **320**, 609-611.

Ferris FG, Fyfe WS, Beveridge TJ (1987) Bacteria as nucleation sites for authigenic minerals in a metal contaminated lake sediment. *Chemical Geology* **63**, 225-232.

Felsenstein J (1985) Confidence limits on phylogenies: an approach using the bootstrap. *Evolution* **39,** 783-791.

Flores GE, Campbell JH, Kirshtein JD, Meneghin J, Podar M, Steinberg JI, Seewald JS, Tivey MK, Voytek MA, Yang ZK, Reysenbach AL (2011) Microbial community structure of hydrothermal deposits from geochemically different vent fields along the Mid-Atlantic Ridge. *Environmental Microbiology* **13**, 2158-2171.

Francis CA, Obraztsova AY, Tebo BM (2000) Dissimilatory metal reduction by the facultative anaerobe *Pantoe agglomerans* SP1. *Applied and Environmental Microbiology* **66**, 543-548.

Fredrickson JK, Zachara JM, Kennedy D, Dong H, Onstott T, Hinman N, Li SM (1998) Biogenic iron mineralization accompanying the dissimilatory reduction of hydrous ferric oxide by a groundwater bacterium. *Geochimica et Cosmochimica Acta* **62**, 3239–3257.

Gadd GM (1992) Metals and microorganisms: a problem of definition. *FEMS Microbiology Letters* **100**, 197–204.

Gadd GM (2004) Microbial influence on metal mobility and application for bioremediation. *Geoderma* **122**, 109–119.

Gadd GM (2008) Bacterial and fungal geomicrobiology: a problem with communities? *Geobiology* **6**, 278–284.

Gaspard S, Vasquez F, Holliger C (1998) Localization and solubilization of the iron(III) reductase of *Geobacter sulfurreducens*. *Applied and Environmental Microbiology* **64**, 3188-3194.

Gilmour C, Riedel G (2009) Biogeochemistry of trace metals and metalloids, pp. 7–15. In *Encyclopedia of Inland Waters*, Likens GE (ed.), Elsevier, Amsterdam.

Gogarten JP, Rausch T, Bernasconi P, Kibak H, Taiz L (1989) Molecular evolution of H^+ ATPases. I. *Methanococcus* and *Sulfolobus* are monophyletic with respect to eukaryotes and eubacteria. *Zeitschrift für Naturforschung, A Journal of Biosciences*, Section C **44**, 641-650.

Gold T (1992) The deep, hot biosphere. *Proceeds of the National Academy of Sciences USA* **89**, 6045-6049.

Goldfarb MS, Converse DR, Holland HD, Edmond JM (1983) The genesis of hot spring deposits on the East Pacific Rise, 21°N, *Economic Geology Monograph* **5**, 184-197.

Goldstein SJ, Murrell MT, Janecky DR, Delaney JR, Clague DA (1991) Geochronology and petrogenesis of MORB from the Juan de Fuca and Gorda Ridges by U-238 Th-230 disequilibrium. *Earth and Planetary Science Letters* **107**, 25-41.

Gorby YA, Lovley DR (1991) Electron transport in the dissimilatory iron reducer GS-15. *Applied and Environmental Microbiology* **57**, 867-870.

Gorby YA, Yanina S, McLean JS, Rosso KM, Moyles D, Dohnalkova A, Beveridge TJ, Chang IS, Kim BH, Kim KS, Culley DE, Reed SB, Romine MF, Saffarini DA, Hill EA, Shi L, Elias DA, Kennedy DW, Pinchuk G, Watanabe K, Ishii S, Logan B, Nealson KH, Fredrickson JK (2006) Electrically conductive bacterial nanowires produced by *Shewanella oneidensis strain MR-1* and other microorganisms. *Proceedings of the National Academy of Sciences USA* **103**, 11,358-11,363.

Hamilton WA, Characklis WG (1989) Relative activities of cells in suspension and in biofilms, pp. 199-219. In *Structure and Function of Biofilms*, Characklis WG, Wilderer P (eds.), John Wiley, New York.

Hansel CM, Benner SG, Neiss J, Dohnalkova A, Kukkadapu RK, Fendorf S (2003) Secondary mineralization pathways induced by dissimilatory iron reduction of ferrihydrite under advective flow. *Geochimica et Cosmochimica Acta* **67**, 2977-2992.

Hansel CM, Benner SG, Fendorf S (2005) Competing Fe(II)-induced mineralization pathways of ferrihydrite. *Environmental Science & Technology* **39**, 7147-7153.

Hassett KL, Stecher LC, Hendrickson DN (1980) Polymer-anchored metal oxide particles: 1. Superparamagnetic magnetite microcrystals stabilized by lignosulfonate. *Inorganic Chemistry* **19**, 416-422.

Haymon R (1983) Growth history of hydrothermal black smoker chimneys. *Nature* **301**, 695-698.

Heberling C, Lowell R, Liu L, Fisk MR (2010) Extent of the microbial biosphere in the oceanic crust. *Geochemistry Geophysics Geosystems* **11**, Q08003.

Hedrick DB, Pledger RD, White DC, Baross JA (1992) In situ microbial ecology of hydrothermal vent sediments. *FEMS Microbiology Ecology* **101**, 1-10.

Hentscher M, Bach W (2012) Geochemically induced shifts in catabolic energy yields explain past ecological changes of diffuse vents in the East Pacific Rise 9°50′N area. *Geochemical Transactions* **13**, 2.

Hobbie JE, Daley RJ, Jasper S (1977) Use of nucleopore filters for counting bacteria by microscopy. *Applied and Environmental Microbiology* **33**, 1225-1228.

Hoehler TM (2007) An energy balance concept of habitability. *Astrobiology* **7**, 824-838.

Holden JF, Breier JA, Rogers KL, Schulte MD, Toner BM (2012) Biogeochemical processes at hydrothermal vents: microbes and minerals, bioenergetics, and carbon fluxes. *Oceanography* **25**, 196-208.

Holland ME, Baross JA (2003) Limits to life in hydrothermal systems, pp. 235-249. In *Mass and Energy Transfer in Hydrothermal Systems*, P.E. Halbach, V. Tunnicliffe, andJ.R. Hein, (eds) Proceedings of the 89th Dahlem Workshop, Dahlem University Press, Berlin.

Hooft EEE, *et al.* (2010) A seismic swarm and regional hydrothermal and hydrologic perturbations: The northern Endeavour Segment, February, 2005. *Geochemistry Geophysics Geosystems* **11**, Q12015.

Huang PM, Wang MC, Wang MK (2004) Mineral-organic-microbial interactions, pp. 486-499. In *Encyclopedia of Soils in the Environment*, Hillel D, Rosenzweig C, Powlson DS, Scow KM, Singer MJ, Sparks DL, Hatfield J (eds.), Elsevier, Amsterdam.

Huber JA, Holden JF (2007) Modeling the impact of diffuse vent microorganisms along mid-ocean ridges and flanks. pp. 215-231 In *Magma to Microbe: Modeling Hydrothermal*

Processes at Oceanic Spreading Centers, Lowell RP, Seewald JS, Metaxas A and Perfit MR (eds.), American Geophysical Union, Washington, DC.

Huber JA, Butterfield DA, Baross JA (2003) Bacterial diversity in a subseafloor habitat following a deep-sea volcanic eruption. *FEMS Microbiology Ecology* **43**, 393-409.

Huber JA, Mark Welch DB, Morrison HG, Huse SM, Neal PR, Butterfield DA, Sogin ML (2007) Microbial population structures in the deep marine biosphere. *Science* **318**, 97-100.

Hubas C, Jesus B, Passarelli C, Jeanthon C (2011) Tools providing new insight into coastal anoxygenic purple bacterial mats: review and perspectives. Research in Microbiology **162**, 858-868

Hugenholtz P & Goebel BM (2001). The polymerase chain reaction as a tool to investigate microbial diversity in environmental samples, pp. 31-42. In Rochelle, P. A. (ed.) Environmental Molecular Microbiology: Protocols and Applications. Horizon Scientific Press, Norfolk, UK.

Jamieson JW, Hannington MD, Clague DA, Kelley DS, Delaney JR, Holden JF, Tivey MK, Kimpe LE (2013) Sulfide geochronology along the Endeavour Segment of the Juan de Fuca Ridge, *Geochemistry Geophysics Geosystems* **14**, 2084-2099.

Jannasch HW, Mottl MJ (1985) Geomicrobiology of deep-sea hydrothermal vents. *Science* **229**, 717-725.

Jin Q and Bethke CM (2005) Predicting the rate of microbial respiration in geochemical environments. *Geochimica et Cosmochimica Acta* **69**, 1133–1143.

Johnson HP, Hutnak M, Dziak RP, Fox CG, Urcuyo I, Cowen JP, Nabelek J, Fisher C (2000) Earthquake-induced changes in a hydrothermal system on the Juan de Fuca mid-ocean ridge. *Nature* **407**, 174-177.

Jumpertz CM, Rimbert JN (1993) Identification and characterization of the iron compounds in bone marrow by means of Mössbauer spectroscopy. *BioMetals* **6**, 207-212.

Kallmeyer J, Pockalny R, Adhikari R, Smith DC, D'Hondt S (2012) Global distribution of subseafloor sedimentary biomass. *Proceedings of the National Academy of Science USA* **109**, 16,213-16,216.

Kalska-Szostko B, Zubowska M, Satula D (2006) Studies of the magnetite nanoparticles by means of Mössbauer spectroscopy. *Acta Physica Polonica A* **109**, 365-369.

Karsten JL, Hammond SR, Davis EE, Currie RG (1986) Detailed geomorphology and neotectonics of the Endeavour Segment, Juan de Fuca Ridge: New results from Seabeam swath mapping. *Geological Society of America Bulletin* **97**, 213-221.

Kashefi K, Lovley DR (2000) Reduction of Fe(III), Mn(IV), and toxic metals at 100°C by *Pyrobaculum islandicum*. *Applied and Environmental Microbiology* **66**, 1050-1056.

Kashefi K, Lovley DR (2003) Extending the upper temperature limit for life. *Science* **301**, 934.

Kashefi K, Holmes DE, Reysenbach AL, Lovley DR (2002) Use of Fe(III) as an electron acceptor to recover previously uncultured hyperthermophiles: isolation and characterization of *Geothermobacterium ferrireducens* gen. nov., sp. nov. *Applied and Environmental Microbiology* **68**, 1735-1742.

Kashefi K, Tor JM, Holmes DE, Gaw Van Praagh CV, Reysenbach AL, Lovley DR (2002) *Geoglobus ahangari* gen. nov., sp. nov., a novel hyperthermophilic archaeon capable of oxidizing organic acids and growing autotrophically on hydrogen with Fe(III) serving as the sole electron acceptor. *International Journal of Systematic and Evolutionary Microbiology* **52**, 719-728.

Kashefi K, Moskowitz BM, Lovley DR (2008) Characterization of extracellular minerals during dissimilatory Fe(III) and U(VI) reduction at 100°C by *Pyrobaculum islandicum*. *Geobiology* **6**, 147-154.

Kato S, Takano Y, Kakegawa T, Oba H, Inoue K, Kobayashi C, Utsumi M, Marumo K, Kobayashi K, Ito Y, Ishibashi J, Yamagishi A (2010) Biogeography and biodiversity in sulfide structures of active and inactive vents at deep-sea hydrothermal fields of the southern Mariana Trough. *Applied and Environmental Microbiology* **76**, 2968-2979.

Kelley DS, Delaney JR, Yoerger DR (2001) Geology and venting characteristics of the Mothra hydrothermal field, Endeavour segment, Juan de Fuca Ridge. *Geology* **29**, 959-962.

Kelley DS, Baross JA, Delaney JR (2002) Volcanoes, fluids, and life at mid-ocean ridge spreading centers. *Annual Review of Earth and Planetary Sciences* **30**, 385-491.

Kelley DS, Carbotte SM, Caress DW, Clague DA, Delaney JR, Gill JB, Hadaway H, Holden JF, Hooft EEE, Kellogg JP, Lilley MD, Stoermer, Toomey D, Weekly R, Wilcock WSD (2012) Endeavour Segment of the Juan de Fuca Ridge: one of the most remarkable places on Earth. *Oceanography* **25**, 44-61.

Koch AL, Schmidt TM (1991) The first cellular bioenergetic process: Primitive generation of a proton motive force. *Journal of Molecular Evolution* **33**, 297–304.

Konstantinidis KT, Tiedje JM (2005) Genomic insights that advance the species definition for prokaryotes. *Proceedings of the National Academy of Sciences U S A* **102**, 2567-2572.

Konstantinidis KT, Ramette A, Tiedje JM (2006) The bacterial species definition in the genomic era. *Philosophical Transactions of the Royal Society B Biological Sciences* **361**, 1929-1940

Kormas KA, Tivey MK, Von Damm K, Teske A (2006) Bacterial and archaeal associated with distinct mineralogical layers of a white smoker spire from a deep-sea hydrothermal vent site (9°N, East Pacific Rise), *Environmental Microbiology* **8**, 909-920.

Koski RA, Jonasson IR, Kadko DC, Smith VK, Wong FL (1994) Compositions, growth mechanisms, and temporal relations of hydrothermal sulfide-sulfate-silica chimneys at the northern Cleft segment, Juan de Fuca Ridge, *Journal of Geophysical Research* **99**, 4813-4832.

Kristall B, Kelley DS, Hannington MD, Delaney JR (2006) Growth history of a diffusely venting sulfide structure from the Juan de Fuca Ridge: a petrological and geochemical study. *Geochemistry Geophysics Geosystems* **7**, Q07001.

Lane MD (2007) Mid-Infrared emission spectroscopy of sulfate and sulfide-bearing minerals. *American Mineralogist* **92**, 1-18.

Lane MD (2008) Sulfide minerals studied using thermal emission spectroscopy, *Lunar and Planetary Science XXXIX*, Abstract 2205, Lunar and Planetary Institute, Houston.

Lane MD, Bishop JL, Dyar MD, Hiroi T, Mertzman SA, Bish DL, King PL, Rogers AD (submitted) Mid-infrared emission spectroscopy and visible/near-infrared reflectance spectroscopy of Fe-sulfate minerals. *American Mineralogist*.

Larkin M, *et al.* (2007) ClustalW and ClustalX version 2.0. *Bioinformatics* **23**, 2947-2948.

Leang C, Coppi MV, Lovley DR (2003) OmcB, a *c*-type polyheme cytochrome, involved in Fe(III) reduction in *Geobacter sulfurreducens*. *Journal of Bacteriology* **185**, 2096-2103.

Li YL, Pfiffner SM, Dyar MD, Vali H, Konhauser K, Cole DR, Rondinone AJ, Phelps TJ (2009) Degeneration of biogenic superparamagnetic magnetite. *Geobiology* **7**, 25-34.

Lilley MD, Butterfield DA, Olson EJ, Lupton JE, Macko SA, McDuff RE (1993) Anomalous CH_4 and NH_4^+ concentrations at an unsedimented mid-ocean-ridge hydrothermal system. *Nature* **364**, 45-47.

Lilley MD, Butterfield DA, Lupton JE, Olson EJ (2003) Magmatic events can produce rapid changes in hydrothermal vent chemistry. *Nature* **422**, 878-881.

Lipp JS, Morono Y, Inagaki F, Hinrichs KU (2008) Significant contribution of Archaea to extant biomass in marine subsurface sediments. *Nature* **454**, 991-994.

Lonergan DJ, Jenter HL, Coates JD, Phillips EJP, Schmidt TM, Lovley DR (1996) Phylogenetic analysis of dissimilatory Fe(III)-reducing bacteria. *Journal of Bacteriology* **178**, 2402-2408.

Lovley DR (1991) Dissimilatory Fe(III) and Mn(IV) reduction. *Microbiology Reviews* **55**, 259-287.

Lovley DR (1993) Dissimilatory metal reduction. *Annual Review of Microbiology* **47**, 263-290.

Lovley DR (2004) Origins: Genesis, Evolution and Diversity of Life. Series: Cellular Origin, Life in Extreme Habitats and Astrobiology. Seckbach J (Eds) 709. Springer.

Lovley DR, Coates JD (2000) Novel forms of anaerobic respiration of environmental relevance. *Current Opinions in Microbiology* **3**:252-256.

Lovley DR, Goodwin S (1988) Hydrogen concentrations as an indicator of the predominant terminal electron-accepting reactions in aquatic sediments. *Geochimica et Cosmochimica Acta* **52**, 2993-3003.

Lovley DR, Phillips EJP (1988) Novel mode of microbial energy metabolism: organic carbon oxidation coupled to dissimilatory reduction of iron or manganese. *Applied and Environmental Microbiology* **54**, 1472–1480.

Lovley DR, Stolz JF, Nord GL, Phillips EJP (1987) Anaerobic production of magnetite by a dissimilatory iron-reducing microorganism. *Nature* **330**, 252-254.

Lovley DR, Holmes DE, Nevin KP (2004) Dissimilatory Fe(III) and Mn(IV) reduction. *Advances in Microbial Physiology* **49**, 219-286.

Lozupone C, Knight R (2005) UniFrac: a new phylogenetic method for comparing microbial communities. *Applied and Environmental Microbiology* **71**, 8228-8235.

Lyubutin IS, Lin CR, Lu SZ, Siao YJ, Korzhetsky YV, Dmitrieva TV, Dubinskaya YL, Pokatilov VS, Konovalova AO (2011) High-temperature redistribution of cation

vacancies and irreversible magnetic transitions in the Fe1-xS nanodisks observed by Mössbauer spectroscopy and magnetic measurements. *Journal of Nanoparticle Research* **13**, 5507-5517.

Magnuson TS, Hodges-Myerson AL, Lovley DR (2000) Characterization of a membrane-bound NADH-dependent Fe^{3+} reductase from the dissimilatory Fe^{3+}-reducing bacterium *Geobacter sulfurreducens*. *FEMS Microbiology Letters* **185**, 205-211.

Manceau A, Combes JM (1988) Structure of Mn and Fe oxides and oxyhydroxides: a topological approach by EXAFS. *Physics and Chemistry of Minerals*. **15**, 283-295.

Marquez-Linares F, Uwakweh ONC, Lopez N, Chavez E, Polanco R, Morant C, Sanz JM, Elizalde E, Neira C, Nieto S, Roque-Malherbe R (2011) Study of the surface chemistry and morphology of single walled carbon nanotube-magnetite composites. *Journal of Solid State Chemistry* **184**, 655-666.

Marsili E, Baron DB, Shikhare ID, Coursolle D, Gralnick JA, Bond DR (2008) *Shewanella* secretes flavins that mediate extracellular electron transfer. *Proceedings of the National Academy of Sciences of the United States of America* **105**, 3968-3973

McCollom TM, Shock EL (1997) Geochemical constraints on chemolithoautotrophic metabolism by microorganisms in seafloor hydrothermal systems. *Geochimica et Cosmochimica Acta* **61**, 4375-4391.

McDonald D, Price MN, Goodrich J, Nawrocki EP, DeSantis TZ, Probst A, Knight GL, Hugenholtz P (2012) An improved Greengenes taxonomy with explicit ranks for ecological and evolutionary analyses of bacteria and archaea. *ISME Journal* **6**, 610-618.

McKay CP and Davis WL (1991) Duration of liquid water habitats on early Mars. *Icarus* **90**, 214-221.

McNeill DF 1990 Biogenic magnetite from surface Holocene carbonate sediments, Great Bahama Bank, *Journal of Geophysical Research* **95**, 4363-4372,

Mehta MP, Baross JA (2006) Nitrogen fixation at 92°C by a hydrothermal vent archaeon. *Science* **15,** 1783-1786.

Meyer JL, Akerman NH, Proskurowski G, Huber JA (2013), Microbiological characterization of post-eruption “snowblower” vents at Axial Seamount, Juan de Fuca Ridge. *Frontiers in Microbiology* **4**, 153.

Murad E (1992) Magnetic properties of fine-grained materials, pp. 339-349. In *Studies of Magnetic Properties of Fine Particles and their Relevance in Materials Science*, Dormann JL, Fiorani D (eds.) Elsevier Science, Amsterdam.

Murad E, Johnston JH (1988) Iron oxides and oxyhydroxides, pp. 507-582. In *Mössbauer Spectroscopy Applied to Inorganic Chemistry*, Long GJ (ed.), Plenum, New York.

Murray AE, Hollibaugh JT & Orrego C (1996) Phylogenetic compositions of bacterioplankton from two California estuaries compared by denaturing gradient gel electrophoresis of 16S rRNA fragments. *Applied Environmental Microbiology* **62,** 2676-2680.

Myers CR, Nealson KH (1988) Bacterial manganese reduction and growth with manganese oxide as the sole electron acceptor. *Science* **240**, 1319-1321.

Nakagawa S, Takai K, Inagaki F, Chiba H, Ishibashi J, Kataoka S, Hirayama H, Nunoura T, Horikoshi K, Sako Y (2005) Variability in microbial community and venting chemistry in a sediment-hosted backarc hydrothermal system: impacts of subseafloor phase-separation. *FEMS Microbiology Ecology* **54**, 141-155.

Nazaries L, Pan Y, Bodrossy L, Baggs EM, Millard P, Murrell JC, Singh BK (2013) Evidence of microbial regulation of biogeochemical cycles from a study on methane flux and land use change. *Applied and Environmental Microbiology* **79**, 4031-4040.

Nealson K, Myers CR (1990) Iron reduction by bacteria: a potential role in the genesis of banded iron formations. *American Journal of Science* **290-A**, 35-45

Noffke N, Christian D, Wacey D, Hazen RM (2013) Microbially induced sedimentary structures recording an ancient ecosystem in the ca. 3.48 billion-year-old dresser formation, Pilbara, western Australia. *Astrobiology* **13**, 1103-1124.

Olins HC, Rogers DR, Frank KL, Vidoudez C, Girguis PR (2013) Assessing the influence of physical, geochemical and biological factors on anaerobic microbial primary productivity within hydrothermal vent chimneys. *Geobiology* **11**, 279-293.

Olsson-Francis K, Cockell CS (2010) Experimental methods for studying microbial survival in extraterrestrial environments. *Journal of Microbiological Methods* **80**, 1-3.

Opatkiewicz AD, Butterfield DA, Baross JA (2009) Individual hydrothermal vents at Axial Seamount harbor distinct subseafloor microbial communities. *FEMS Microbiology Ecology* **70**, 413-424.

Orellana R, Leavitt JJ, Comolli LR, Csencsits R, Janot N, Flanagan KA, Gray AS, Leang C, Izallalen M, Mester T, Lovley DR (2013) U(VI) reduction by a diversity of outer surface *c*-type cytochromes of *Geobacter sulfurreducens*. *Applied and Environmental Microbiology* **79**, 6369-6374

Pagé A, Tivey MK, Stakes DS, Reysenbach AL (2008) Temporal and spatial archaeal colonization of hydrothermal vent deposits. *Environmental Microbiology* **10**, 874-884

Phillips EJP, Lovley DR (1987) Determination of Fe(III) and Fe(II) in oxalate extracts of sediments. *Soil Science Society of America Journal* **51**, 938-941.

Pierson B, Oesterle A, Murphy GL (1987) Pigments, light penetration, photosynthetic activity in the multi-layered microbial mats of Great Sippewissett Salt Marsh, Massahucsetts. *FEMS Microbial Ecology* **45**, 365-376

Pieters CM (1983) Strength of mineral absorption features in the transmitted component of near-infrared reflected light: First results from RELAB. *Journal of Geophysical Research* **88**, 9534-9544

Pley U, Schipka J, Gambacorta A, Jannasch HW, Fricke H, Rachel R, Stetter KO (1991) *Pyrodictium abyssi* sp. nov. represents a novel heterotrophic marine archaeal hyperthermophile growing at 110°C. *Systematic and Applied Microbiology* **14**, 245-253.

Pope KO, Kieffer SW and Ames DE (2006) Impact melt sheet formation on Mars and its implication for hydrothermal systems and exobiology. *Icarus* **183**, 1-9

Price RE, Lesniewski R, Nitzsche KS, Meyerdierks A, Saltikov C, Pichler T, Amend JP (2013) Archaeal and bacterial diversity in an arsenic-rich shallow-sea hydrothermal system undergoing phase separation. *Frontiers of Microbiology* **4**, 158

Proskurowski G, Lilley MD, Brown TA (2004) Isotopic evidence of magmatism and seawater bicarbonate removal at the Endeavour hydrothermal system. *Earth and Planetary Science Letters* **225**, 53-61.

Purvis OW, Pawlik-Skowronska B (2008). Lichens and metals, pp. 175-200. In *Stress in Yeasts and Filamentous Fungi*, Avery SV, Stratford M and Van West P (eds) Elsevier, Amsterdam.

Reguera G, McCarthy KD, Mehta T, Nicoll JS, Tuominen MT, Lovley DR (2005) Extracellular electron transfer via microbial nanowires. *Nature* **435**, 1098-1101.

Rickard D (1969) The chemistry of iron sulphide formation at low temperatures. *Stockholm Contributions in Geology* **26**, 67–95.

Riddihough R (1984) Recent movements of the Juan-de-Fuca plate system. *Journal of Geophysical Research* **89**, 6980-6994.

Roberts AP, Weaver R (2005) Multiple mechanisms of remagnetization involving sedimentary greigite. *Earth and Planetary Science Letters* **231**, 263-277.

Roberts JL (1947) Reduction of ferric hydroxide by strains of *Bacillus polymyxa*. *Soil Science* **63**, 135-140.

Robigou V, Delaney JR, Stakes DS (1993) Large massive sulfide deposits in a newly discovered active hydrothermal system, the High-Rise Field, Endeavour Segment, Juan de Fuca Ridge. *Geophysical Research Letters* **20**, 1887-1890.

Rothschild LJ (1990) Earth analogs for Martian life. Microbes in evaporites, a new model system for life on Mars. *Icarus* **88,** 246-260.

Ruff SW, Christensen PR, Barbera PW and Anderson DL (1997) Quantitative thermal emission spectroscopy of minerals: A laboratory technique for measurement and calibration. *Journal of Geophysical Research* **102,** 14899-14913.

Runov EV (1926) Die reduktion der eisenoxyde auf microbiologichem wege. *Vestn. Bakter-Agronomich. Stantsii* **24**, 75-82.

Saffarini DA, Blumerman SL, Mansoorabadi KJ (2002) Role of menaquinones in Fe(III) reduction by membrane fractions of *Shewanella putrefaciens*. *Journal of Bacteriology* **184**, 846-848.

Saitou N & Nei M (1987) The neighbor-joining method: a new method for reconstructing phylogenetic trees. *Molecular Biology and Evolution* **4,** 406-425.

Seeliger S, Cord-Ruwisch R, Schink B (1998) A periplasmic and extracellular *c*-type cytochrome of *Geobacter sulfurreducens* acts as a ferric iron reductase and as an electron carrier to other acceptors or to partner bacteria. *Journal of Bacteriology* **180,** 3686-3691.

Schloss PD, Westcott SL, Ryabin T, Hall JR, Hartmann M, Hollister EB, Lesniewski RA, Oakley BB, Parks DH, Robinson CJ, Sahl JW, Stres B, Thallinger GG, Van Horn DJ, Weber CF (2009) Introducing Mothur: open-source, platform-independent, community-supported software for describing and comparing microbial communities. *Applied and Environmental Microbiology* **75**, 7537-7541.

Schrenk MO, Kelley DS, Delaney JR, Baross JA (2003) Incidence and diversity of microorganisms within the walls of an active deep-sea sulfide chimney. *Applied and Environmental Microbiology* **69**, 3580-3592.

Schwertmann U, Taylor RM (1977) Iron oxides, in Dixon JB, Weed SB (eds) Madison, Minerals in soil environments: *Soil Sciences Society of America* 145-180.

Seyfried WE, Seewald JS, Berndt ME, Ding K, Foustoukos DI (2003) Chemistry of hydrothermal fluids from the Main Endeavour Field, northern Juan de Fuca Ridge: Geochemical controls in the aftermath of June 1999 seismic events. *Journal of Geophysical Research* **108**, 2429.

Shannon CE (1948) A mathematical theory of communication. *The Bell System Technical Journal*, **27**, 379-423 and 623-656.

Skinner BJ (1983) Submarine volcanic exhalations that form mineral deposits: An old idea now proven correct, pp 557-569. In *Hydrothermal Processes at Seafloor Spreading Centers*, NATO Conference Series 12.

Slobodkin A, Reysenbach AL, Strutz N, Dreier M, Wiegel J (1997) *Thermoterrabacterium ferrireducens* gen. nov., sp. nov., a thermophilic anaerobic dissimilatory Fe(III)-reducing bacterium from a continental hot spring. *International Journal of Systematic Bacteriology* **47**, 541-547.

Slobodkin A, Jeanthon C, L'Haridon S, Nazina T, Miroshnichenko M, Bonch-Osmolovskaya E (1999) Dissimilatory reduction of Fe(III) by thermophilic bacteria and archaea in deep subsurface petroleum reservoirs of Western Siberia. *Current Microbiology* **39**, 99-102.

Slobodkin A, Campbell B, Cary SC, Bonch-Osmolovskaya E, Jeanthon C (2001) Evidence for the presence of thermophilic Fe(III) reducing microorganisms in deep-sea hydrothermal vents at 13°N (East Pacific Rise). *FEMS Microbiology Ecology* **36**, 235-243.

Starowicz M, Starowicz P, Żukrowski J, Przewoźnik J, Lemański A, Kapusta C, Banaś J (2011) Electrochemical synthesis of magnetic iron oxide nanoparticles with controlled size. *Journal of Nanoparticle Research* **13**, 7167-7176.

Stetter KO, König H, Stackebrandt E (1983) *Pyrodictium* gen. nov., a new genus of submarine disc-shaped sulphur reducing archaebacteria growing optimally at 105°C. *Systematic and Applied Microbiology* **4**, 535–551

Stolz J, Basu P, Oremland R (2002) Microbial transformation of elements: the case of arsenic and selenium. *International Microbiology* **5**, 201-207.

Straub KL, Benz M, Schink B (2001) Iron metabolism in anoxic environments at near neutral pH. *FEMS Microbiology Ecology* **34**, 181-186.

Summit M, Baross JA (2001) A novel microbial habitat in the mid-ocean ridge subseafloor. *Proceedings of the National Academy of Sciences USA* **98**, 2158-2163.

Takai K, Komatsu T, Inagaki F, Horikoshi K (2001) Distribution of archaea in a black smoker chimney structure. *Applied and Environmental Microbiology* **67,** 3618-3629.

Takai K, Gamo T, Tsunogai U, Nakayama N, Hirayama H, Nealson KH, Horikoshi K (2004) Geochemical and microbiological evidence for a hydrogen-based, hyperthermophilic subsurface lithoautotrophic microbial ecosystem (HyperSLiME) beneath an active deep-sea hydrothermal field. *Extremophiles* **8,** 269-282.

Takai K, Nakamura K, Toki T, Tsunogai U, Miyazaki M, Miyazaki J, Hirayama H, Nakagawa S, Nunoura T, Horikoshi K (2008) Cell proliferation at 122°C and isotopically heavy CH_4 production by a hyperthermophilic methanogen under high-pressure cultivation. *Proceedings of the National Academy of Science USA* **105**, 10,949-10,954.

Takai K, Nakamura K (2010) Compositional, physiological and metabolic variability in microbial communities associated with geochemically diverse, deep-sea hydrothermal vent fluids, pp. 251-283. In *Geomicrobiology: Molecular and Environmental Perspective*, Loy A, Mandl M, Barton LL (eds.), Springer, New York.

Talwani M, Windisch CC, Langseth Jr MG (1971) Reykjanes ridge crest: A detailed geophysical study. *Journal of Geophysical Research* **76**, 473-517.

Tamura K, Dudley J, Nei M & Kumar S (2007) MEGA4: Molecular Evolutionary Genetics Analysis (MEGA) software version 4.0. *Molecular Biology and Evolution* **24,** 1596-1599.

Tamura K, Nei M & Kumar S (2004) Prospects for inferring very large phylogenies by using the neighbor-joining method. *Proceedings of the National Academy of Sciences USA* **101,** 11,030-11,035.

Tamura K, Peterson D, Peterson N, Stecher G, Nei M, Kumar S (2011) MEGA5: molecular evolutionary genetics analysis using maximum likelihood, evolutionary distance, and maximum parsimony methods. *Molecular Biology and Evolution* **28**, 2731-2739

Thomas-Keprta KL, Bazylinski BA, Kirchvink JL, Clemett SJ, McKay DS, Wentworth SJ, Vali H, Gibson JEK, Romanek CS (2000a) Elongated prismatic magnetite crystals in ALH84001 carbonate globules: potential Martian magnetofossils. *Geochimica et Cosmochimica Acta* **64**, 4049-4081.

Thomas-Keprta KL, Clemett SJ, Bazylinski DA, Kirschvink JL, McKay DS, Wentworth SJ, Vali H, Gibson JEK, McKay MF, Romanek CS (2001) Truncated hexa-octahedral magnetite crystals in ALH84001: presumptive biosignatures. *Proceedings of the National Academy of Sciences. USA* **98**, 2164-2169.

Thompson JR, Marcelino LA, Polz MF (2002) Heteroduplexes in mixed-template amplifications: formation, consequence and elimination by "reconditioning PCR" *Nucleic Acids Research* **30**, 2083-2088

Tivey MK (2004) Environmental conditions within active seafloor vent structures: sensitivitiy to vent fluid composition and fluid flow, pp. 137-152. In *The Subseafloor Biosphere at Mid-Ocean Ridges*, Wilcock WSD, DeLong EF, Kelley DS, Baross JA, Cary SC (eds.), Geophysical Monograph 144, American Geophysical Union Press, Washington, DC.

Tivey MK (2007) Generation of seafloor hydrothermal vent fluids and associated mineral deposits. *Oceanography* **20**, 50-65.

Tivey MK, Delaney JR (1985) Sulfide deposits from the Endeavour Segment of the Juan de Fuca Ridge. *Marine Mining* **5**, 165-179.

Tivey MK, Delaney JR (1986) Growth of large sulfide structures on the Endeavour Segment of the Juan de Fuca Ridge. *Earth and Planetary Science Letters* **77**, 303-317.

Tivey MK, and Singh S (1997) Nondestructive imaging of fragile sea-floor vent deposit samples. *Geology* **25**, 931-934.

Tivey MK, Stakes DS, Cook TL, Hannington MD, Petersen S (1999) A model for growth of steep-sided vent structures on the Endeavour Segment of the Juan de Fuca Ridge: results of a petrological and geochemical study. *Journal of Geophysical Research* **104**, 22,859-22,883.

Tor JM, Lovley DR (2001) Anaerobic degradation of aromatic compounds coupled to Fe(III) reduction by *Ferroglobus placidus*. *Environmental Microbiology* **3**, 281-287.

Tor JM, Kashefi K, Lovley DR (2001) Acetate oxidation coupled to Fe(III) reduction in hyperthermophilic microorganisms. *Applied and Environmental Microbiology* **67**, 1363-1365.

Uroz S, Calvaruso C, Turpault MP, Frey-Klett P (2009) Mineral weathering by bacteria: ecology, actors and mechanisms. *Trends in Microbiology* **17**, 378–387.

Vali H, Weiss B, Li YL, Sears SK, Kim SS, Kirschvink JL, Zhang CL (2004) Formation of tabular single-domain magnetite induced by *Geobacter metallireducens* GS-15. *Proceedings of the National Academy of Sciences USA* **101**, 16,121-16,126.

Van Ark EM, Detrick RS, Canales JP, Carbotte SM, Harding JJ, Kent GM, Nedimovic MR, Wilcock WSD, Diebold JB, Babcock JM (2007) Seismic structure of the Endeavour Segment, Juan de Fuca Ridge: Correlations with seismicity and hydrothermal activity, *Journal of Geophysical Research* **112**, B02401.

Van Cappellen P, Viollier E, Roychoudhury AN, Clark L, Ingall E, Lowe K, DiChristina T (1998) Biogeochemical cycles of manganese and iron at the oxic-anoxic transition of a stratified marine basin (Orca Basin, Gulf of Mexico). *Environmental Science & Technology* **32**, 2931-2939.

Vargas M, Kashefi K, Blunt-Harris EL, Lovley DR (1998) Microbiological evidence for Fe(III) reduction on early Earth. *Nature* **395**, 65-67.

Ver Eecke HC, Kelley DS, Holden JF (2009) Abundances of hyperthermophilic autotrophic Fe(III) oxide reducers and heterotrophs in hydrothermal sulfide chimneys of the northeastern Pacific Ocean. *Applied and Environmental Microbiology* **75**, 242-245.

Ver Eecke HC, Butterfield DA, Huber JA, Lilley MD, Olson EJ, Roe KK, Evans LJ, Merkel AY, Cantin HV, Holden JF (2012) Hydrogen-limited growth of hyperthermophilic methanogens at deep-sea hydrothermal vents. *Proceedings of the National Academy of Sciences USA* **109**, 13,674-13,679.

Ver Eecke HC, Akerman NH, Huber JA, Butterfield DA, Holden JF (2013) Growth kinetics and energetics of a deep-sea hyperthermophilic methanogen under varying environmental conditions. *Environmental Microbiology Reports* **5**, 665-671.

Volkl P, Huber R, Drobner E, Rachel R, Burggraf S, Trincone A, Stetter KO (1993) *Pyrobaculum aerophilum sp. nov.*, a novel nitrate-reducing hyperthermophilic archaeum. *Applied and Environmental Microbiology* **59**, 2918-2926.

Volpe AM, Goldstein SJ (1993) Ra-226 Th-230 disequilibrium in axial and off-axis mid-ocean ridge basalts, *Geochimica et Cosmochimica Acta* **57**, 1233-1241.

von Canstein H, Ogawa J, Shimizu S, Lloyd JR (2008) Secretion of flavins by *Shewanella* species and their role in extracellular electron transfer. *Applied and Environmental Microbiology* **74**, 615-623.

Von Damm KL (1995) Controls on the chemistry and temporal variability of seafloor hydrothermal fluids, pp. 222-247. In *Seafloor Hydrothermal Systems: Physical, Chemical, Biological, and Geological Interactions*, Humpries SE, Zierenberg RA, Mullineaux LS, Thomson RE (eds.), Geophysical Monograph 91, American Geophysical Union, Washington, DC.

Von Damm KL, Edmond JM, Grant B, Measures CI (1985) Chemistry of submarine hydrothermal solutions at 21°N, East Pacific Rise. *Geochimica et Cosmochimica Acta* **49**, 2197-2220.

Walker JCG (1984) Suboxic diagenesis in banded iron formations. *Nature* **309**, 340-342.

Wang Q, Garrity GM, Tiedje JM, Cole JR (2007) Naive Bayesian classifier for rapid assignment of rRNA sequences into the new bacterial taxonomy. *Applied and Environmental Microbiol*ogy **73**, 5261-5267.

Weber KA, Achenbach LA, Coates JD (2006) Microorganisms pumping iron: anaerobic microbial iron oxidation and reduction. *Nature Reviews Microbiology* **4**, 752-764.

Weiss BP, Kim SS, Kirschvink JL, Kopp RE, Sankaran M, Kobayashi A, Komeili A (2004) Ferromagnetic resonance and low-temperature magnetic tests for biogenic magnetite. *Earth and Planetary Science Letters* **224**, 73-89.

Werner JJ, Koren O, Hugenholtz P, DeSantis TZ, Walters WA, Caporaso JG, Angenent LT, Knight R, Ley RE (2012) Impact of training sets on classification of high-throughput bacterial 16S rRNA gene surveys. *ISME Journal* **6**, 94-103.

Whitman WB, Coleman DC, Wiebe WJ (1998) Prokaryotes: the unseen majority. *Proceedings of the National Academy of Sciences USA* **95**, 6578-6583.

Wilcock WSD, Hooft EEE, Toomey DR, McGill PR, Barclay AH, Stakes DS, Ramirez TM (2009) The role of magma injection in localizing black-smoker activity. *Nature Geosciences* **2**, 509-513.

Zając M, Freindl K, Ślęzak T, Ślęzak M, Spiridis N, Wilgocka-Ślęzak D, Korecki J (2011) Electronic and magnetic properties of ultra-thin epitaxial magnetite films on MgO(001). *Thin Solid Films* **519,** 5588-5595.

Zeigler Allen L, Ishoey T, Novotny MA, McLean JS, Lasken RS, Williamson SJ (2011) Single virus genomics: a new tool for virus discovery. *PLoS ONE* **6**, e17722.

Zhou H, Li J, Peng X, Meng J, Wang F, Ai Y (2009) Microbial diversity of a sulfide black smoker in Main Endeavour hydrothermal vent field, Juan de Fuca Ridge. *Journal of Microbiology* **47**, 235-247.

Zillig W, Holz I, Janekovic D, Klenk HP, Imsel E, Trent J, Wunderl S, Forjaz VC, Coutinho R, Ferreira T (1990) *Hyperthermus butylicus*, a hyperthermophilic sulfur-reducing archaebacterium that ferments peptides. *Journal of Bacteriology* **172**, 3959-3965.